ORNL-4617
(ENDF-139)
UC-34 — Physics

A RE-EVALUATION OF NATURAL IRON NEUTRON AND GAMMA-RAY PRODUCTION CROSS SECTIONS — ENDF/B MATERIAL 1124

S. K. Penny
W. E. Kinney

OAK RIDGE NATIONAL LABORATORY
operated by
UNION CARBIDE CORPORATION
for the
U.S. ATOMIC ENERGY COMMISSION

Printed in the United States of America. Available from
National Technical Information Service
U.S. Department of Commerce
5285 Port Royal Road, Springfield, Virginia 22151
Price: Printed Copy $3.00; Microfiche $0.95

ORNL-4617
(ENDF-139)

Contract No. W-7405-eng-26

NEUTRON PHYSICS DIVISION

A RE-EVALUATION OF NATURAL IRON NEUTRON AND GAMMA-RAY PRODUCTION CROSS SECTIONS – ENDF/B MATERIAL 1124

S. K. Penny* and W. E. Kinney

NOTE

This Work Funded by

DEFENSE ATOMIC SUPPORT AGENCY

Under Subtask PC10301

APRIL 1971

*Mathematics Division.

OAK RIDGE NATIONAL LABORATORY
Oak Ridge, Tennessee
operated by
UNION CARBIDE CORPORATION
for the
U. S. ATOMIC ENERGY COMMISSION

CONTENTS

A RE-EVALUATION OF NATURAL IRON NEUTRON AND GAMMA-RAY PRODUCTION CROSS SECTIONS – ENDF/B MATERIAL 1124

S. K. Penny and W. E. Kinney

Abstract

Recent data and good agreement between calculated and experimental cross sections prompted the re-evaluation of natural iron neutron and gamma-ray production cross sections for ENDF/B use with the aim of improving angular distributions and extending inelastic level excitation cross sections. Calculations are described and are shown to be in good agreement with experiment. Below 2 MeV, neutron elastic scattering cross sections and cross sections for inelastic scattering to levels in ^{56}Fe are obtained from experimental results. Above 2 MeV, neutron elastic scattering cross sections and cross sections for inelastic scattering to levels in ^{56}Fe up to an excitation energy of 4.116 MeV are obtained from calculations. Cross sections for inelastic scattering to the continuum are obtained from fits to experimental results. The total cross sections are the evaluated cross sections of Irving and Straker from 330 keV to 15 MeV and those of the U.K. evaluation DFN-91 from 10^{-5} eV to 330 keV. The (n,p) and (n,α) cross sections were taken from the U.K. evaluation DFN-91, while the (n,2n) cross sections are those of ENDF/B material 1122. The (n,γ) cross sections were taken from U.K. DFN-91. The gamma-ray production cross sections and associated gamma-ray spectra were calculated from the evaluated (n,n') and (n,γ) cross sections together with known and assumed branching ratios. The evaluated cross sections are presented in graphical form.

I. INTRODUCTION

Previous ENDF/B* evaluations of natural iron neutron cross sections have been found to be deficient in at least two respects:[1] the partial inelastic cross sections are not given above 5 MeV, and the elastic scattering angular distributions above 4.6 MeV do not agree well with experiment at and beyond the first minimum.

Neutron elastic and inelastic scattering cross sections above 4 MeV have recently been measured,[1,2] and model calculations have been found to be in good agreement with the data. Macklin *et al.*[3] have recently taken preliminary data with fine resolution on the excitation of the 0.846-MeV level in ^{56}Fe from threshold to 2 MeV.

In view of the calculational successes and the new data, we have re-evaluated natural iron neutron cross sections with the intention of improving angular distributions, inelastic level excitation cross sections, cross sections for inelastic scattering into the continuum, inelastic gamma-ray production cross sections, and the associated gamma-ray spectra. Outside these areas we have borrowed freely from previous evaluations and cross-section sets, notably from the UKAEA Nuclear Data Library and the evaluation of the total cross section by Irving and Straker.[4] Table I lists these borrowed evaluations. When more than one evaluation is listed in Table I then the evaluations are identical.

The element iron has four naturally occurring isotopes. ^{56}Fe is the dominant isotope in determining the neutron cross sections of the element, and the other isotopes make only minor contributions. The fractional abundances and associated isotopic masses[5] are given in Table II.

Table I. List of Evaluations Having Some Data Identical With Present Evaluation – ENDF-MAT-1124

Reaction	Evaluation
Total	10^{-5} eV to 330 keV UK DFN-91 330 keV to 15 MeV ENDF MAT-1101
(n,2n)	ENDF MAT-1108 ENDF MAT-1122
(n,γ)	UK DFN-91
(n,p)	UK DFN-64 ENDF MAT-1101 UK DFN-91
(n,α)	UK DFN-64 ENDF MAT-1101 UK DFN-91

*Evaluated Nuclear Data File of the National Neutron Cross Section Center, Brookhaven National Laboratory.

Table II. Abundances and Masses of Iron Isotopes

Isotopes	Abundance	Mass
^{54}Fe	0.0582	53.93962
^{56}Fe	0.9166	55.93494
^{57}Fe	0.0219	56.93540
^{58}Fe	0.0033	57.93328

Table III. Neutron Reaction Q Values for Iron Isotopes

Reaction	Q Value (MeV)			
	^{54}Fe	^{56}Fe	^{57}Fe	^{58}Fe
(n,γ)	+9.2987	+7.6415	+10.0424	+6.5848
(n,n')	−1.4330	−0.846	−0.0144	−0.814
(n,p)	+0.0890	−2.9191	−1.9130	−5.7140
(n,α)	+0.8484	+0.3220	+2.4017	−1.3868
(n,2n)	−13.6189	−11.2040	−7.6415	−10.0424
(n,d)	−6.6272	−7.9651	−8.3362	−9.7310
(n,t)	−12.4220	−11.9319	−9.3492	−12.1212
(n,^{3}He)	−7.6947	−10.5348	−11.9224	−13.7164
(n,αn)	−8.4212	−7.6194	−7.3195	−7.6407
(n,pn)	−8.8517	−10.1896	−10.5607	−11.9555
(n,2p)	−7.4714	−11.9990	−11.3921	
(n,2α)	−8.0971	−8.8259	−5.5230	−9.1867

Numerous neutron interactions with the iron isotopes are energetically possible for neutrons with energies less than 15.0 MeV, the upper energy limit of this study. The Q values for possible reactions are given in Table III.[6]

Only a few of the reactions listed in Table III have significant cross sections in the energy range in this study. The (n,γ) reaction was included for all the isotopes. The (n,p), (n,α), and (n,2n) neutrons were included only for ^{54}Fe and ^{56}Fe. The inelastic scattering cross section included the contribution of ^{56}Fe and only that due to the excitation of the first level in ^{54}Fe.

Because of the strong reliance we have placed on calculations, we shall first discuss them and compare calculated results with experiment. The evaluated neutron cross sections are discussed in Section III and the gamma-ray production cross sections are discussed in Section IV. We present as many of the evaluated cross sections as possible in graphical form, dispensing with tables which may readily be obtained from the ENDF/B magnetic tape.

II. NEUTRON CROSS-SECTION CALCULATIONS AND COMPARISON WITH EXPERIMENT

Calculation of Neutron Elastic and Inelastic Scattering Cross Sections

Central to the calculation of neutron elastic and inelastic scattering cross sections is the optical model.[7] Optical model fits to elastic scattering data yield optical model parameters which can be used to interpolate and extrapolate elastic differential cross sections to energies and angles at which no measurements have been made. These optical model parameters are also used to compute penetrabilities in statistical model calculations[8-10] of compound nucleus contributions to elastic and inelastic scattering. Finally, the parameters are used to calculate the distorted waves in a Distorted-Wave-Born-Approximation (DWBA)[11] calculation of direct interaction contributions to inelastic scattering.

In the fitting of the elastic scattering data to find the best optical model parameters, some estimate must be made for the compound nucleus contributions to elastic scattering. This is done initially by performing statistical model calculations with more-or-less standard optical model parameters. The elastic data are then fitted to find the best first-iteration parameters, and another set of statistical model calculations are performed with these parameters. If the compound elastic contributions differ significantly from the starting values, the iteration is repeated and continued to convergence.

Differential Elastic Scattering Cross Sections

To obtain the optical model real and imaginary potential depths as a linear function of incident neutron energy, we fitted ORNL data from 4.60 to 8.56 MeV,[1] using the code GENOA,[12] varying only the constant parts of the potential depths, with the other parameters fixed at values given in Table IV. Two iterations were

Table IV. Optical Model Parameters for Neutron Channels

Real well depth	53.95 − 0.267 E† (MeV)
Real well radius	1.166 f
Real well diffuseness	0.646 f
Imaginary well depth‡	7.401 (MeV)
Imaginary well radius	1.225 f
Imaginary well diffuseness	0.6259 f
Spin orbit well depth	6.523 MeV
Spin orbit well radius	1.166 f
Spin orbit well diffuseness	0.646 f

†E is incident neutron energy (MeV) in laboratory system.
‡Woods-Saxon derivative.

required for convergence of the compound elastic cross sections. The calculated elastic angular distributions are compared with experimental data in Fig. 1 where the calculated values have been normalized to integrals of the experimental data at each energy. The abbreviations we use, the energies, the energy spreads, and the reference numbers for the investigators whose data are shown are given in Table V. The calculated values agree with the ORNL data as they should. The calculations are lower than the broad resolution DUKE data beyond

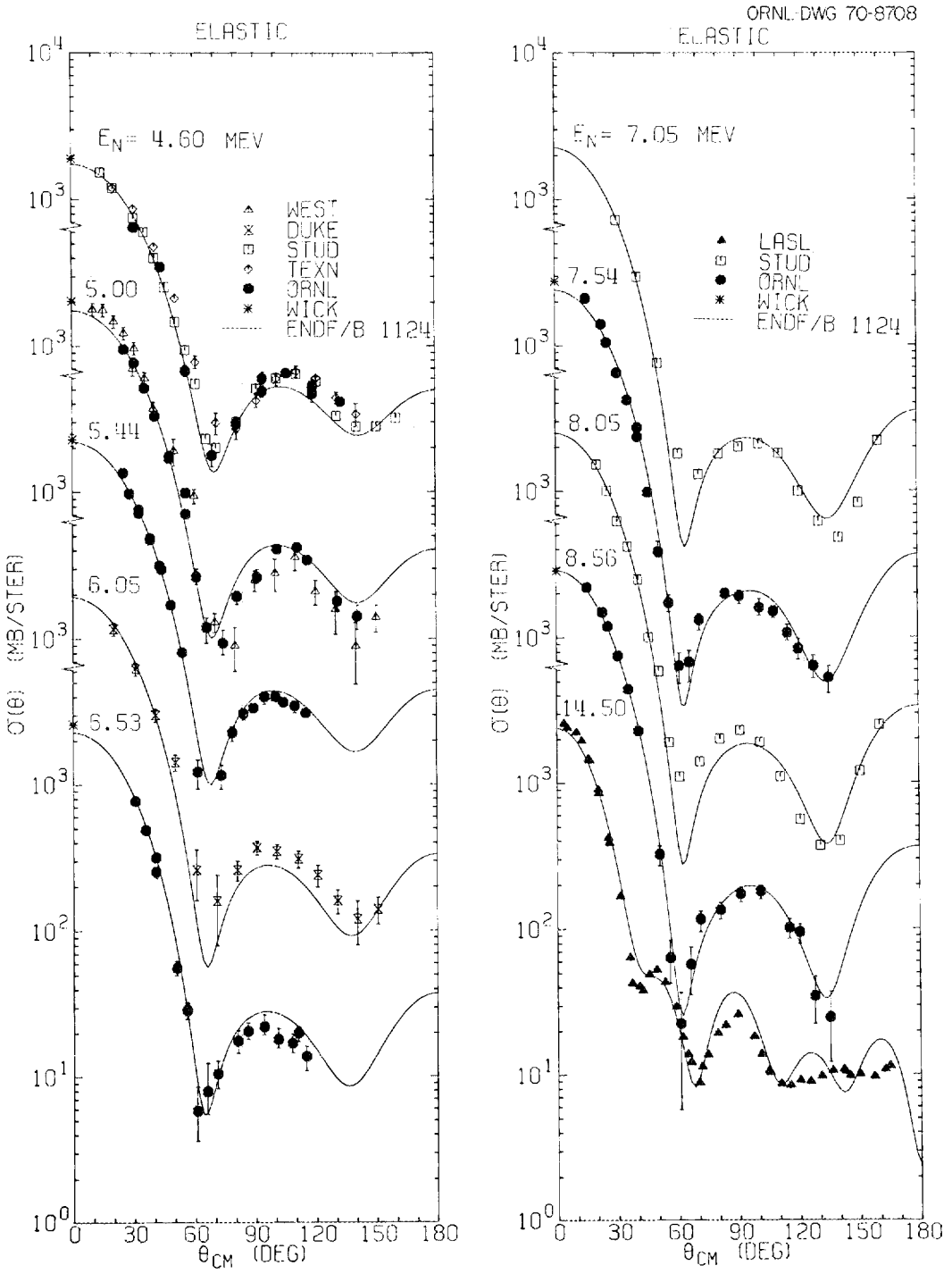

Fig. 1. A Comparison of Calculated and Experimental Differential Elastic Scattering Cross Sections. WICK indicates Wick's Limit.

the first minimum at 6.05 MeV and also are lower than the STUD data around the first minimum at 8.05 MeV. It is interesting that the calculations extrapolate so well to 14.5 MeV, matching the second minimum, although the first minimum is not well described and the structure in the calculations beyond 100° is not evident in the data.

Table V. The Abbreviations, Energies, and Reference Numbers for Investigators Whose Elastic Scattering Data are Compared With Calculations

Abbreviation	Energy (MeV)	Reference
WEST	5.00 ± 0.10	13
DUKE	6.05 ± 0.23	14
STUD	4.56 ± 0.05	2
	7.05 ± 0.09	
	8.05 ± 0.09	
TEXN	4.70 ± 0.09	15
LASL	2.52 ±0.047	16
	3.00 ± 0.043	
	3.50 ± 0.040	
	4.00 ± 0.037	
	4.50 ± 0.033	
	5.00 ± 0.030	
	14.5 ± 0.4	17
ORNL	4.60 ± 0.05	1
	5.00 ± 0.05	
	5.44 ± 0.17	
	6.53 ± 0.03	
	7.54 ± 0.06	
	8.56 ± 0.08	
	4.19 ± 0.08	
	4.46 ± 0.07	
	5.18 ± 0.05	
	5.50 ± 0.05	
	6.00 ± 0.13	
	6.13 ± 0.04	
	6.37 ± 0.13	
	7.60 ± 0.10	
	8.50 ± 0.08	
	8.56 ± 0.05	
ALD	0.98 ± 0.10	18
	1.40 ± 0.09	
	1.61 ± 0.08	
	1.79 ± 0.08	
	1.99 ± 0.07	
	2.01 ± 0.07	
	2.20 ± 0.07	
	2.39 ± 0.07	
	2.61 ± 0.06	
	2.81 ± 0.06	
	3.01 ± 0.06	
	3.06 ± 0.06	
	3.99 ± 0.06	

Cross Sections for Inelastic Scattering to Discrete Levels in ^{56}Fe

Cross sections for inelastic scattering to ^{56}Fe discrete levels by compound nucleus formation and decay were computed by statistical model theory with the computer code HELENE.[19] This code incorporates the Hauser-Feshbach statistical model[8] with Porter-Thomas width-fluctuation corrections.[9] Competition with continuum states is taken into account as well as competition from other reactions. The penetrabilities are computed directly from an optical model with no spin-orbit coupling. The 41 levels that were used for ^{56}Fe are listed in Table VI, together with the spins and parities used in the calculations.[20] Competition from (n,α) and (n,p) reactions was included, the characteristics of the levels in the ^{53}Cr and ^{56}Mn residual nuclei being given in Table VII.[21,22] This competition was not significant for neutron energies below 7 MeV. The optical model parameters for the neutron channels were those shown in Table IV; the α- and p-channel parameters are listed in Table VIII.[23,24] The continuum cutoff energies were 5.25 MeV, 2.782 MeV, and 0.213 MeV, respectively, for the n-, α-, and p-channels.

Table VI. Energy Levels of ^{56}Fe

Energy (MeV)	Jπ	Energy (MeV)	Jπ
0.000	0+	4.296	0+
0.846	2+	4.388	2+
2.084	4+	4.450	(2+)*
2.654	2+	4.501	3+
2.939	0+	4.531	3–
2.957	2+	4.545	(2+)
3.119	1+	4.602	(0+)
3.122	4+	4.650	(3–)
3.368	2+	4.676	(3–)
3.388	6+	4.728	(1–)
3.445	3+	4.866	(2+)
3.450	1+	4.871	(3–)
3.600	0+	5.017	(3–)
(3.601)	(0+)	5.032	(2+)
3.605	2+	5.044	(2+)
3.747	6+	5.130	(4+)
3.829	2+	5.135	(3–)
3.856	3+	5.191	(1–)
4.046	4+	5.196	(4+)
4.099	3+	5.243	(2+)
4.116	4+		

*Assumed spins and parities are enclosed in parentheses.

Table VII. Energy Levels of ^{53}Cr and ^{56}Mn

^{53}Cr		^{56}Mn	
Energy (MeV)	Jπ	Energy (MeV)	Jπ
0.000	3/2−	0.000	3+
0.565	1/2−	0.026	2+
1.008	5/2−	0.110	1+
1.285	(7/2−)*		
1.537	(7/2−)		
1.971	(3/2−)		
2.169	(1/2−)		
2.227	(5/2−)		
2.324	3/2−		
2.454	(1/2−)		
2.664	(5/2−)		
2.667	(1/2−)		
2.715	(3/2−)		

*Assumed spins and parities are enclosed in parentheses.

Table VIII. Optical Model Parameters for Alpha Particle and Proton Channels

	Alpha	Proton
Real well depth	78.60 (MeV)	46.60 (MeV)
Real well radius	1.58 f	1.28 f
Real well diffuseness	0.48 f	0.65 f
Imaginary well depth	15.50 (MeV)†	10.00 (MeV)‡
Imaginary well radius	1.58 f	1.28 f
Imaginary well diffuseness	0.48 f	0.53 f

†Woods-Saxon.

‡Woods-Saxon derivative.

The continuum level density parameters are given in Table IX.[19,25] The cross sections for exciting the continuum were calculated only for competition with discrete levels. The evaluated cross sections for exciting the continuum as discussed in Section III were determined experimentally.

The 0.846-MeV and 4.531-MeV levels in ^{56}Fe may be excited by direct interaction (DI) as well as by compound nucleus formation and decay (CN). A DWBA calculation was performed with the code JULIE[26] using optical model parameters of Table IV and a deformation parameter of 0.26 for the 0.846-MeV level and 0.2 for the 4.531-MeV level to account for the DI contributions.[24] Assuming independence of DI and CN processes, the calculated DI and CN cross sections were added to give the cross sections for inelastic scattering to these levels.

Table IX. Continuum Level Density Parameters

	^{56}Fe	^{53}Cr	^{56}Mn
ϵ_x (MeV)	9.2	8.2	4.6
ϵ_0 (MeV)	0.8	−0.71	−1.19
T (MeV)	1.26	1.41	1.07
a (MeV^{-1})	6.75	5.88	7.27
b	0	0	0
c (MeV^{-1})	8.77	7.37	9.45
Δ (MeV)	2.81	1.35	0

The calculated differential cross sections for inelastic scattering to the 0.846-MeV level in ^{56}Fe is compared with experimental results in Fig. 2 where agreement is seen to be reasonable. The DI contribution increases while the CN contribution decreases with increasing energy, the scattering being all DI at 14.5 MeV and the angular distribution being highly anisotropic. The calculated differential cross sections for inelastic scattering to higher levels agreed with experimental data within the experimental errors.

Calculated level excitation cross sections for inelastic scattering to resolvable levels and groups of levels in ^{56}Fe are compared with experimental results in Fig. 3 where agreement is seen to be good.

Nonelastic and Integrated Elastic Cross Sections

Experimental measurements have been made of both the nonelastic and the integrated elastic cross sections for natural iron and there is some interest in comparing the corresponding evaluated cross sections with the experimental results.

Figure 4 compares the evaluated nonelastic cross section as a function of energy from 1 to 15 MeV with experimental measurements of the nonelastic cross section as given in reference 27. The evaluated nonelastic cross section was averaged over 50-keV intervals for the purpose of this comparison. From 1 to 2.1 MeV, the nonelastic cross section is made up almost entirely of the cross section for inelastic scattering to the 0.846-MeV level in ^{56}Fe. This evaluated inelastic cross section in this energy range is based on the high resolution preliminary experimental data of Macklin[3] *et al.* as described in Section III. From 2.1 to 9 MeV the nonelastic cross section is essentially equal to the total inelastic cross section. In this energy range the evaluated cross sections for inelastic scattering to discrete

levels were calculated as described above while those for inelastic scattering to the continuum were obtained from experimental data as discussed in Section III. Above 9 MeV (n,2n), (n,p), and (n,α) reactions start to contribute to the nonelastic cross section, and in this energy range the cross section for inelastic scattering to the continuum was adjusted so that the evaluated nonelastic cross sections would agree with the experimental results. The fact that the evaluated nonelastic cross section is lower than the experimental data from 2 to 3 MeV implies a discrepancy between the nonelastic and the partial inelastic experimental cross

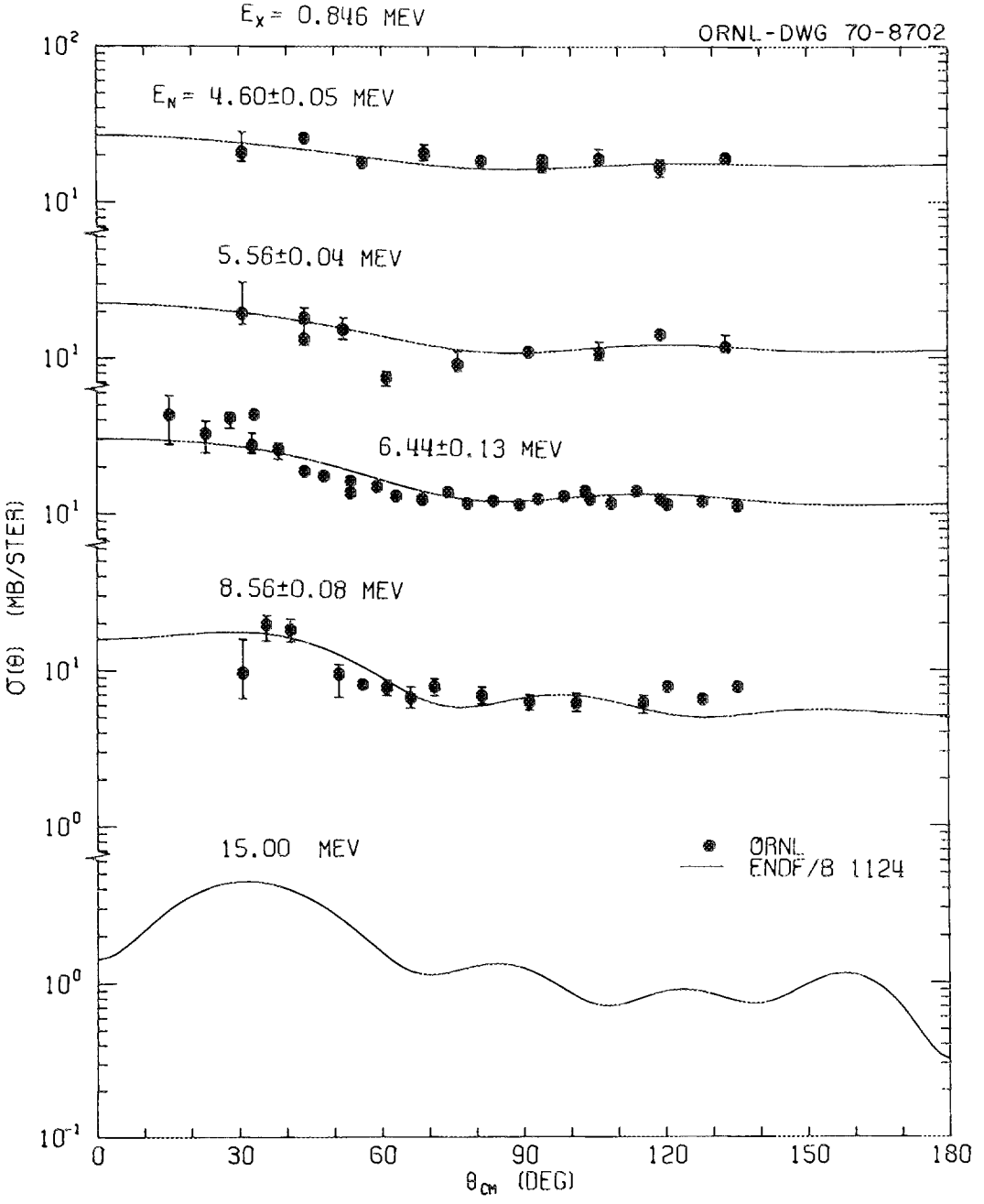

Fig. 2. A Comparison of Calculated and Experimental Differential Cross Sections Per Atom of Natural Iron for Inelastic Scattering to the 0.846-MeV Level in ^{56}Fe.

sections in this energy region. The nonelastic measurements were made by the sphere transmission technique, whereas the partial inelastic data result from time-of-flight experiments. The time-of-flight data require simpler corrections than do the sphere transmission data and should yield the better cross sections.

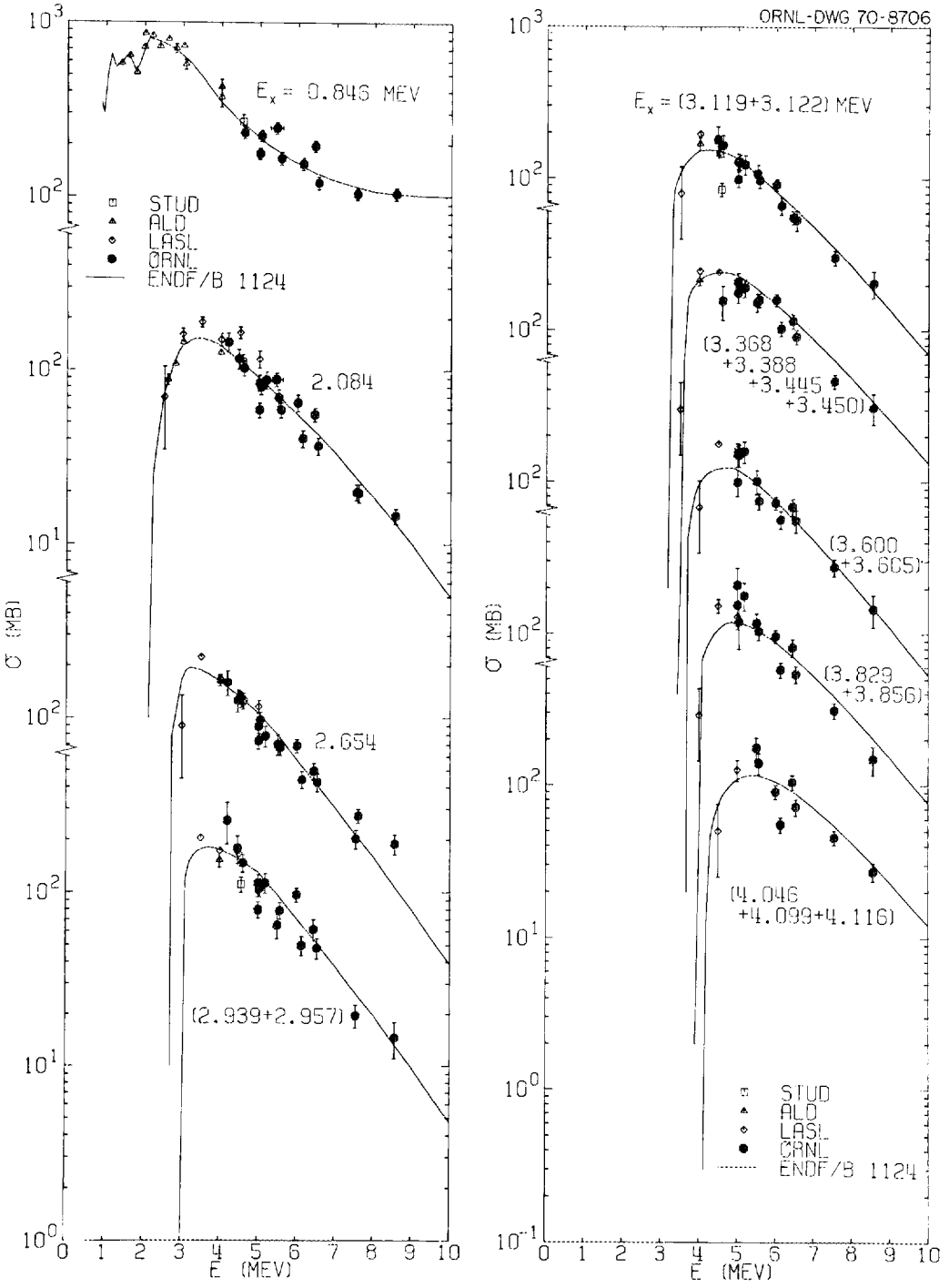

Fig. 3. A Comparison of Evaluated and Experimental Inelastic Scattering Level Excitation Cross Sections.

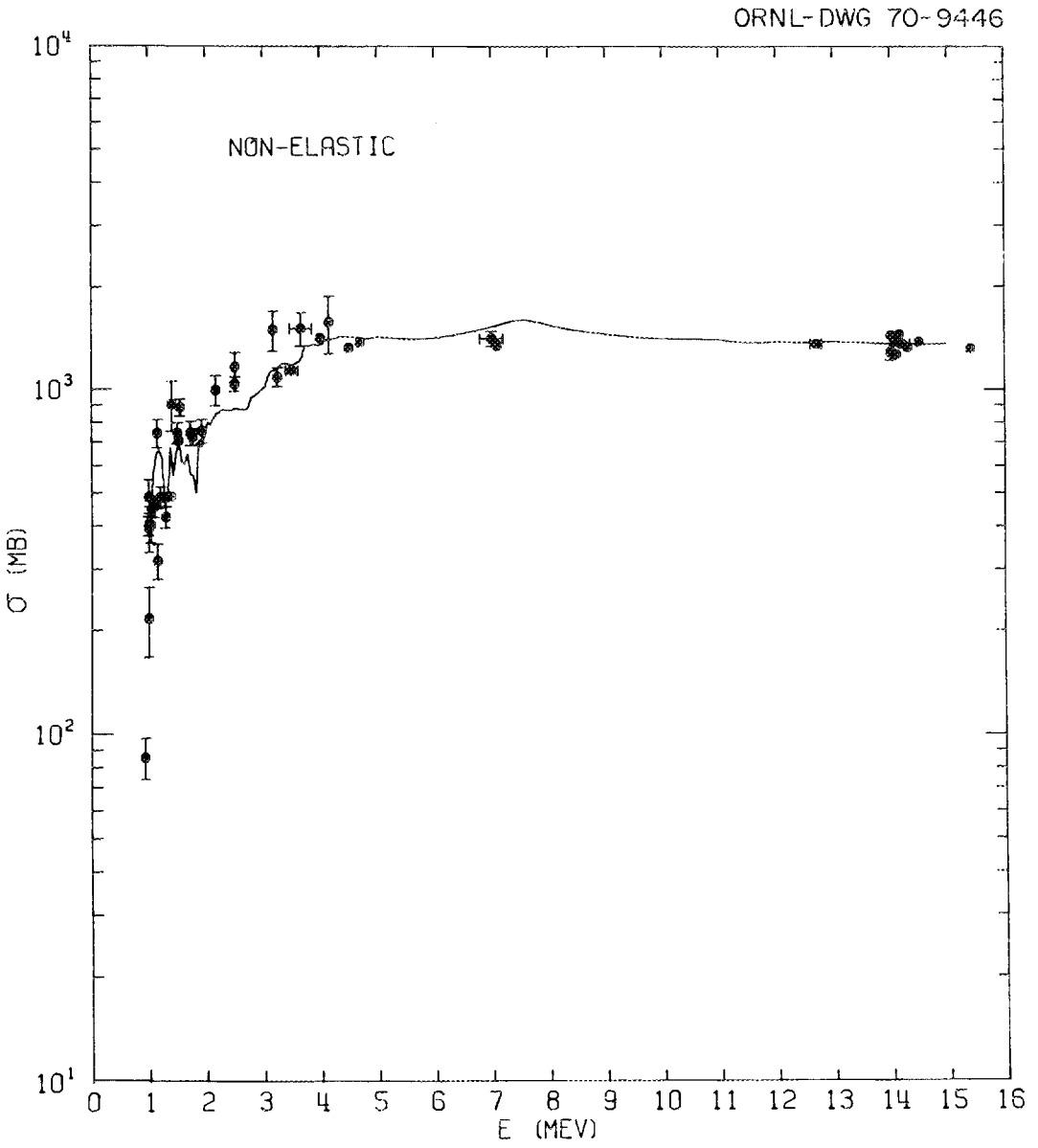

Fig. 4. A Comparison of Evaluated and Experimental Nonelastic Cross Sections.

The integrated elastic scattering cross section is obtained experimentally by measuring the differential elastic scattering cross section at a number of angles and then fitting the data by least squares to a Legendre series to find the integrated cross section. The ENDF/B elastic scattering cross section is defined as the difference between the total and the nonelastic cross sections.

The evaluated elastic scattering cross section for natural iron as a function of energy is compared with experimental data in Fig. 5. The experimental data were obtained from a SCISRS listing* of the available data and from reference 1. The evaluated cross section was averaged over 50-keV intervals for the purpose of comparison. It is in reasonable agreement with the experimental results except in the energy region from 5 to 7 MeV where it is ~10% higher than the data.

*Obtained from National Neutron Cross Section Center, Brookhaven National Laboratory, in March 1970.

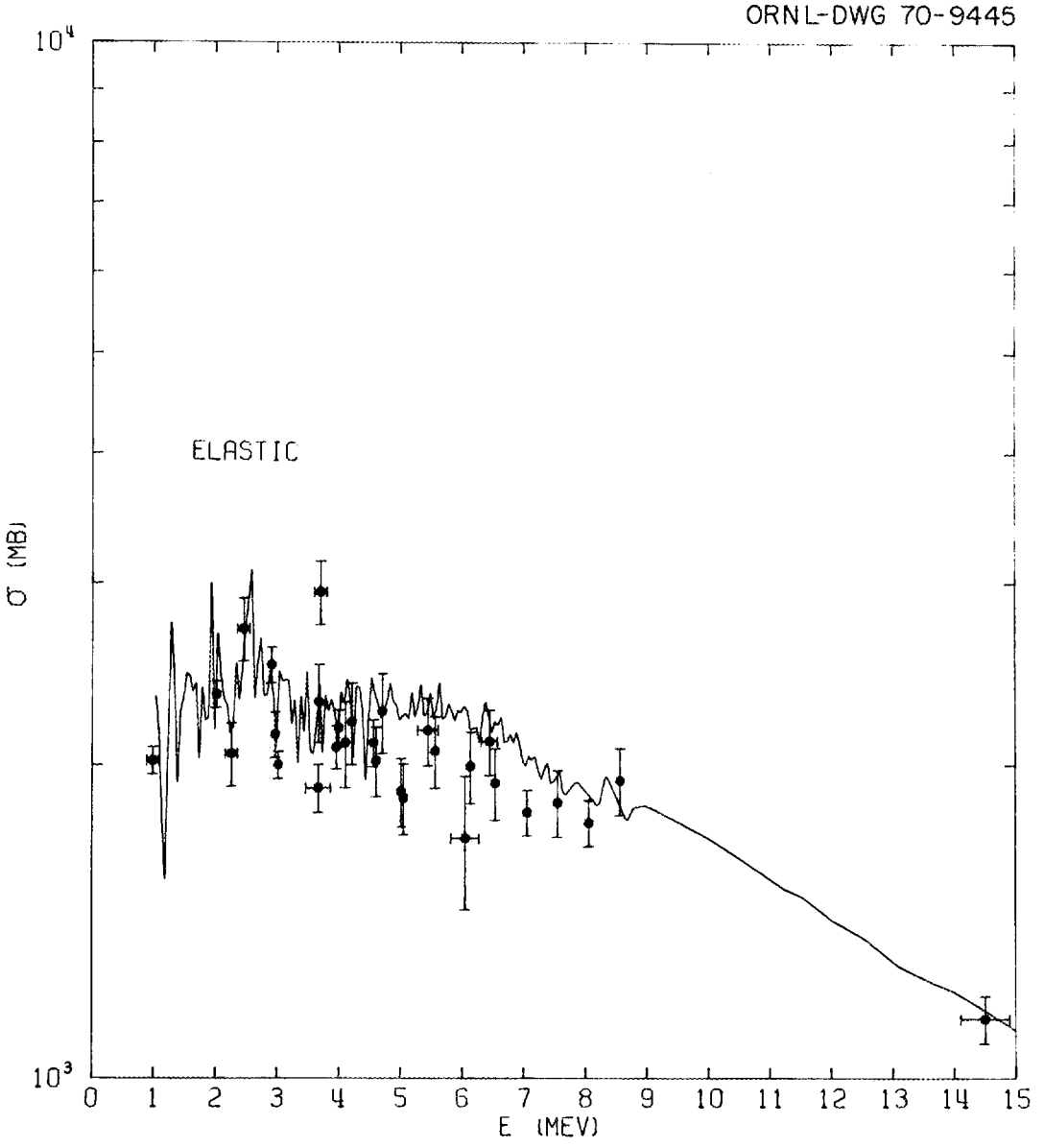

Fig. 5. A Comparison of Evaluated and Experimental Elastic Cross Sections.

III. THE EVALUATED NEUTRON CROSS SECTIONS

The Total Cross Section

The total cross section was taken from two previous evaluations. The evaluation of Irving and Straker[4] was adopted for the energy range 330 keV to 15 MeV. These data were taken from the experiments of Cierjacks *et al.*,[28] Carlson and Cerbone,[29] and Barnard *et al.*[30] Irving and Straker concentrated on eliminating unnecessary points in the experimental data, distinguishing actual structure from statistical fluctuations.

The evaluation of the United Kingdom (DFN-91[31]) was adopted for the energy range 10^{-5} eV to 330 keV. These data reflect the capture measurements of Hockenbury *et al.*[32] Further discussion may be found in the section for the capture cross section. The data are shown in Figs. 6–16.

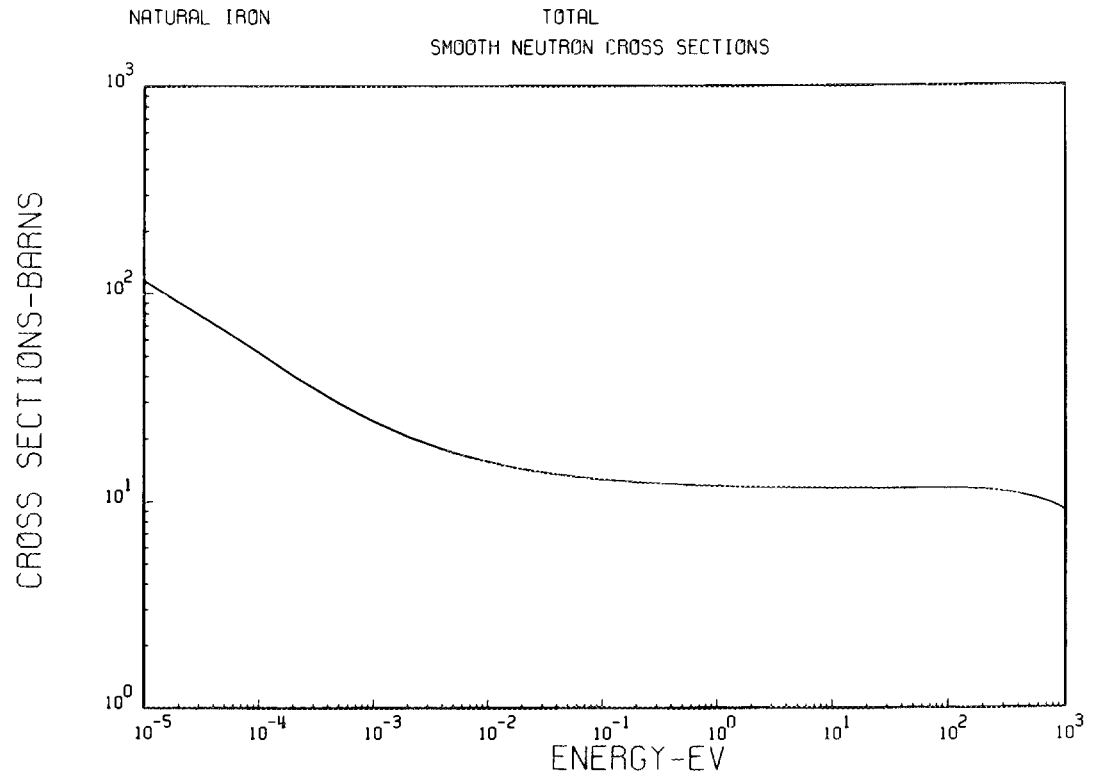

Fig. 6. The Evaluated Total Cross Section From 10^{-5} to 10^3 eV.

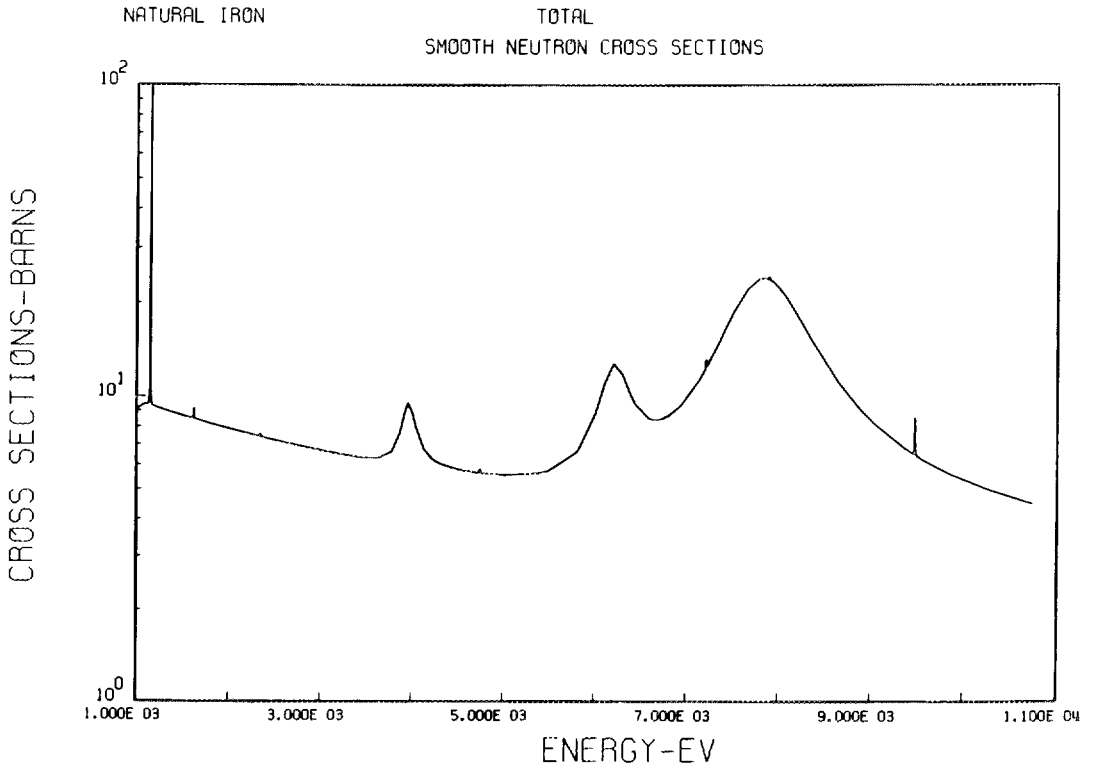

Fig. 7. The Evaluated Total Cross Section From 1 to 11 keV.

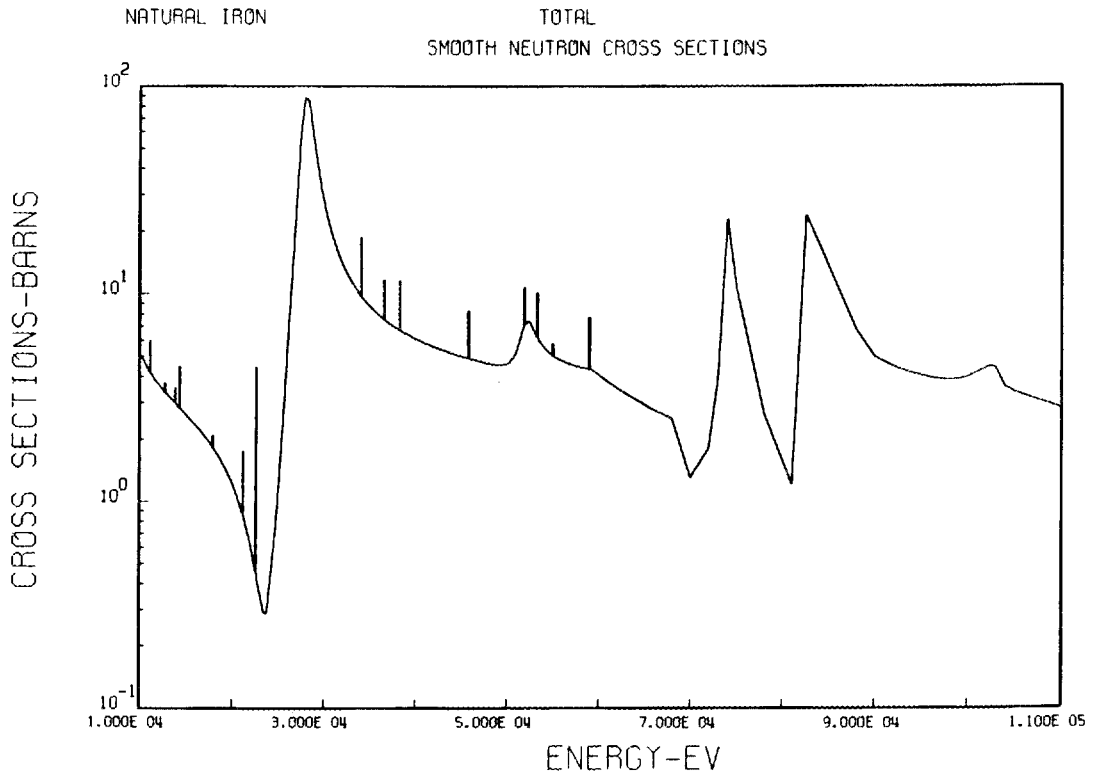

Fig. 8. The Evaluated Total Cross Section From 10 to 110 keV.

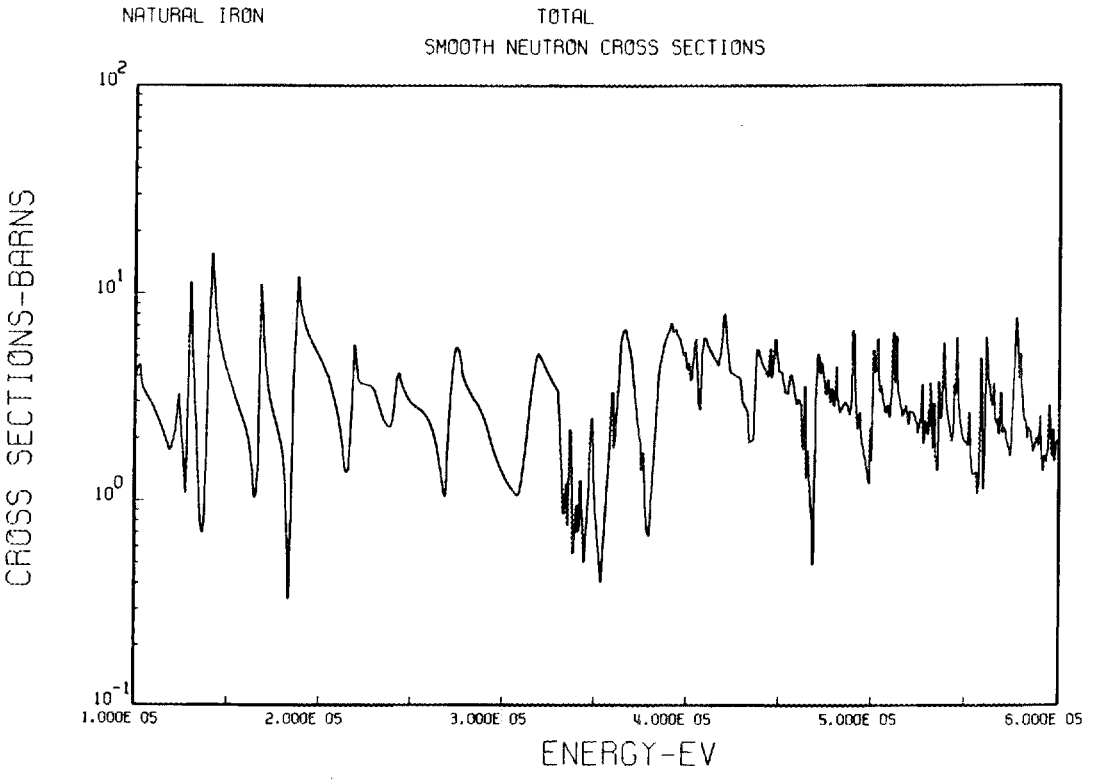

Fig. 9. The Evaluated Total Cross Section From 100 to 600 keV.

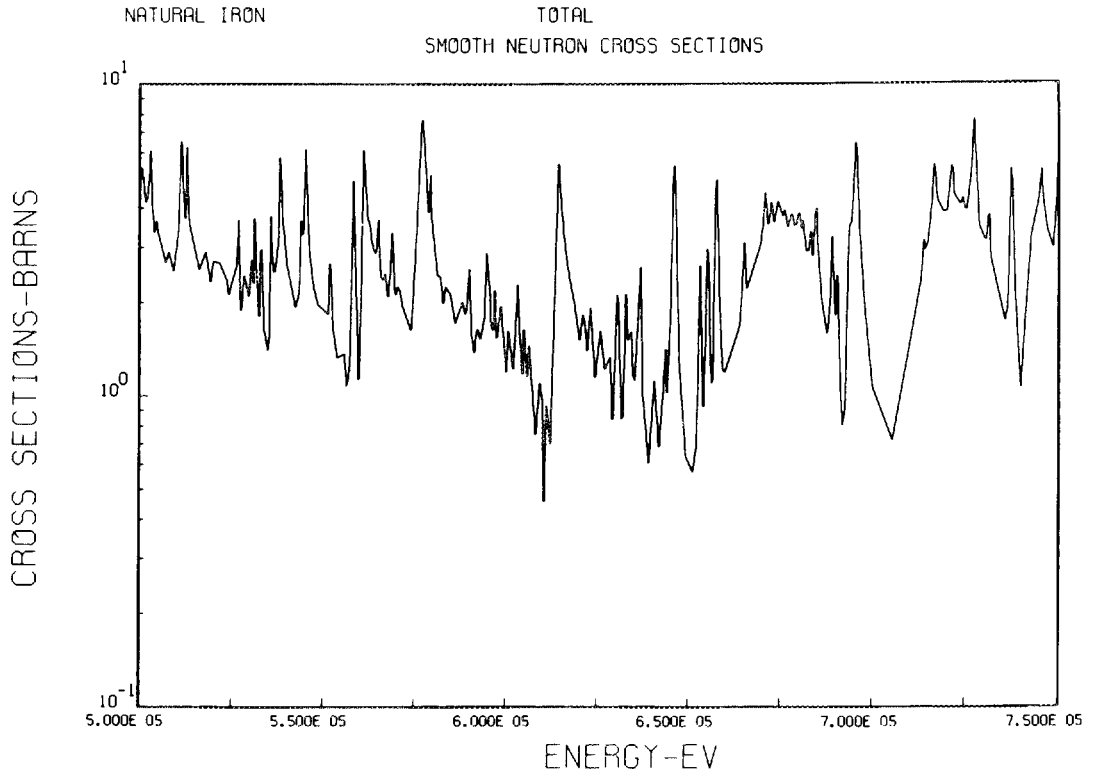

Fig. 10. The Evaluated Total Cross Section From 500 to 750 keV.

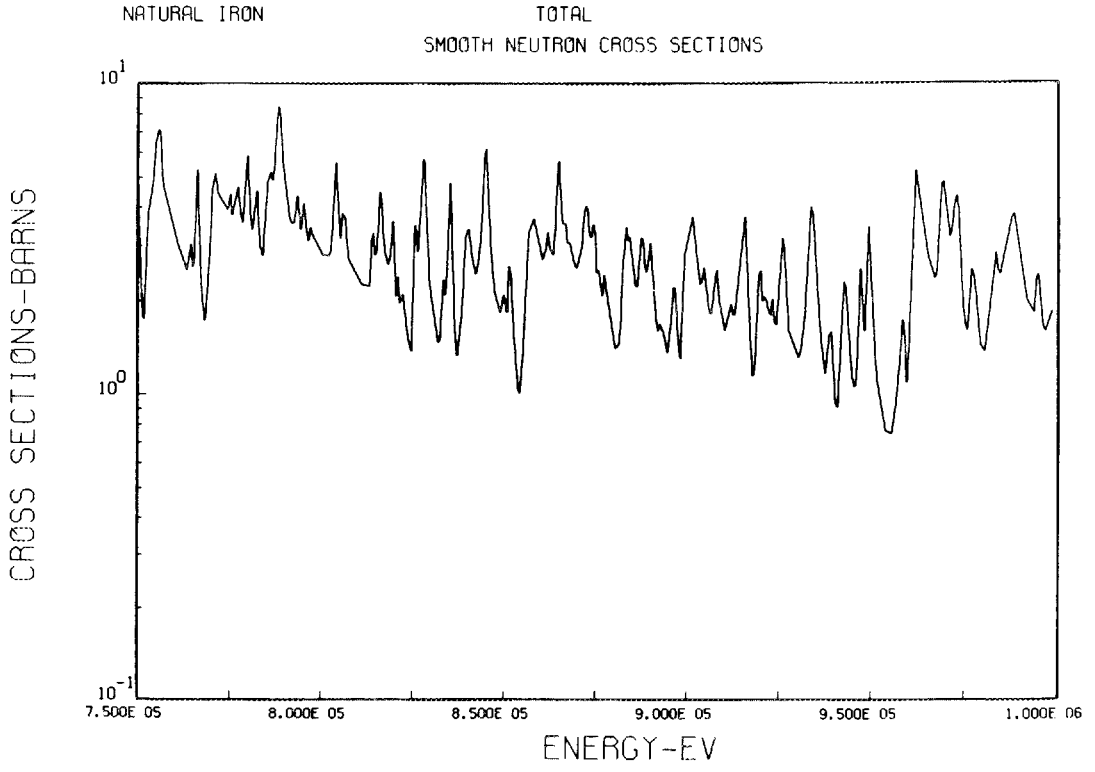

Fig. 11. The Evaluated Total Cross Section From 750 keV to 1 MeV.

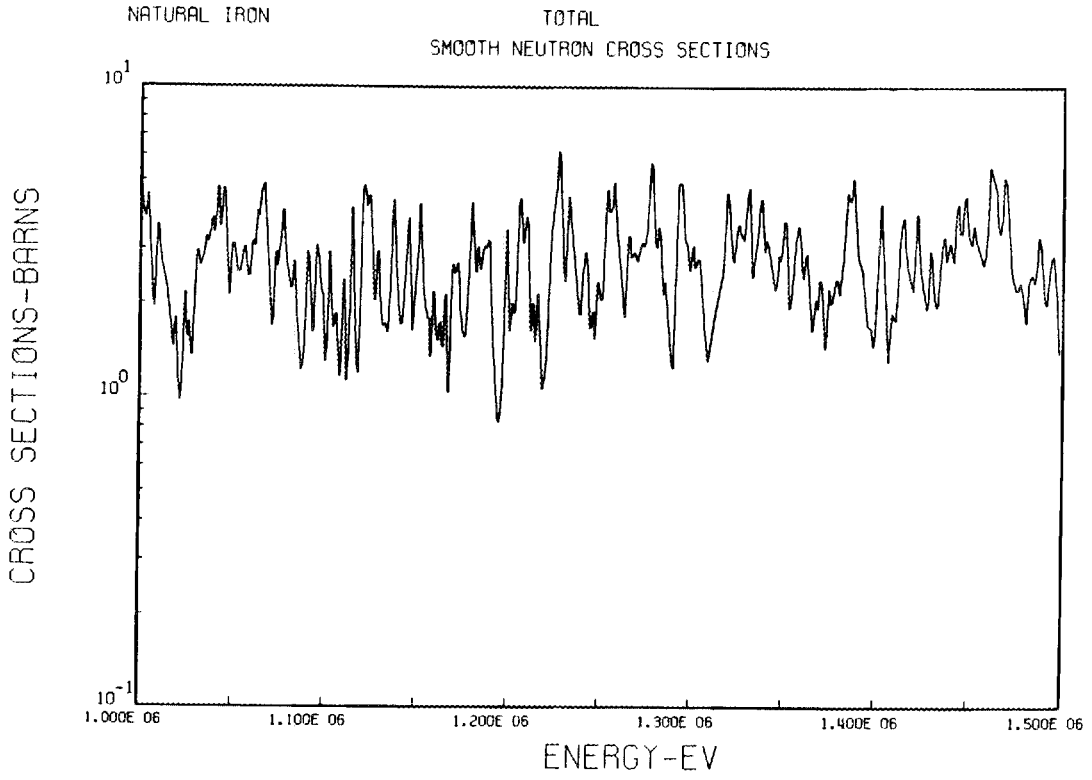

Fig. 12. The Evaluated Total Cross Section From 1 to 1.5 MeV.

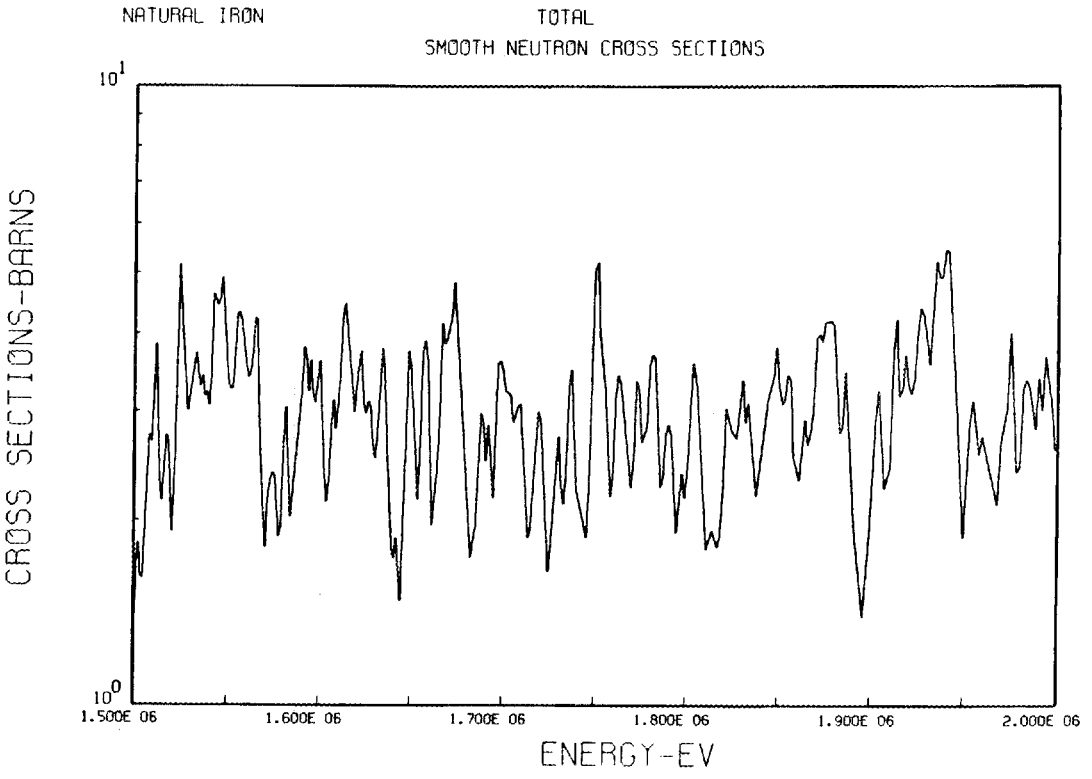

Fig. 13. The Evaluated Total Cross Section From 1.5 to 2 MeV.

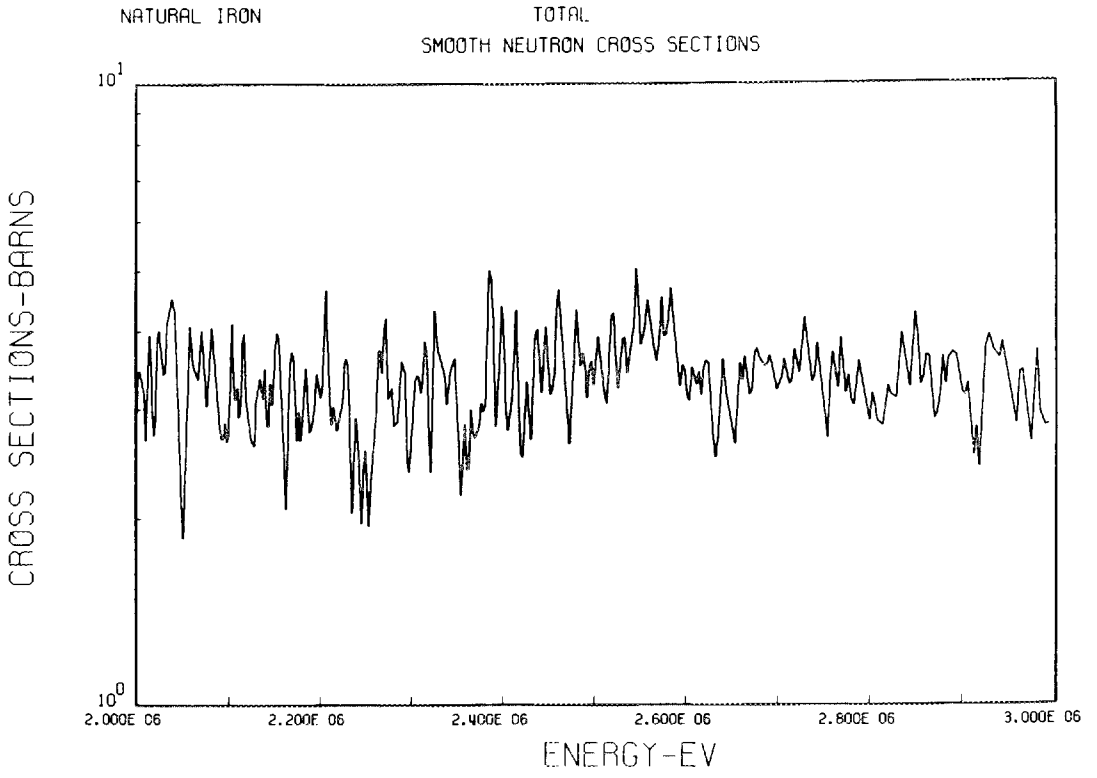

Fig. 14. The Evaluated Total Cross Section From 2 to 3 MeV.

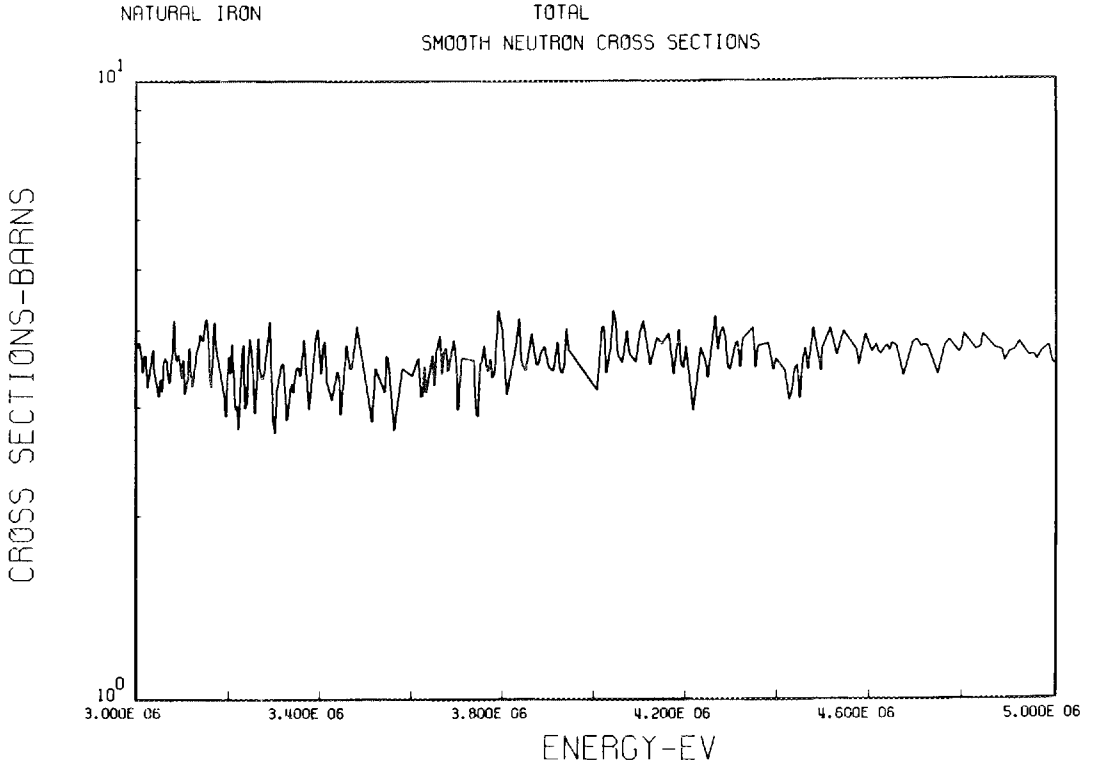

Fig. 15. The Evaluated Total Cross Section From 3 to 5 MeV.

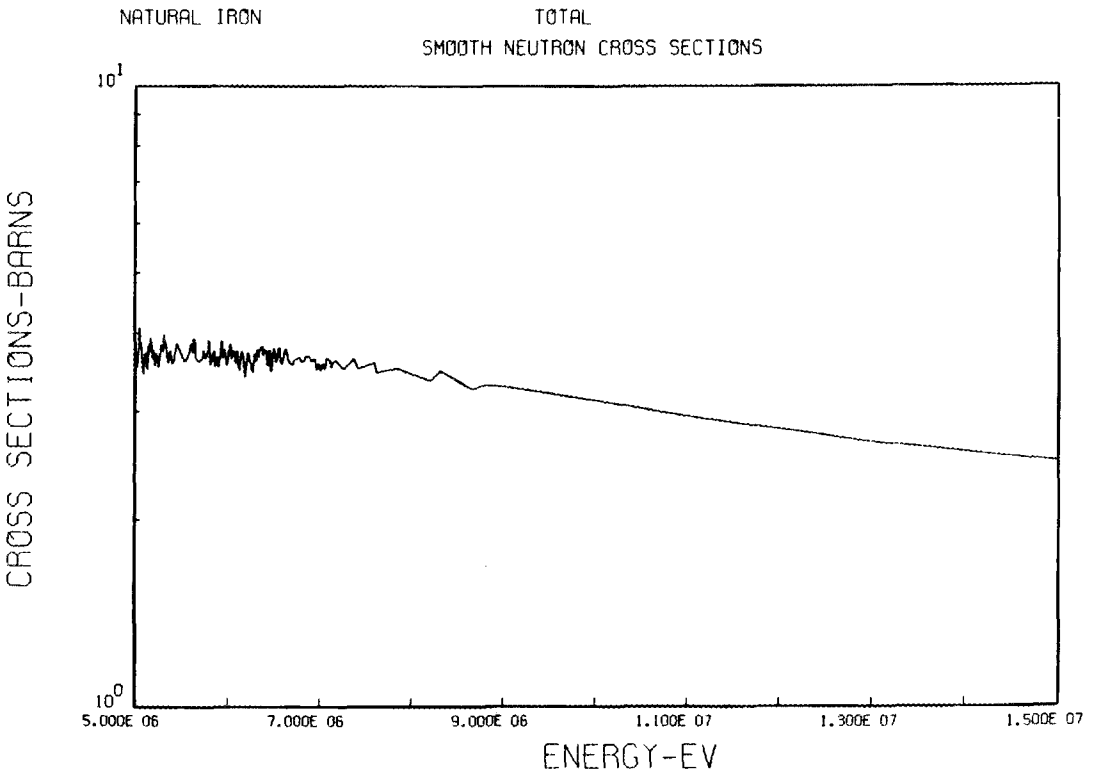

Fig. 16. The Evaluated Total Cross Section From 5 to 15 MeV.

The Elastic Scattering Cross Section

The Integrated Elastic Scattering Cross Section

The elastic scattering cross section was obtained by subtracting the nonelastic from the total cross section. The resulting elastic scattering cross section is shown in Figs. 17–27.

Angular Distributions of Elastically Scattered Neutrons

Cox[33] has measured elastic angular distributions from 0.68 to 1.23 MeV with a resolution of ±10 keV in 9-keV steps. Wells *et al.*[34] have also measured the differential elastic cross section from 0.75 to 0.98 MeV with a resolution of ±3.5 keV, but at only 4–6 angles. Outside this energy interval the data are relatively scarce. Measurements have been made at 0.3[35] and 0.5 MeV[36] with resolutions of ±12.5 and ±25 keV, respectively. Energies and resolutions at which data have been taken between 1.23 and 4 MeV are listed in Table X.

Table X. Energies, Resolutions, and References for Natural Iron Neutron Elastic Differential Cross-Section Measurements Between 1.23 and 4 MeV

E, MeV	Reference
1.37 ± 0.01	37
1.48 ± 0.04	38
1.58 ± 0.04	38
1.66 ± 0.04	38
1.71 ± 0.01	37
2.01 ± 0.01	37
2.20 ± 0.06	39
2.25 ± 0.05	40
2.45 ± 0.05	40
2.50 ± 0.10	41
2.65 ± 0.01	37
3.00 ± 0.025	2
3.20 ± 0.05	42
3.26 ± 0.01	37
3.66 ± 0.20	43
3.67 ± 0.05	15
3.70 ± 0.10	44
4.00 ± 0.025	2

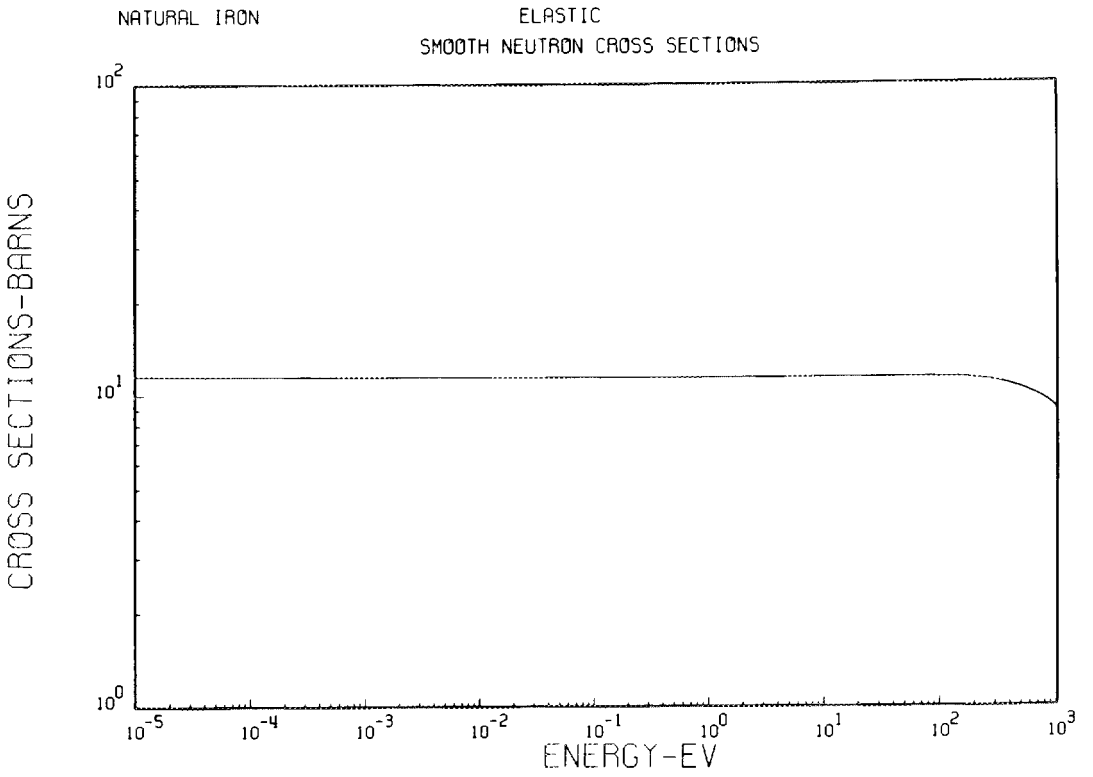

Fig. 17. The Evaluated Elastic Scattering Cross Section From 10^{-5} to 10^3 eV.

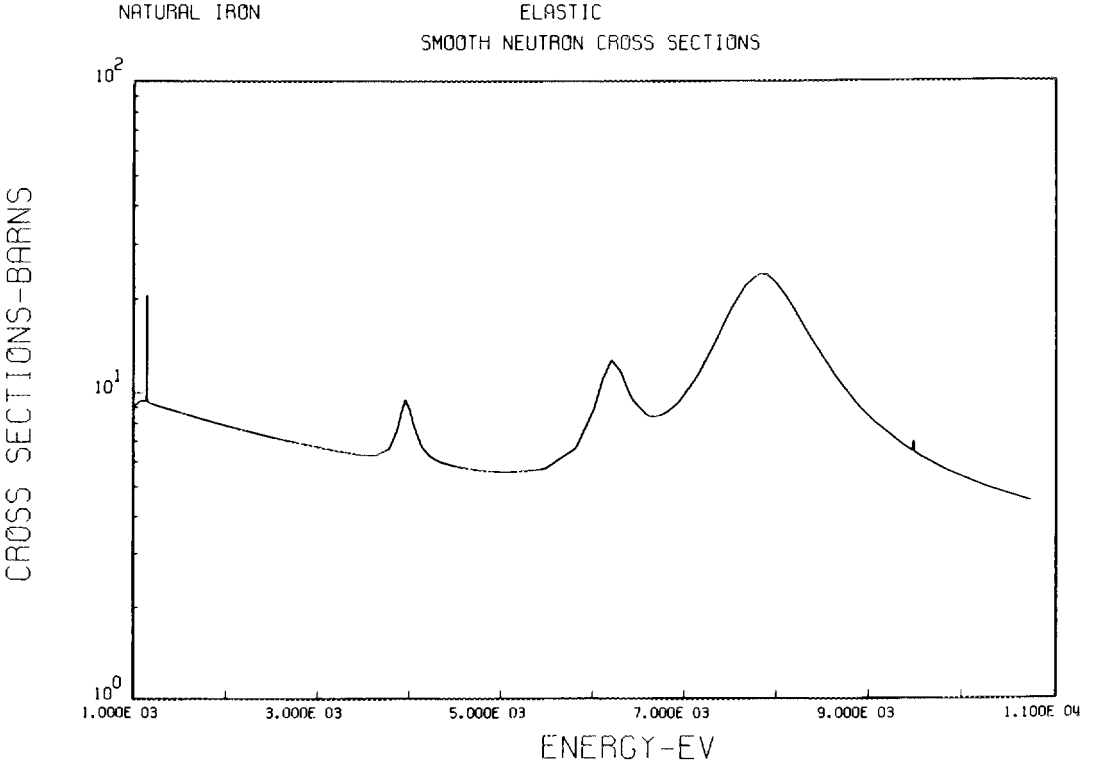

Fig. 18. The Evaluated Elastic Scattering Cross Section From 1 to 11 keV.

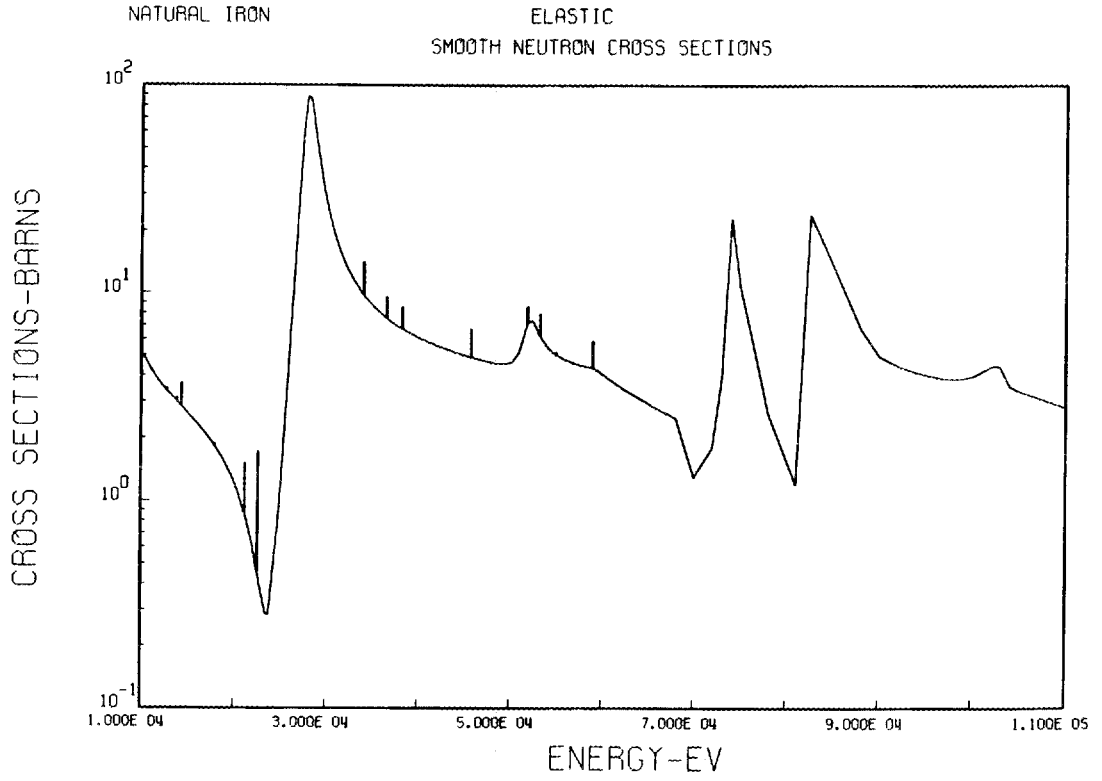

Fig. 19. The Evaluated Elastic Scattering Cross Section From 10 to 110 keV.

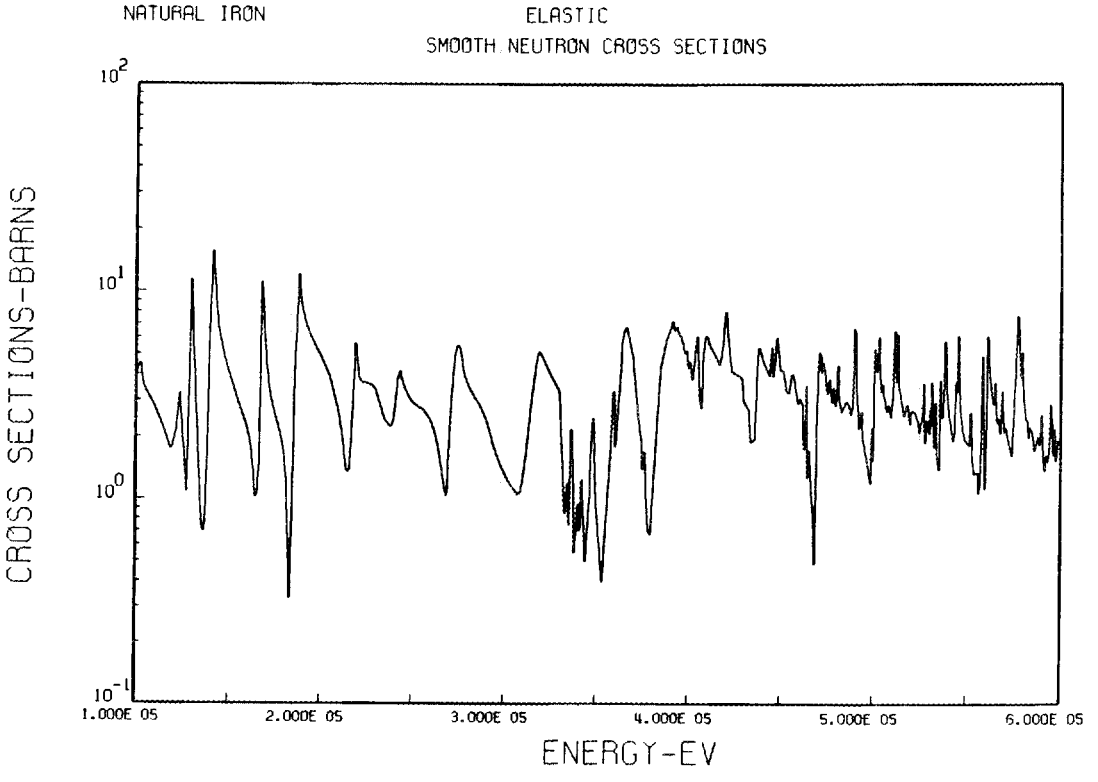

Fig. 20. The Evaluated Elastic Scattering Cross Section From 110 to 600 keV.

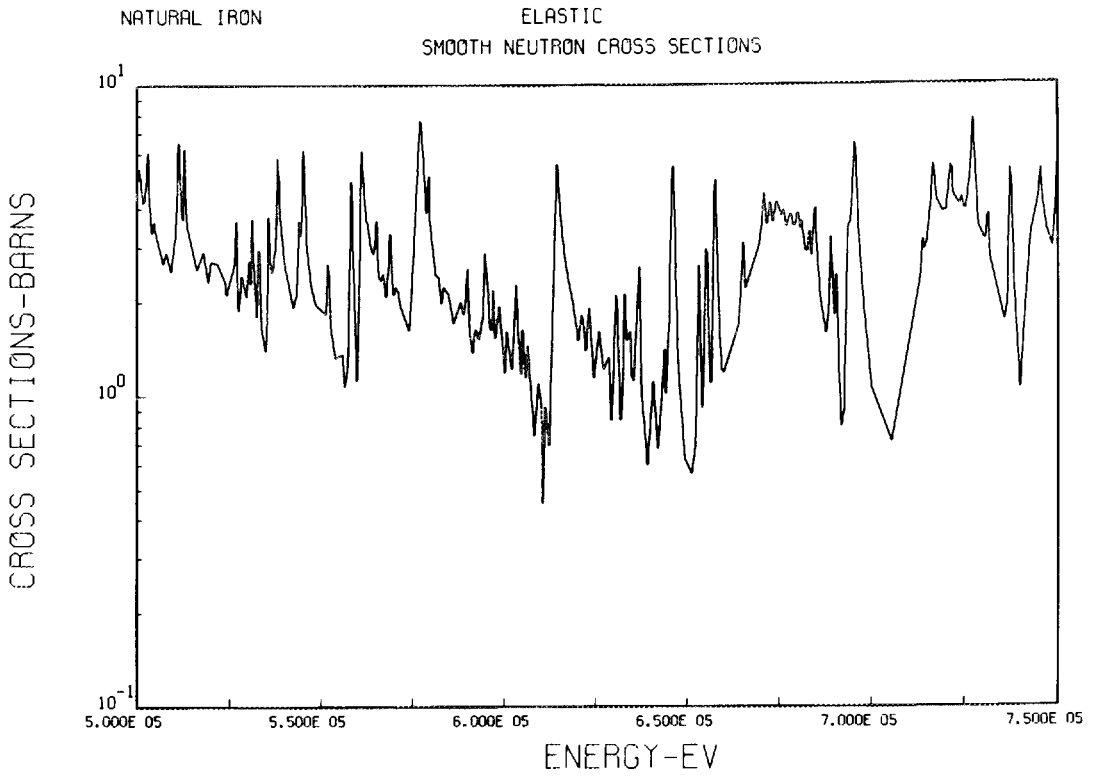

Fig. 21. The Evaluated Elastic Scattering Cross Section From 500 to 750 keV.

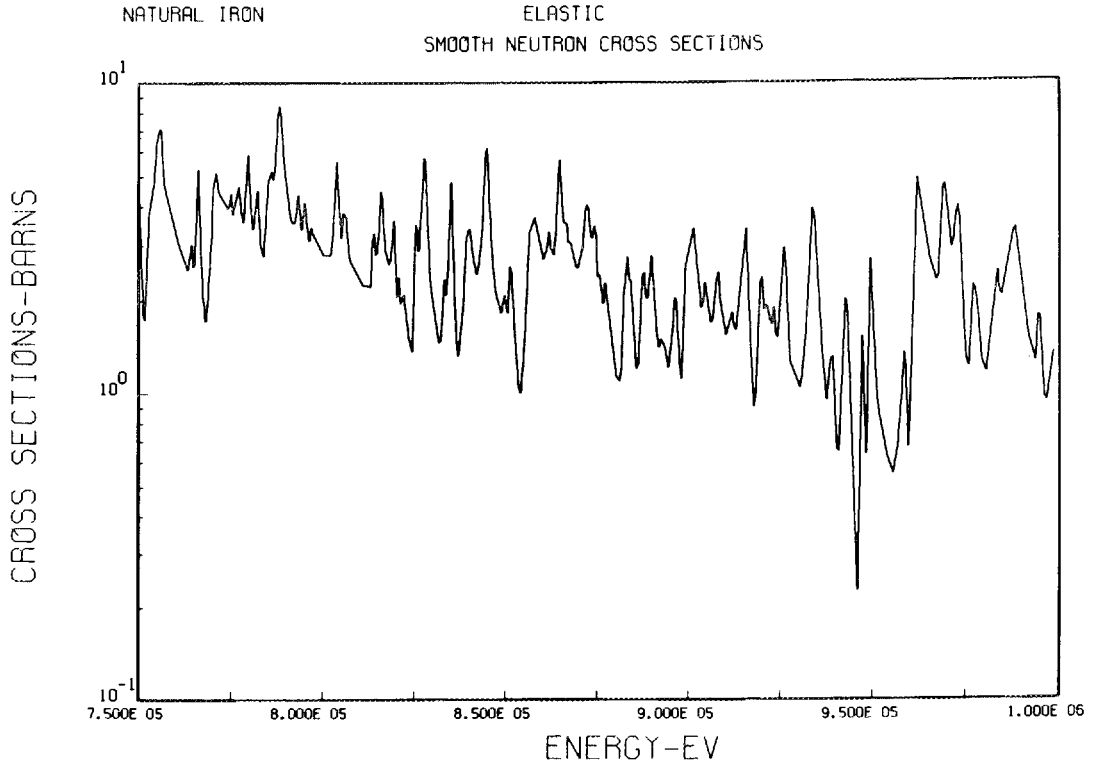

Fig. 22. The Evaluated Elastic Scattering Cross Section From 750 keV to 1 MeV.

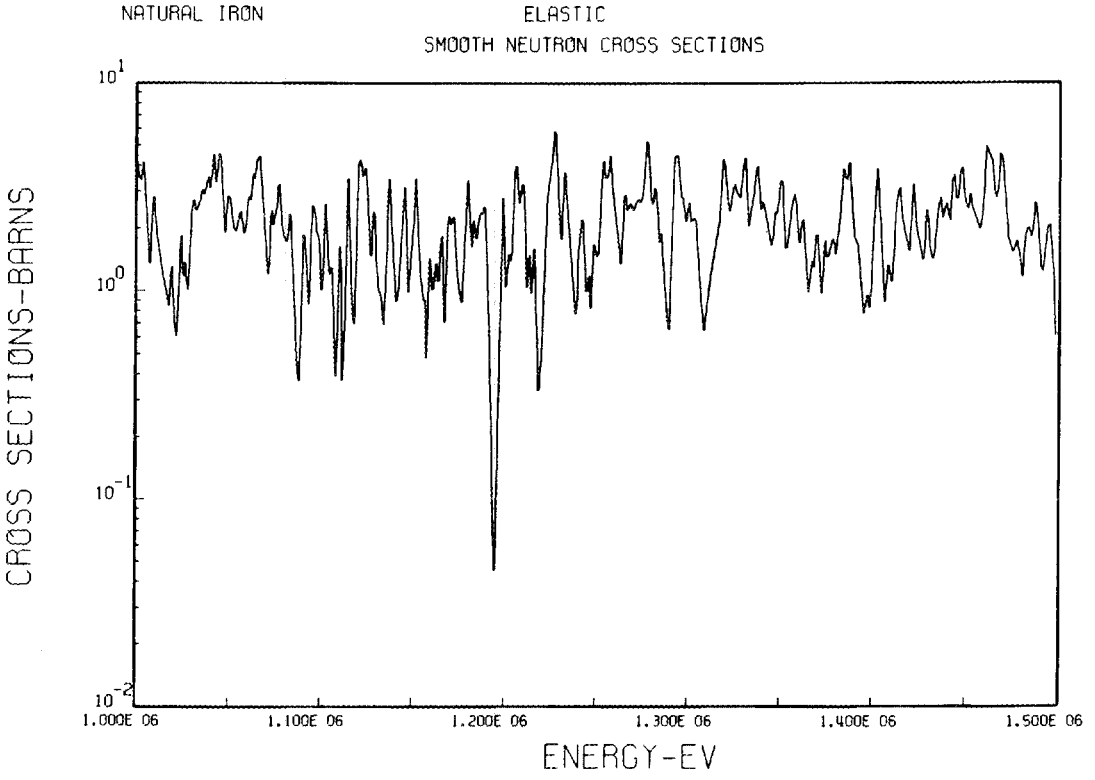

Fig. 23. The Evaluated Elastic Scattering Cross Section From 1 to 1.5 MeV.

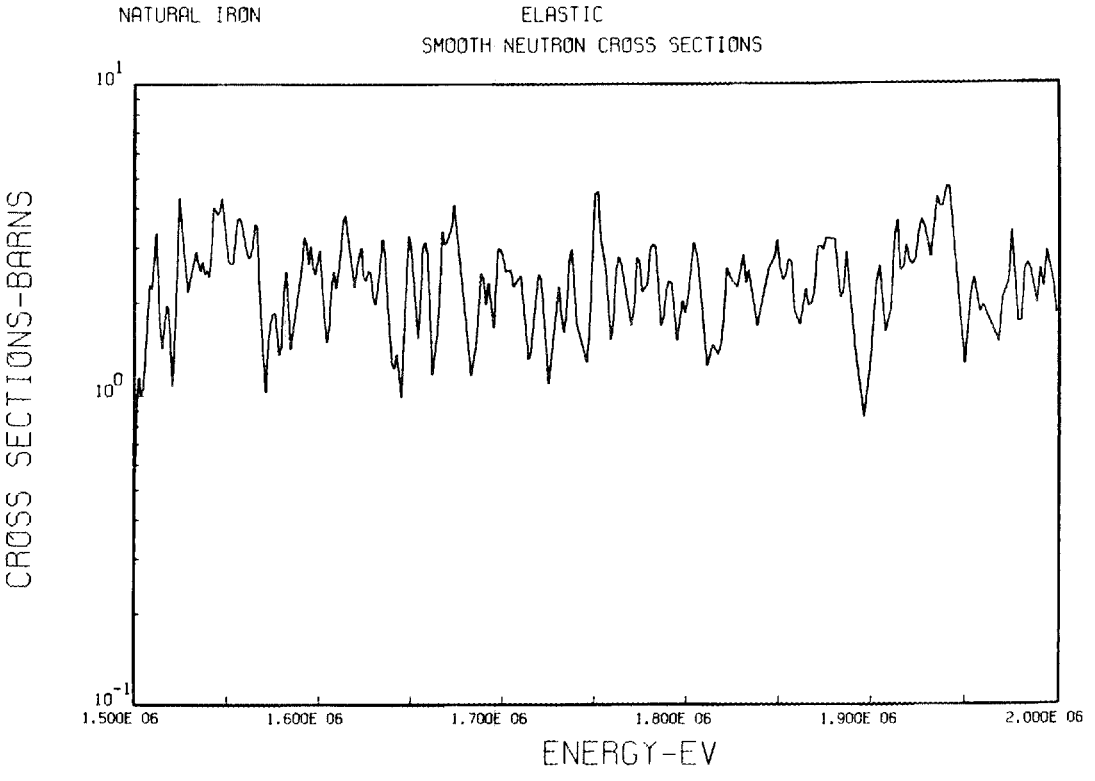

Fig. 24. The Evaluated Elastic Scattering Cross Section From 1.5 to 2 MeV.

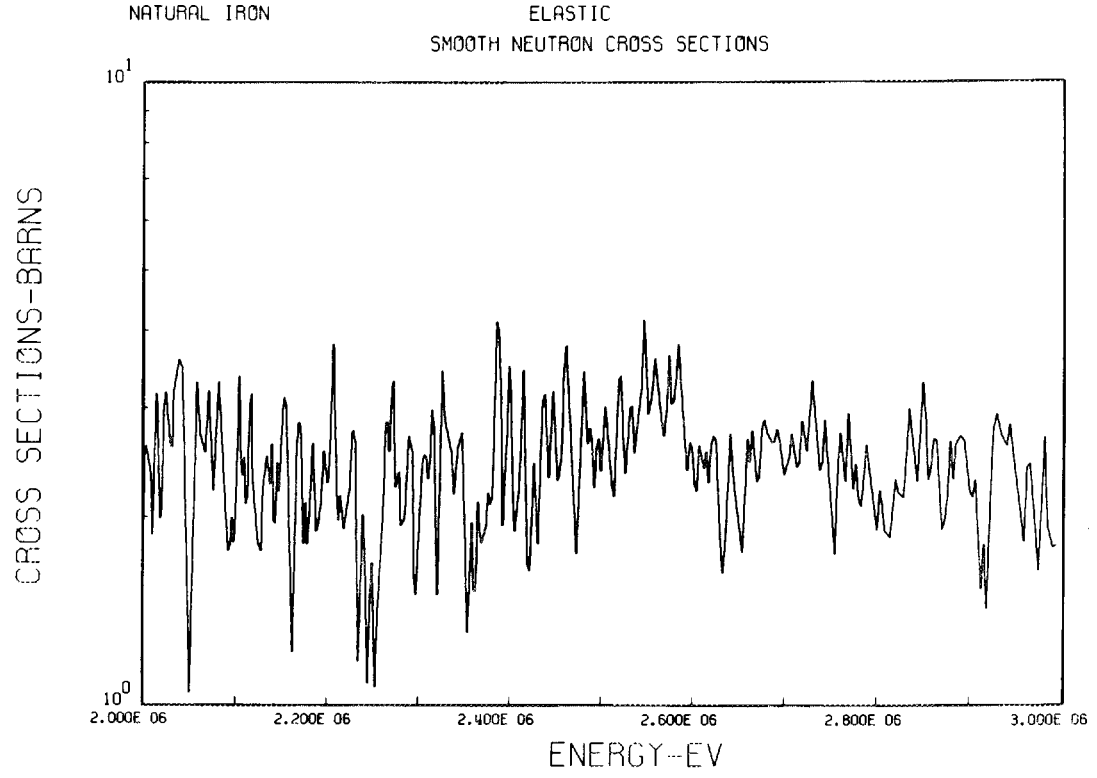

Fig. 25. The Evaluated Elastic Scattering Cross Section From 2 to 3 MeV.

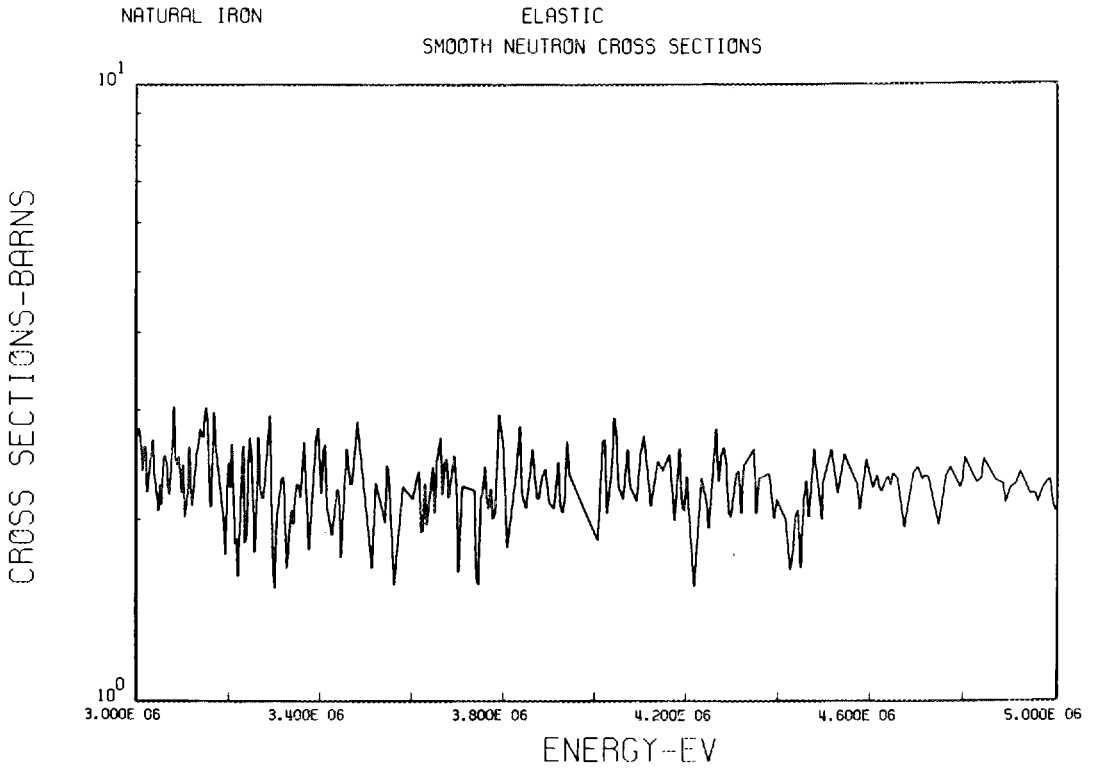

Fig. 26. The Evaluated Elastic Scattering Cross Section From 3 to 5 MeV.

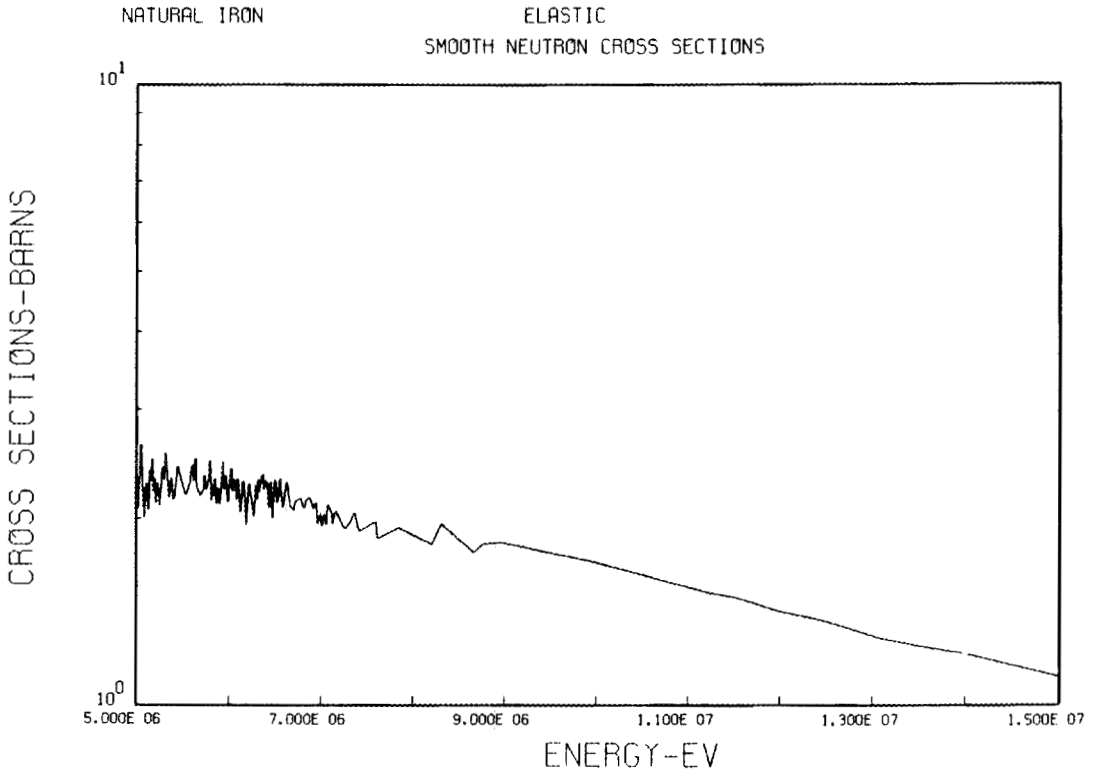

Fig. 27. The Evaluated Elastic Scattering Cross Section From 5 to 15 MeV.

We fitted the differential cross sections between 0.3 and 4 MeV by least squares to a Legendre series, plotting the data with the fits to ensure adequate fitting. P_3 was sufficient below 2 MeV, while P_5 and P_6 had to be used above 2 MeV. Because of the larger energy range and data taken at eight angles rather than at 4–6 angles, we used Cox's data rather than that of Wells, drawing a smooth curve by eye through the data. We also used the results at 0.3 and 0.5 MeV. The coefficients resulting from our Legendre fits to the data and the curves we drew to represent them for a_1, a_2, and a_3 from 0.3 to 1.3 MeV are shown in Fig. 28 where the a's are defined by

$$f(\mu) = \sum_{l=0}^{L} \frac{2l+1}{2} a_l P_l(\mu)$$

where

$f(\mu)$ = the probability of scattering into $d\mu$ about μ,

μ = the cosine of the center-of-mass scattering angle,

$P_l(\mu)$ = the l_{th} Legendre polynomial,

$a_0 = 1$.

Above 1.23 MeV, the Legendre coefficients obtained by optical model and statistical model calculations yielded as reasonable a curve as one could draw to represent the data for coefficients a_3 through a_5. We did adjust the computed a_1 and a_2 to give a better fit to what data are available. There is no doubt that the fluctuations in Cox's data extend both above and below his energy interval but in the absence of data similar to his, a smoothing of the data seems most reasonable. The coefficients from 0.3 to 4 MeV are plotted along with the results of fits to the experimental data in Fig. 29.

Above 4 MeV, the real and imaginary potentials for the optical model were obtained by fits to experimental data; hence, the Legendre coefficients describing the calculated results are tied directly to experiment. The Legendre coefficients from 0.3 to 15 MeV are plotted in Fig. 30.

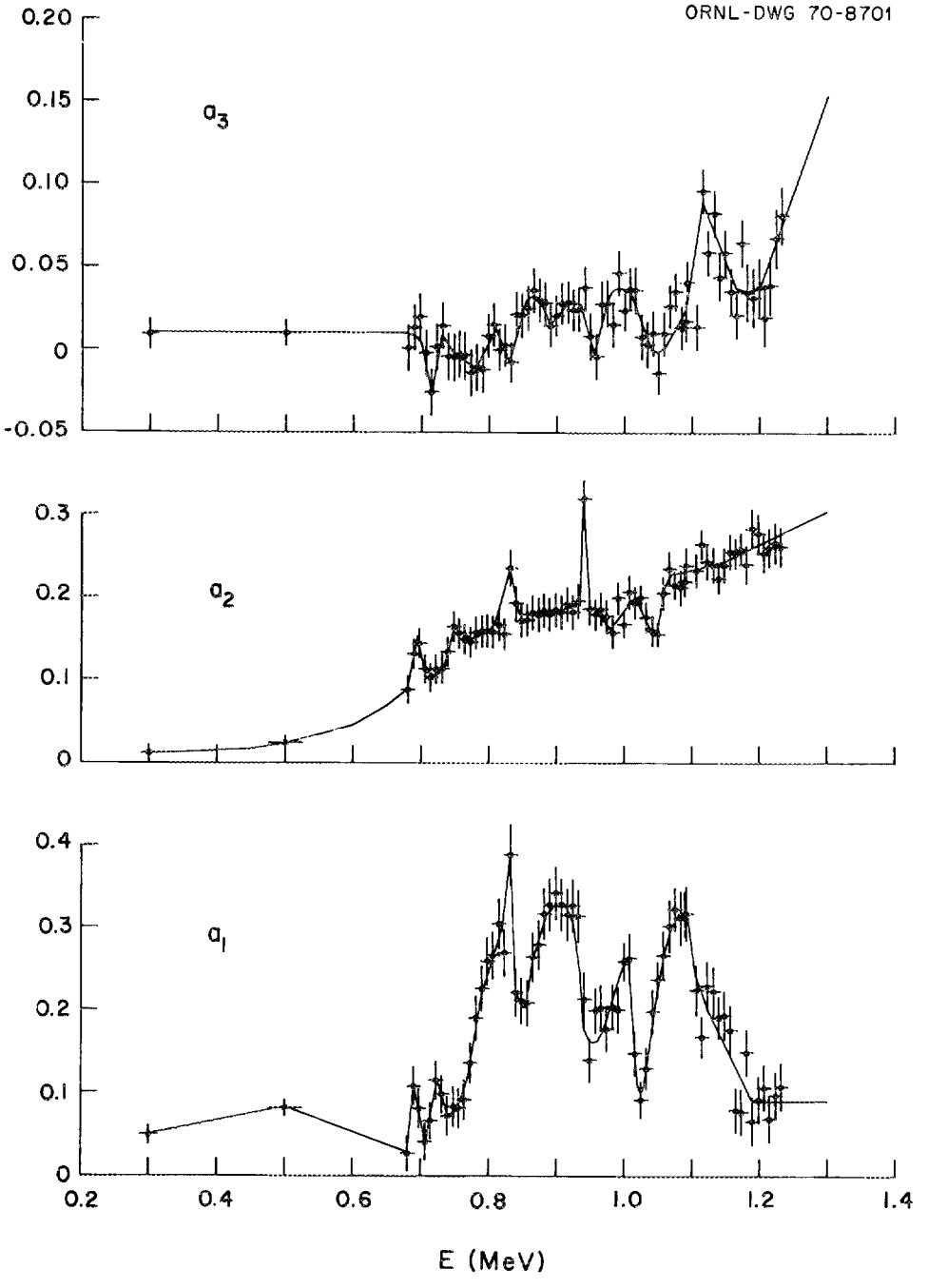

Fig. 28. The Evaluated Values and Experimental Data for the Elastic Legendre Expansion Coefficients a_1, a_2, and a_3 From 0.3 to 1.25 MeV.

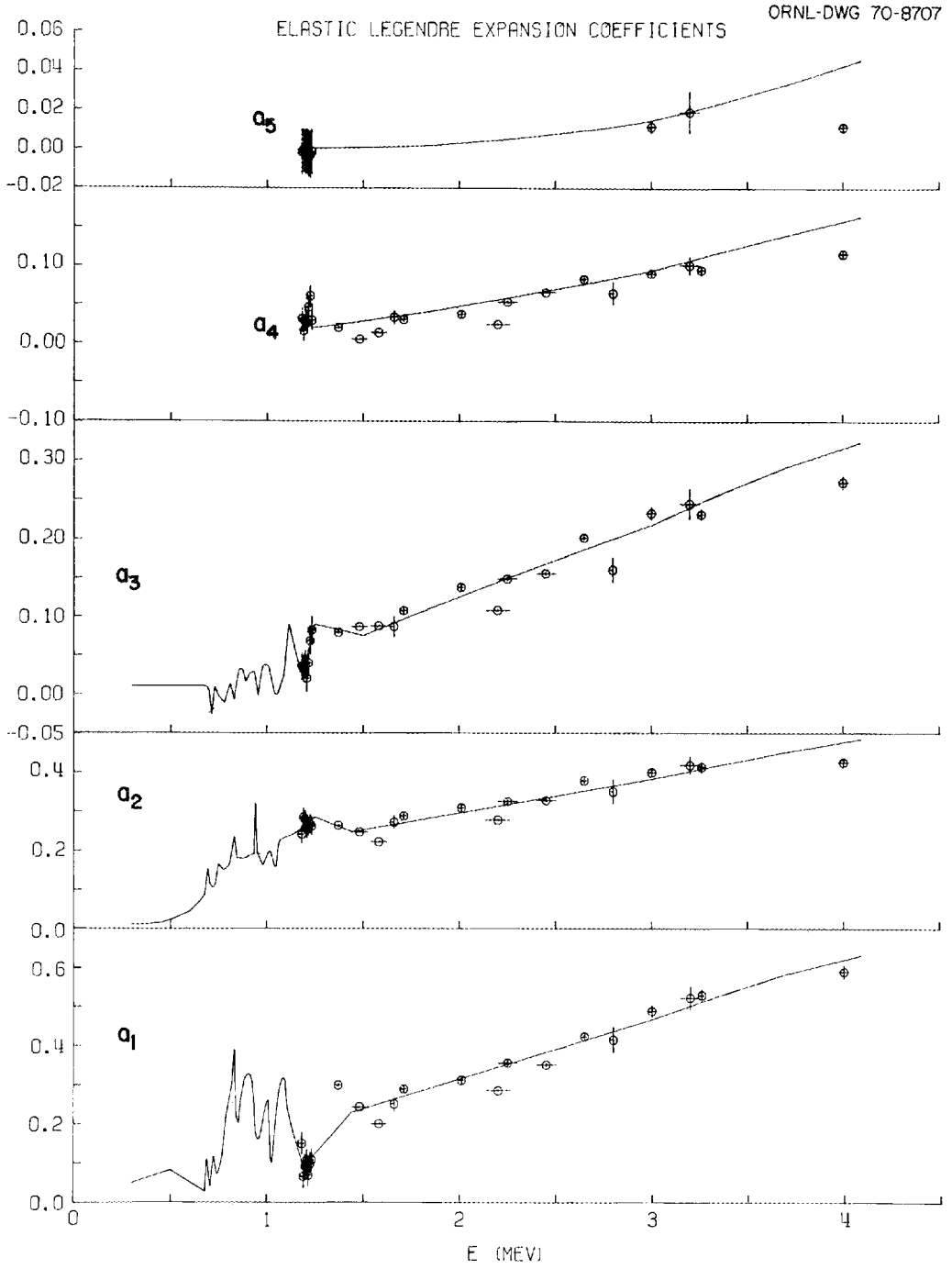

Fig. 29. The Evaluated Values and Experimental Data for the Elastic Legendre Expansion Coefficients a_1 Through a_5 From 0.3 to 4 MeV.

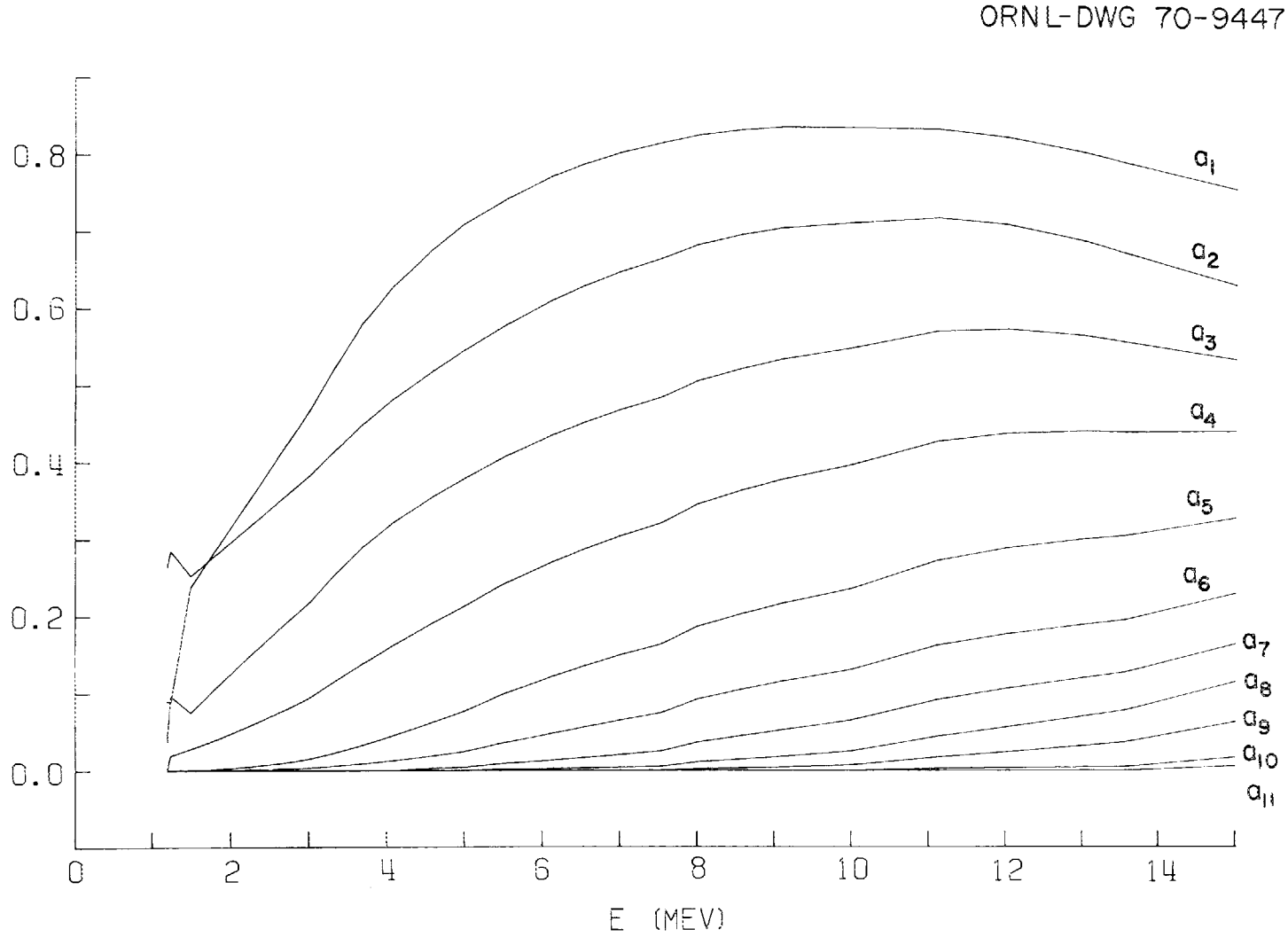

Fig. 30. The Evaluated Elastic Legendre Expansion Coefficients From 1.2 to 15 MeV.

The Cross Sections for Inelastic Scattering to the 0.846-MeV Level in ^{56}Fe

Integrated Cross Section

Macklin *et al.*[3] have recently taken data on the excitation of the 0.846-MeV level in ^{56}Fe from threshold to >2 MeV with the best energy resolution to date, ±~3 keV at 1-MeV neutron energy. These data have yet to be reduced to cross sections. Barnard *et al.*[30] measured the excitation of this level from 0.94 to 1.50 MeV with an energy resolution of ±~7 keV.

We normalized Macklin's data to the results of Barnard *et al.* below 1.5 MeV. From 1.5 to 2.12 MeV we normalized to the ±35-keV resolution measurements of Gilboy and Towle.[18]

Above 2.12 MeV, the evaluated cross sections are a result of calculations as described in Section II.

Angular Distribution

We relied exclusively on calculations to provide the angular distributions for scattering to the 0.846-MeV level in ^{56}Fe over the entire incident neutron energy range. The CN and DI contributions were separately fitted by least squares to Legendre polynomial series, the coefficients weighted by the ratio of the partial (CN or DI)-to-total (CN + DI) inelastic cross sections, and added to arrive at the coefficients for the combined distributions. The coefficients are plotted as a function of energy in Fig. 31 and result in the angular distributions which were shown in Fig. 2.

The Cross Section for Inelastic Scattering to the 1.408-MeV Level in ^{54}Fe

Integrated Cross Section

Even though ^{54}Fe is but 4.82% abundant in natural iron, the 1.408-MeV level is sufficiently excited so that it should be considered. This level is 2^+ and, as with the 0.846-MeV level in ^{56}Fe, may be excited by direct interaction as well as by compound nucleus formation and decay.

The UK-evaluated cross section below 3 MeV was used where there is considerable structure.[4] Since the ^{54}Fe level structure is not too dissimilar to that of ^{56}Fe, we normalized the cross section for the 0.846-MeV level in ^{56}Fe to the U.K. results below 3 MeV and used the normalized results from 3 to 15 MeV for the ^{54}Fe 1.408-MeV level. The cross section for this level is shown in Fig. 32.

Angular Distribution

While the angular distribution of neutrons inelastically scattered to the 1.408-MeV level in ^{54}Fe very likely resembles that of neutrons scattered to the 0.846-MeV level in ^{56}Fe, we have taken the distribution to be isotropic at all energies.

Cross Sections for Inelastic Scattering to Levels in ^{56}Fe With $E_x > 0.846$ MeV

Integrated Cross Sections

There are eighteen levels in ^{56}Fe with $0.846 < E_x \leq 4.116$ MeV which were resolvable in the ORNL data[1] either as individual levels or as groups of levels. As discussed previously, calculational results are in excellent agreement with experiment. Calculated values for each of the 18 levels were therefore used in the evaluation and are shown in Figs. 32–35.

Angular Distributions

The angular distributions calculated by a statistical model, as described previously, were used for neutrons inelastically scattered to each of the 18 levels in ^{56}Fe with $0.846 < E_x \leq 4.116$ MeV. While P_{12} was necessary to describe some of the distributions, the coefficients of odd polynomials are zero because of the symmetry about 90°. Typical behavior of the coefficients as a function of energy is shown in Fig. 36 for scattering to levels of spins 0, 1, 2, and 3.

The Cross Section for Inelastic Scattering to the Continuum

It has been observed[1] that below an excitation energy of ~7 MeV inelastic scattering into the "continuum" shows structure and is not well described by an evaporation model. As suggested by evaporation theory, however, if the cross section for scattering into the continuum is divided by the outgoing neutron energy E' then the plot of the quantity σ/E' versus excitation energy, E_x, is similar in shape at various incident neutron energies. Above an excitation energy of 7 MeV an evaporation model was found to apply.

That portion of the continuum which shows structure extends from E_x = 4.1875 MeV where groups of discrete levels cease being resolvable in the experimental data to E_x = 7.0125 MeV where an evaporation model starts to represent the data. The continuum data were

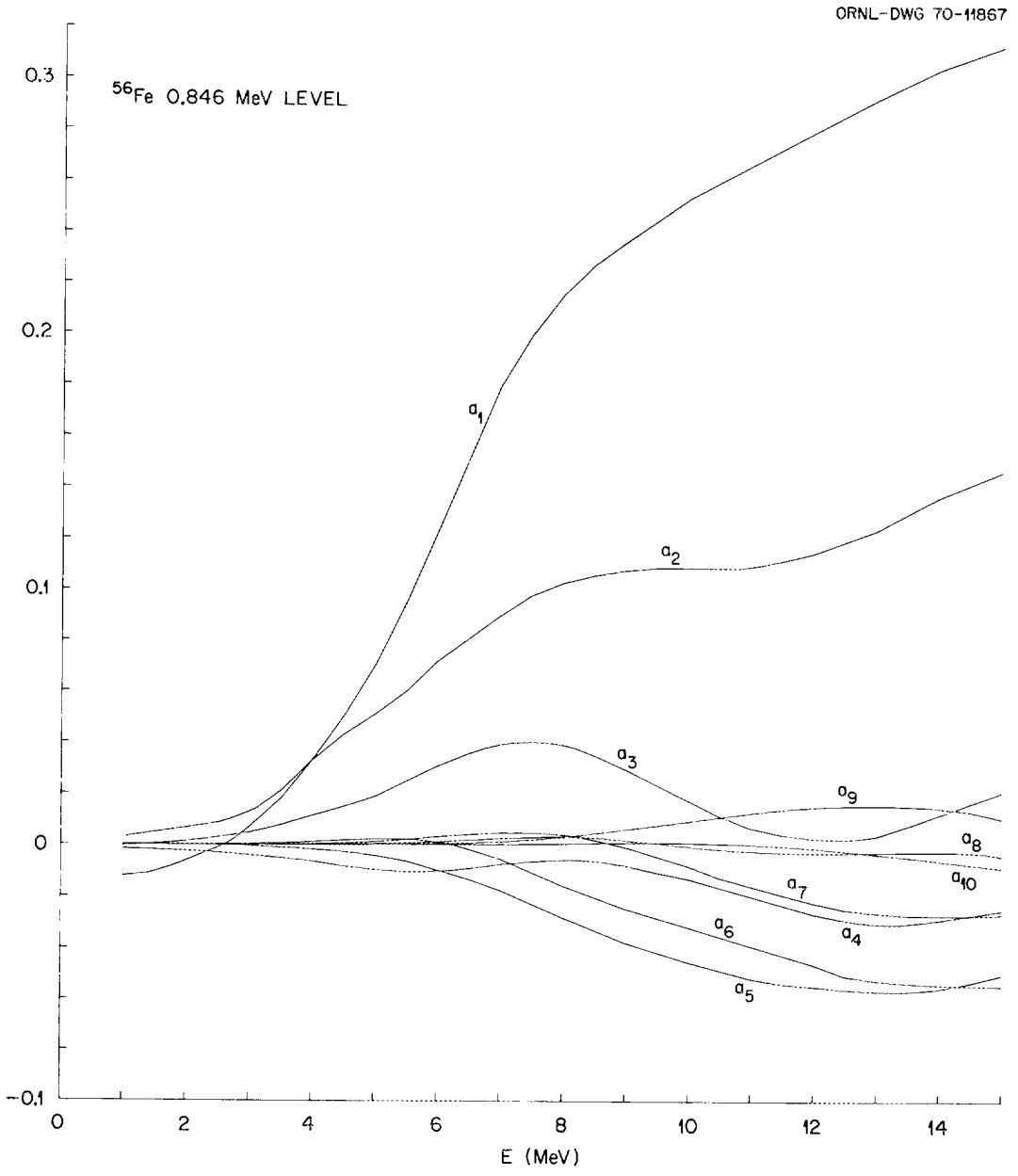

Fig. 31. The Evaluated Legendre Expansion Coefficients for Inelastic Scattering to the 0.846-MeV Level in ^{56}Fe.

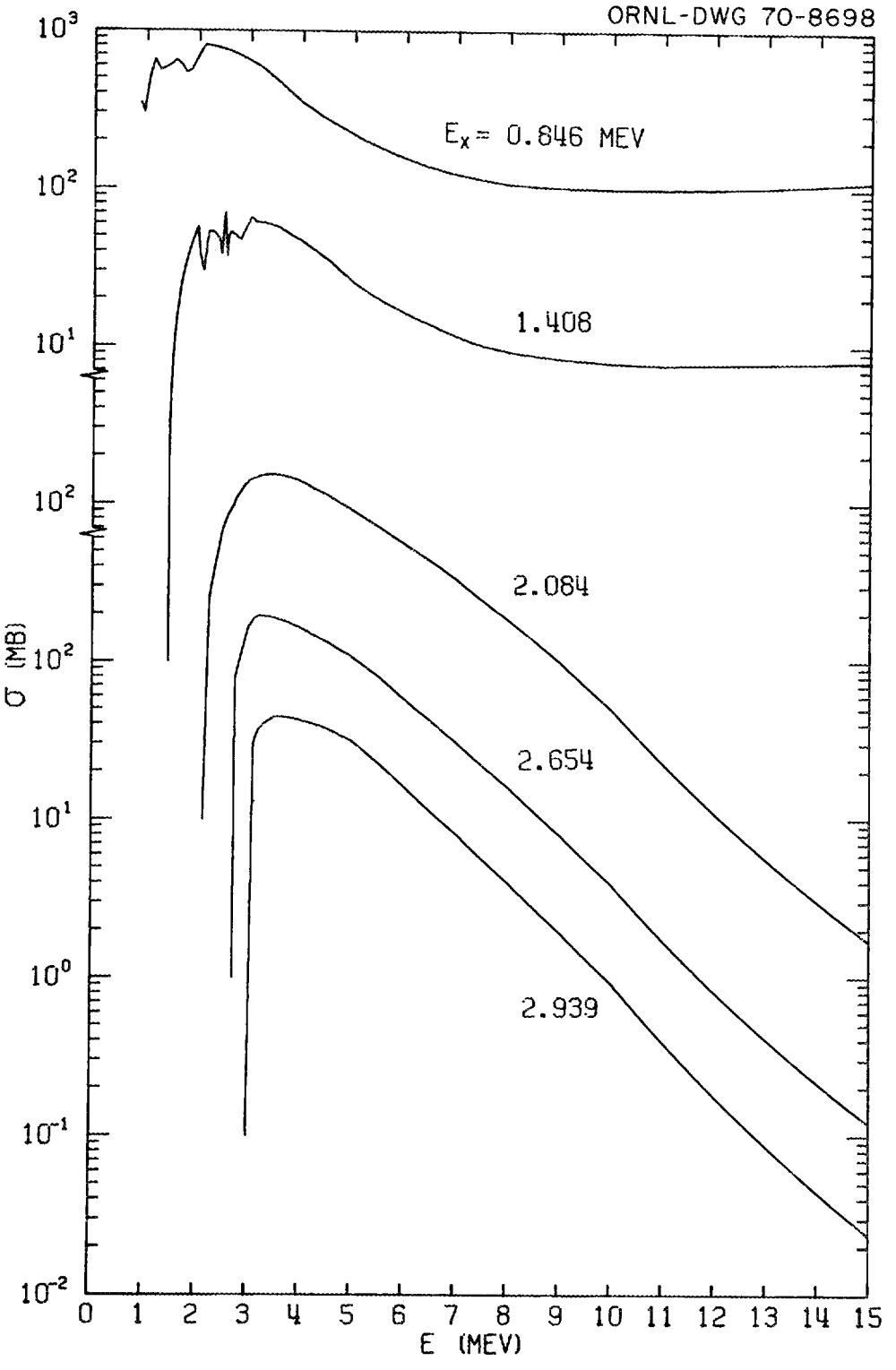

Fig. 32. The Evaluated Inelastic Scattering Level Excitation Cross Section for Excitation Energies E_x = 0.846 MeV to 2.939 MeV.

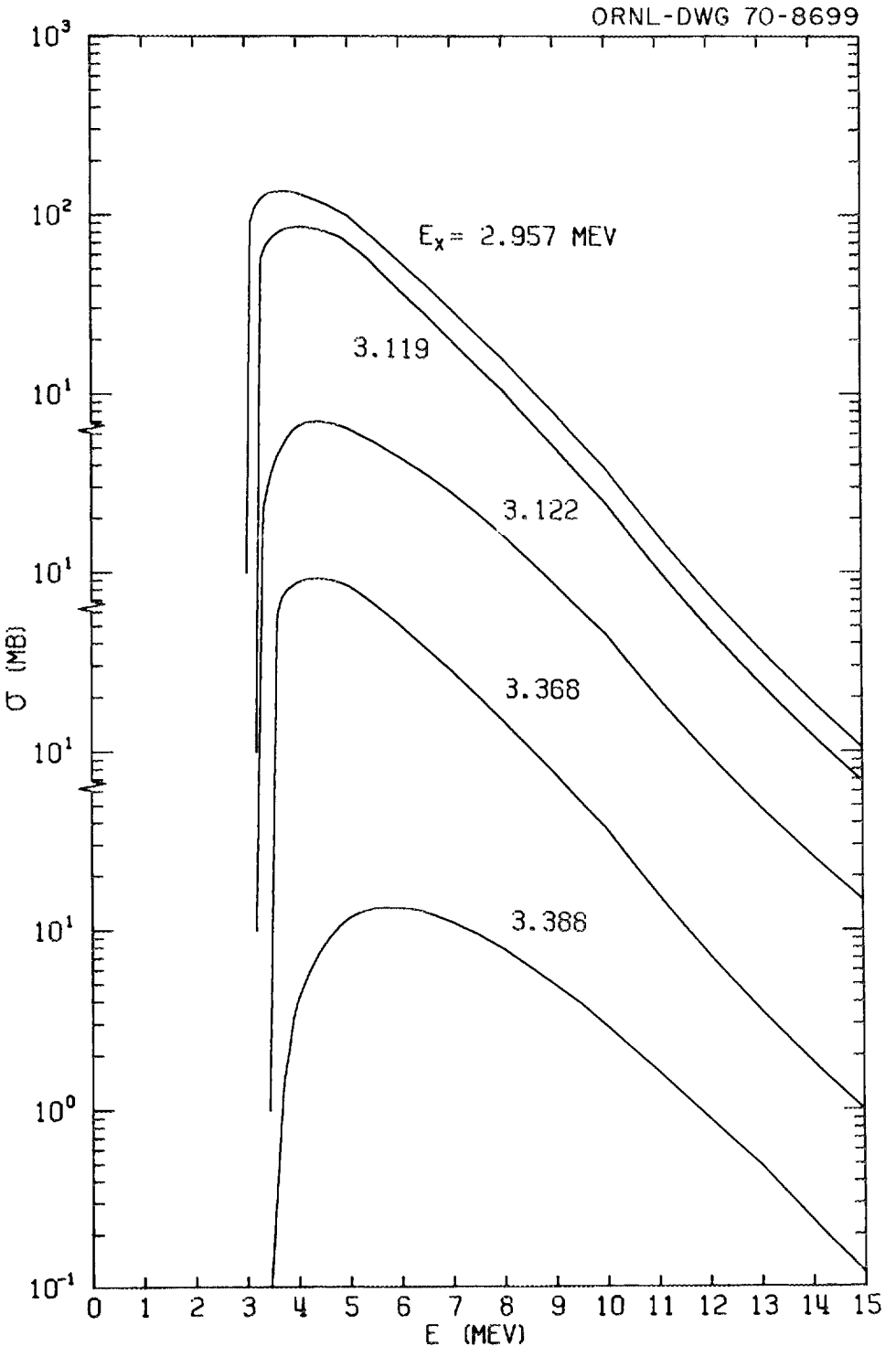

Fig. 33. The Evaluated Inelastic Scattering Level Excitation Cross Section for Excitation Energies E_x = 2.957 to 3.388 MeV.

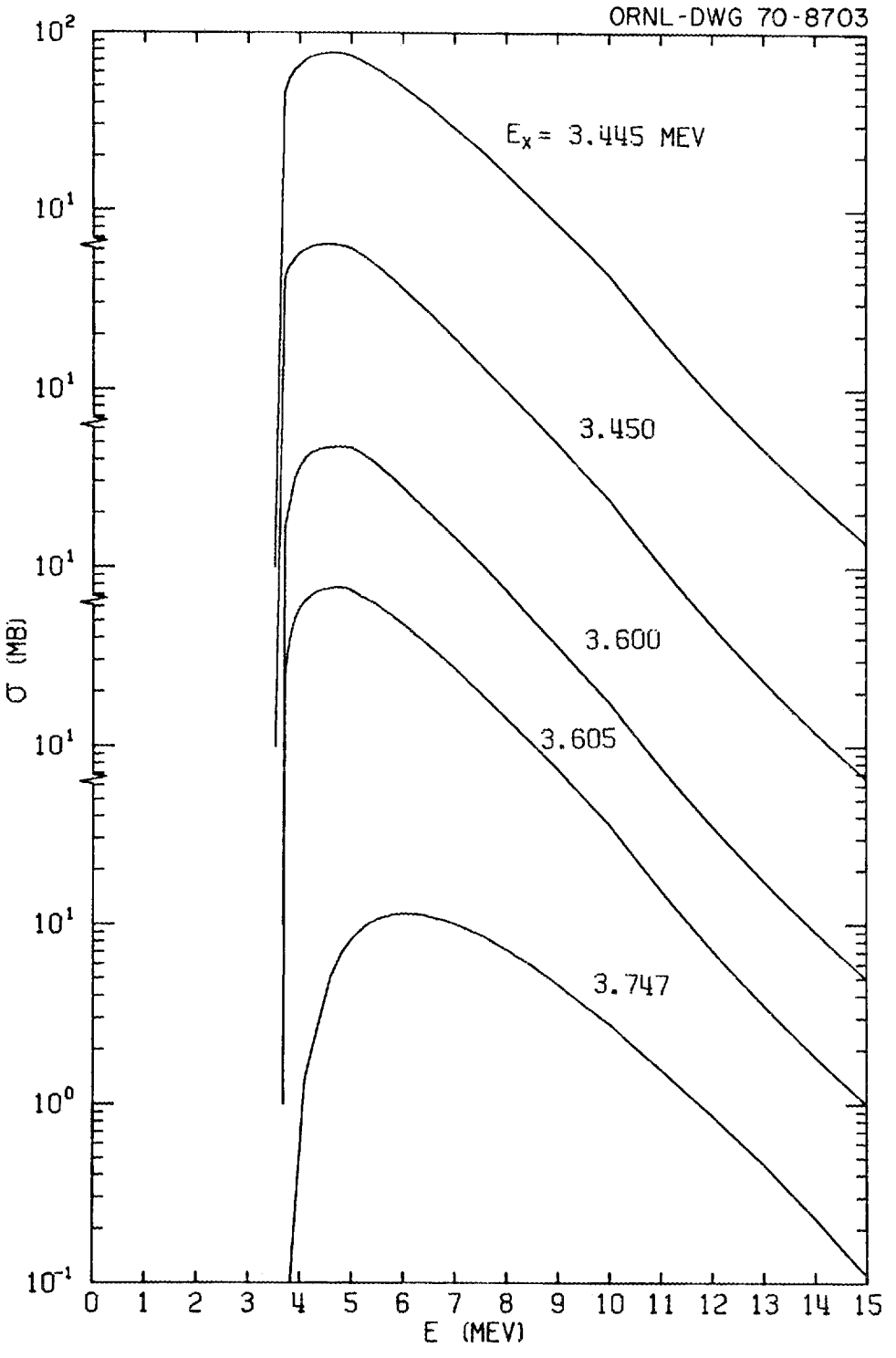

Fig. 34. The Evaluated Inelastic Scattering Level Excitation Cross Section for Excitation Energies E_x = 3.445 to 3.747 MeV.

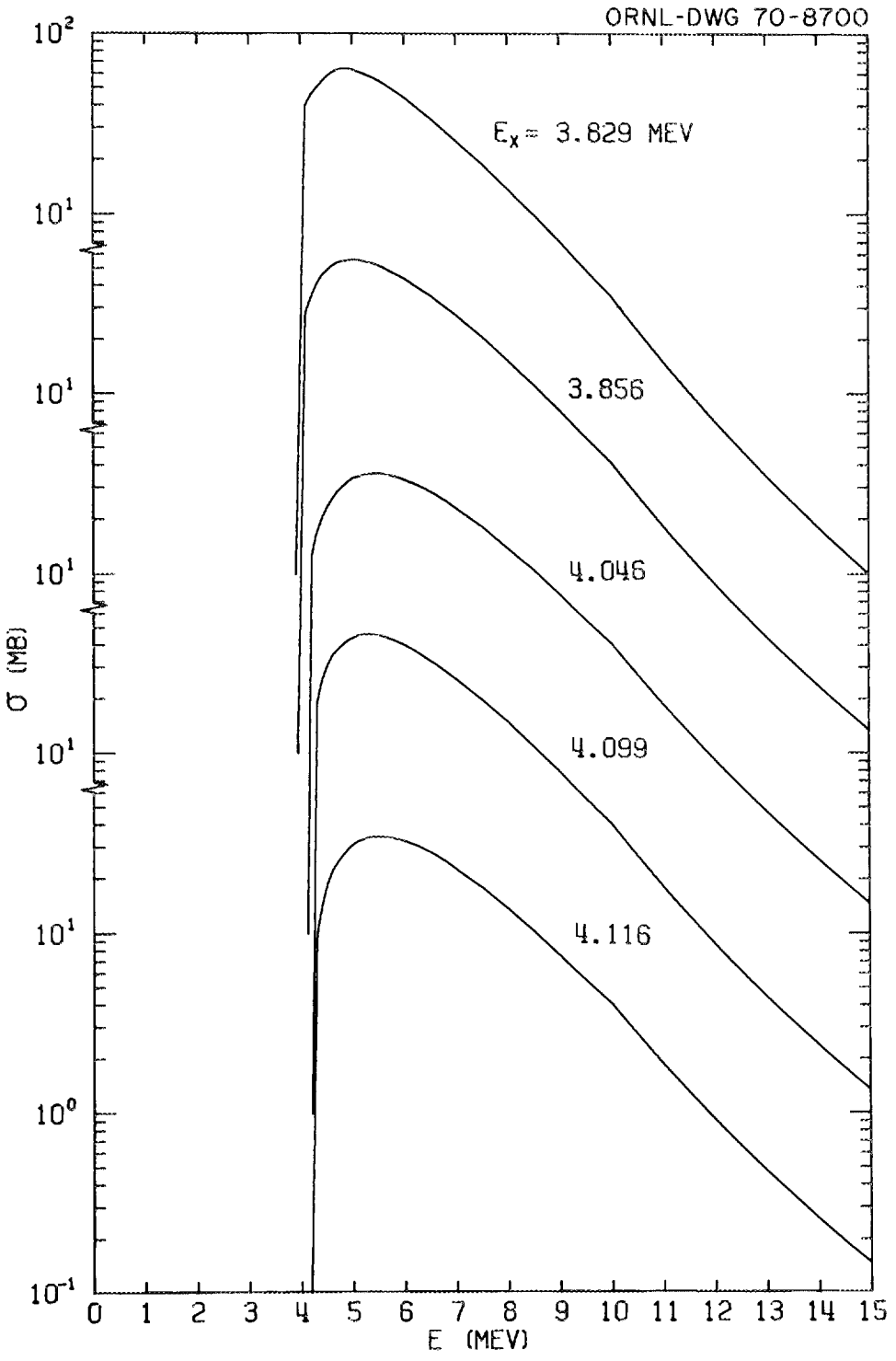

Fig. 35. The Evaluated Inelastic Scattering Level Excitation Cross Section for Excitation Energies E_x = 3.829 to 4.116 MeV.

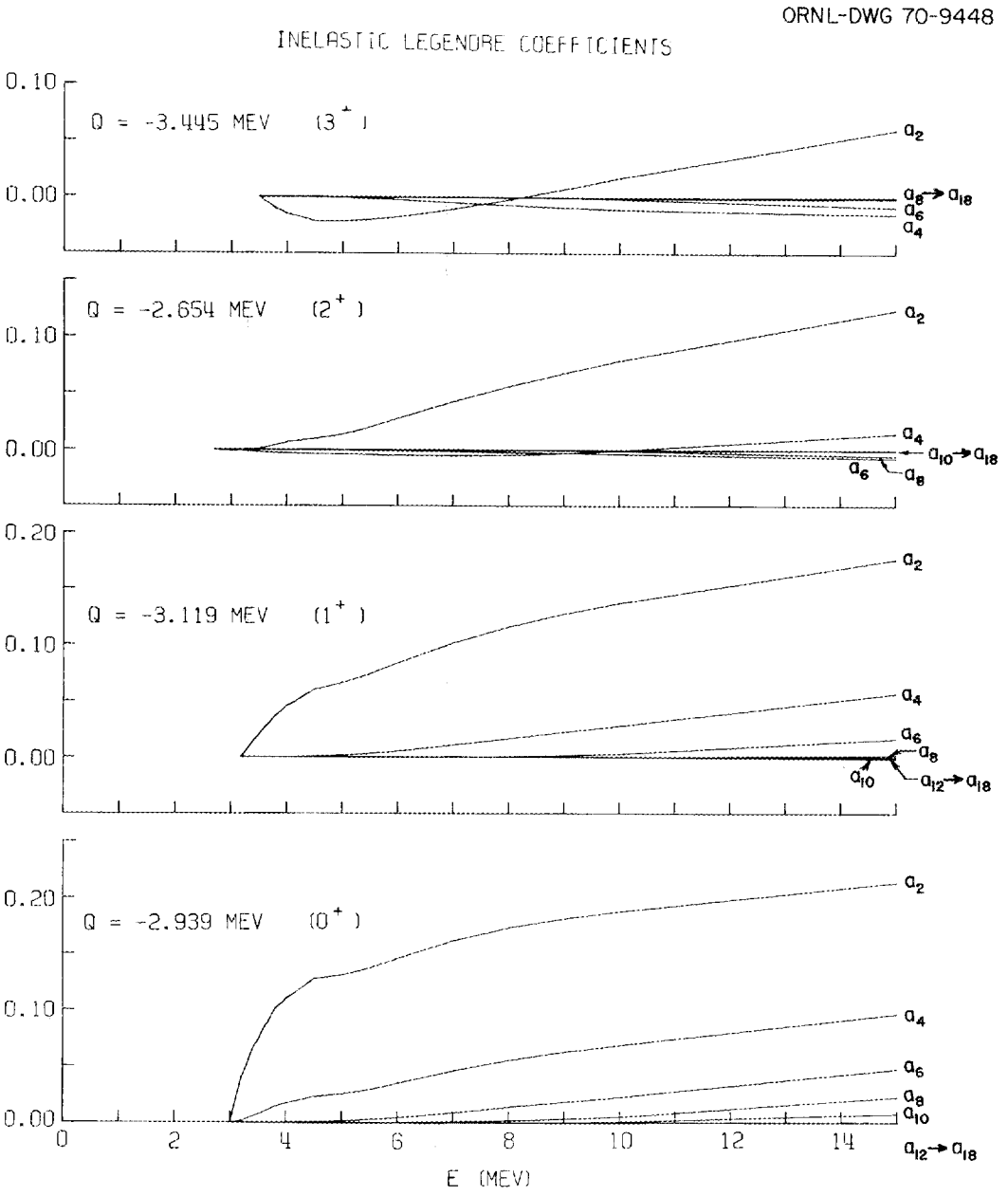

Fig. 36. Typical Legendre Expansion Coefficients for Inelastic Scattering to States of Spins 0, 1, 2, and 3.

reduced to cross sections summed over 25-keV intervals in excitation energy, $\sigma(E\to E_x)\Delta E_x$. By comparing $\sigma(E\to E_x)\Delta E_x/E'$ versus E_x from data taken at E = 6.44, 7.54, and 8.56 MeV, it was found that the cross sections at energy E could be related to those at 8.56 MeV by

$$\sigma(E\to E_x)\Delta E_x/E' = [\sigma(8.56\to E_x)\Delta E_x/E'] \times \exp[0.681(8.56-E)] \ . \quad (1)$$

Above E_x = 7.0125 MeV the cross section could reasonably well be represented by

$$\frac{\sigma(E\to E_x)}{E'} = 36 \exp[0.936(E_x - 7.0125)] \text{mb/(sr - MeV}^2). \quad (2)$$

Now the average laboratory energy of a neutron inelastically scattered to E_x in the continuum assuming isotropic scattering is

$$E' = \frac{1+A^2}{(1+A)^2} E - \frac{A}{1+A} E_x \ . \quad (3)$$

A = mass number.

Converting Eq. (2) to a Maxwellian by substituting for E_x from Eq. (3) yields

$$\sigma(E\to E') = 4\pi \times 36 \exp[0.681(8.56-E)] \times \exp\left[0.936\left(\frac{(1+A)\alpha E}{A} - 7.0125\right)\right] \times E' \exp\left[-0.936 \frac{(1+A)}{A} E'\right] \text{(mb/MeV)} \quad (4)$$

$$\text{where } \alpha = \frac{1+A^2}{(1+A)^2} \ .$$

Even though it is physically impossible for the average E′ to reach 0 since this requires backward scattering in the center of mass, its minimum value differs little from 0 so we shall allow it to be so. Equation (4) can now be used to arrive at the Maxwellian probability for scattering from E to dE′ about E′:

$$p(E\to E') = \frac{E' e^{-E'/\theta}}{I} \quad (5)$$

where

$$I = \theta^2 \left[1 - e^{-(\alpha E - U)/\theta}\left(1 + \frac{\alpha E - U}{\theta}\right)\right]$$

θ = 1.0496 MeV

U = 6.8895 MeV.

Note that ENDF procedures do not consider a constant α multiplying the incident energy E. It must be included for proper normalization.

Integrated Cross Section

To obtain the cross section for scattering into the continuum we performed the integration

$$\int_0^{\alpha E - 4.1140} \left(\frac{\sigma}{E'}\right) E' dE',$$

as a function of E up to 9 MeV.

Above 9 MeV we adjusted the cross section for inelastic scattering into the continuum so that the nonelastic cross section obtained by summing the evaluated partial cross sections would agree with experiment.[27] The cross section for scattering into the continuum is shown in Fig. 37.

Angular Distribution

Experimental data[1] indicate isotropic-angular distributions for neutrons scattered into the continuum, and that is the distribution we have used.

Energy Distribution

As discussed above, the continuum was divided into two regions in excitation energy E_x. The first, for which 4.1875 MeV $\leq E_x \leq$ 7.0125 MeV, shows structure and is tabulated every 0.1 MeV in incident neutron energy from 4.4 to 15 MeV. The outgoing neutron probabilities are given for energy bins 0.05-MeV wide and boundaries on multiples of 0.05 MeV. The second region, for which $E_x > 7.0125$ MeV, is describable by the Maxwellian discussed above.

Typical secondary neutron energy distributions for several incident energies are shown in Fig. 38.

The Total Inelastic Cross Section

The total inelastic cross section obtained by summing the cross sections for inelastic scattering to discrete levels and to the continuum is shown in Figs. 39–44.

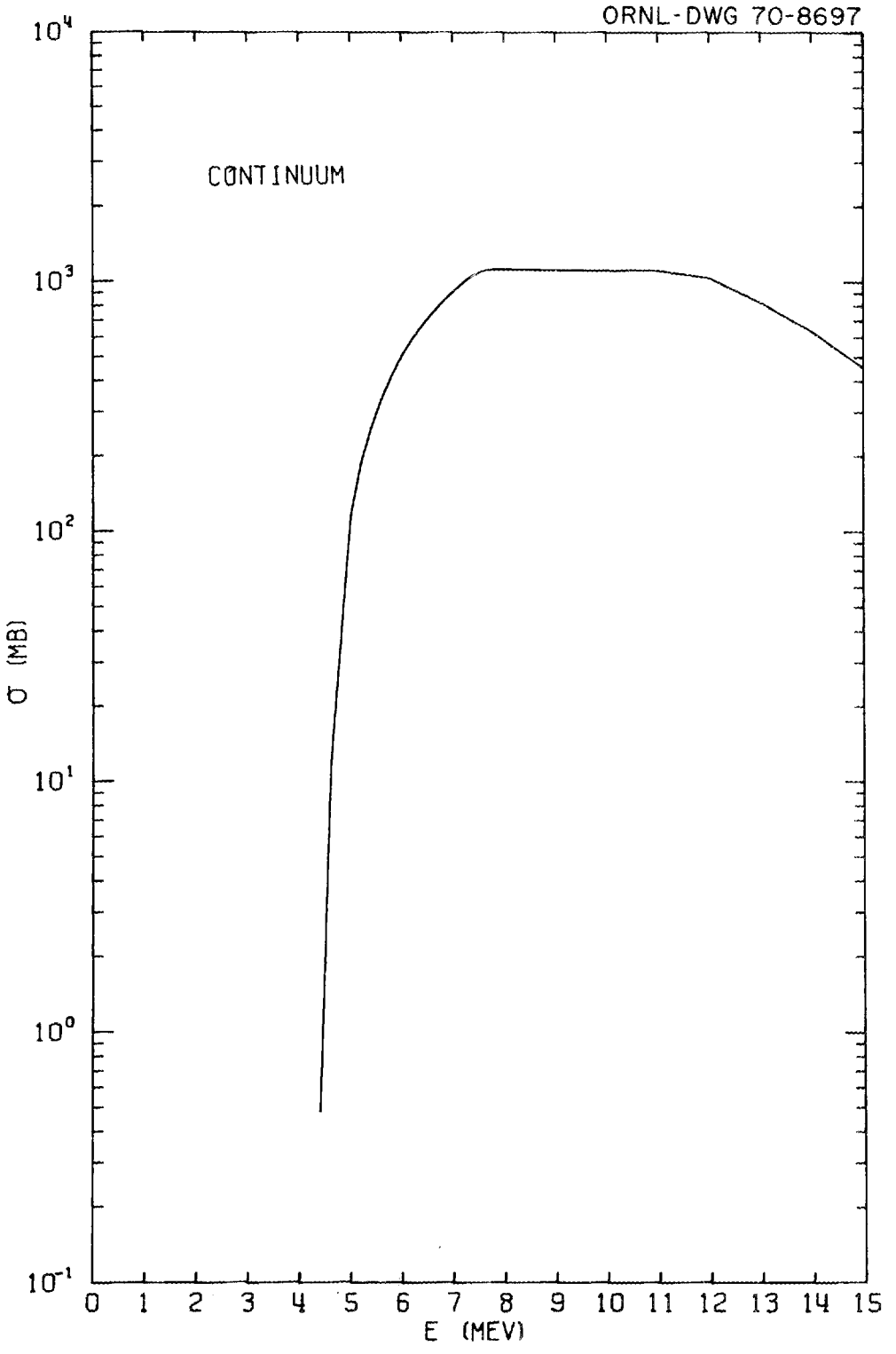

Fig. 37. The Evaluated Cross Section for Inelastic Scattering to the Continuum.

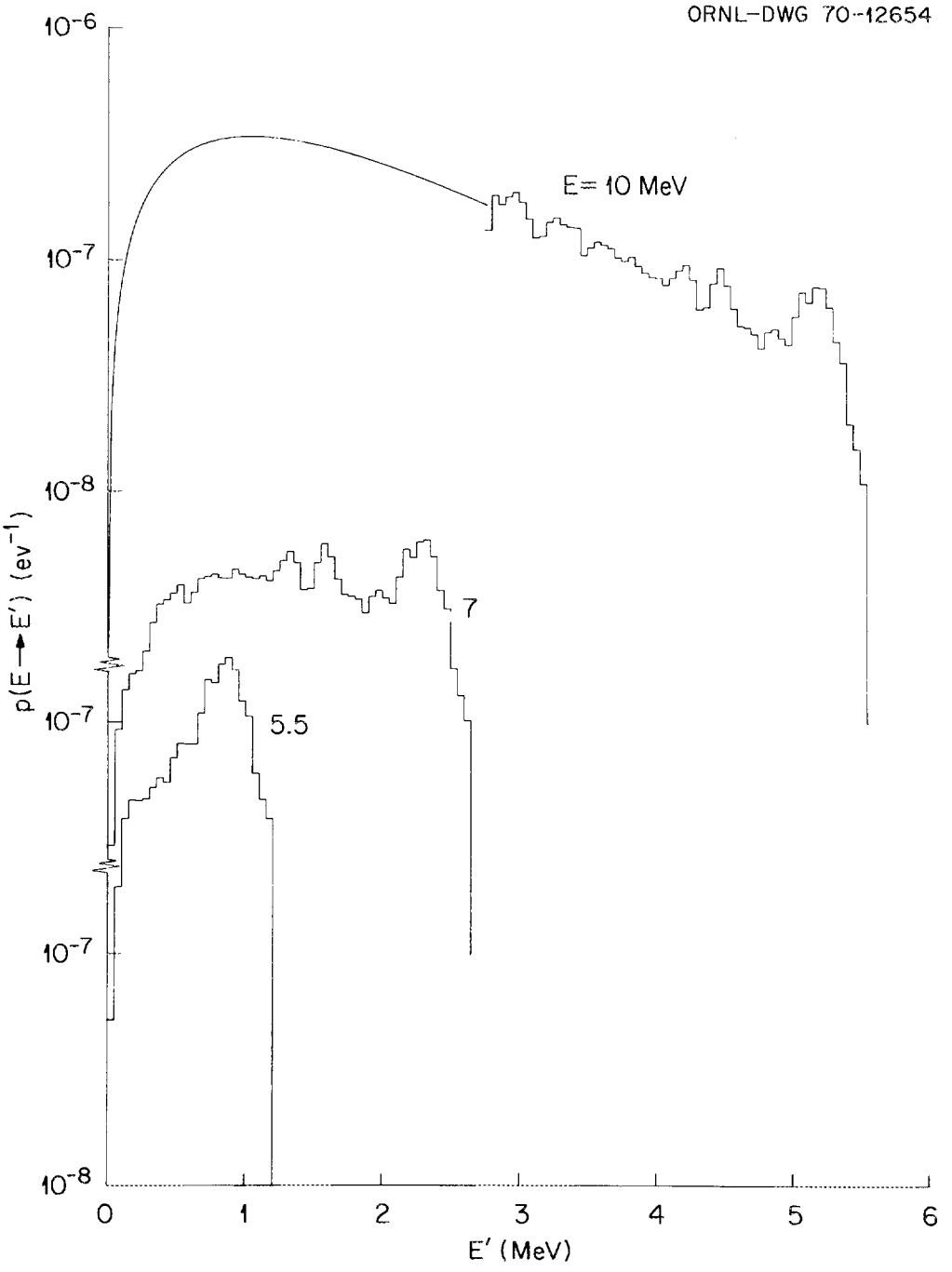

Fig. 38. Representative Secondary Neutron Energy Distributions Resulting From Inelastic Scattering to the Continuum.

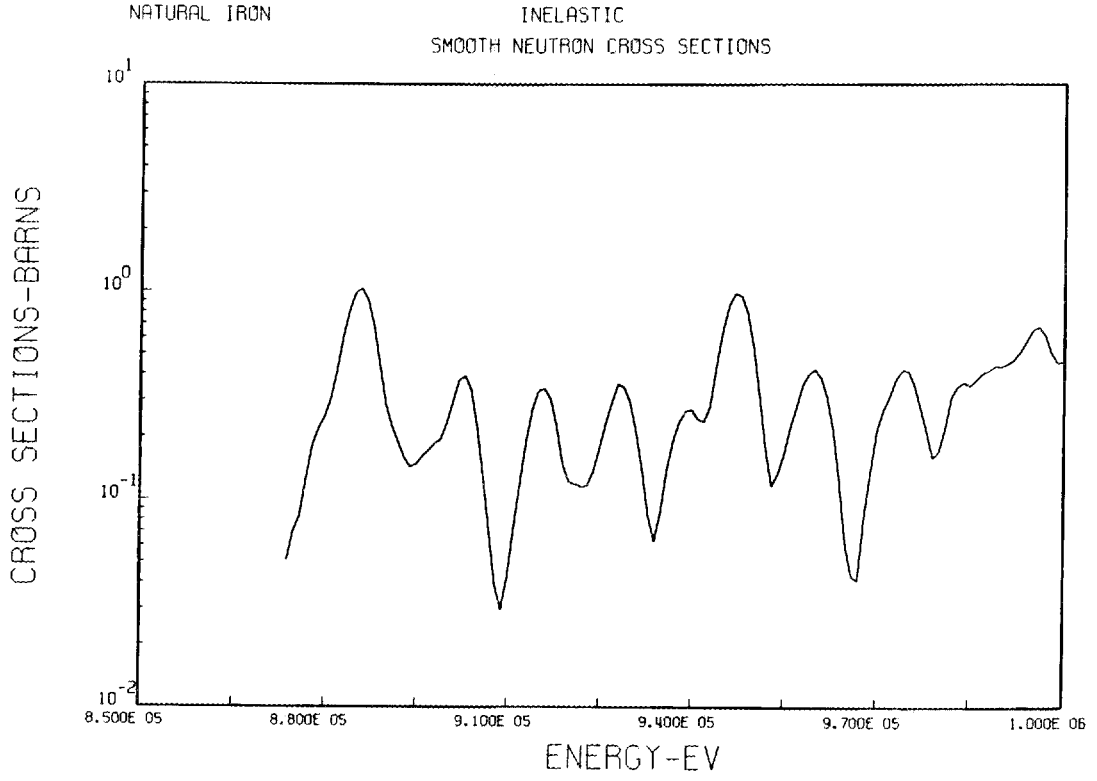

Fig. 39. The Evaluated Inelastic Scattering Cross Section From 850 keV to 1 MeV.

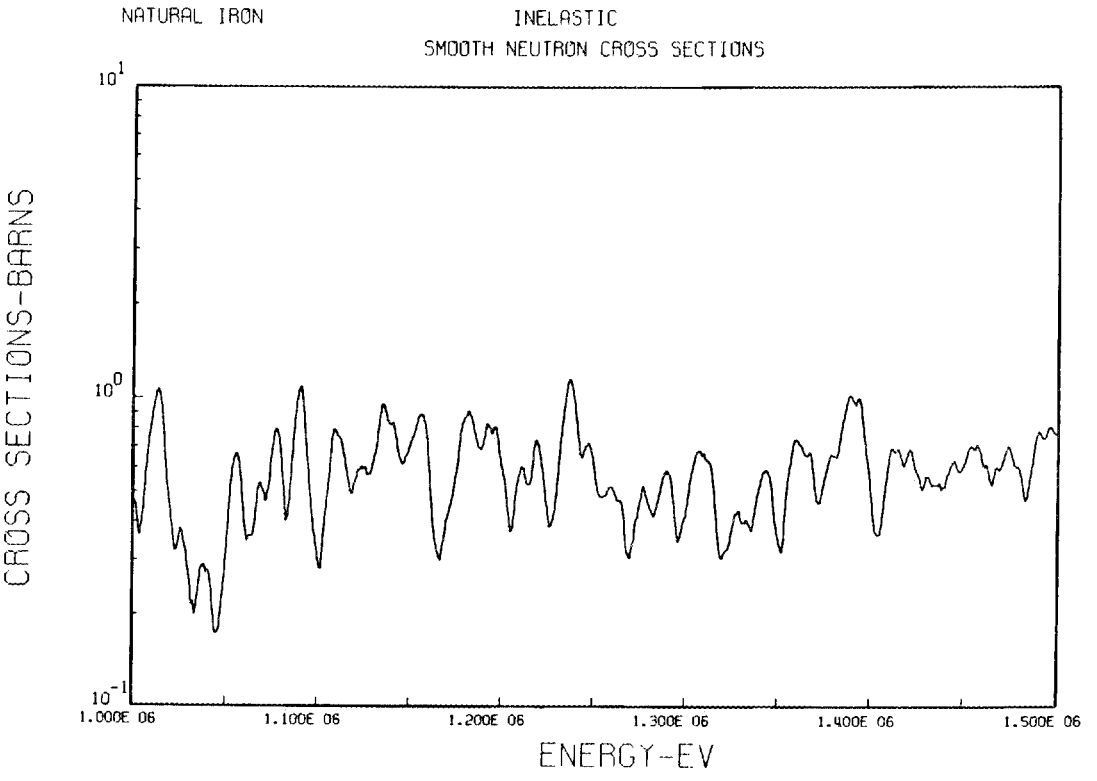

Fig. 40. The Evaluated Inelastic Scattering Cross Section From 1 to 1.5 MeV.

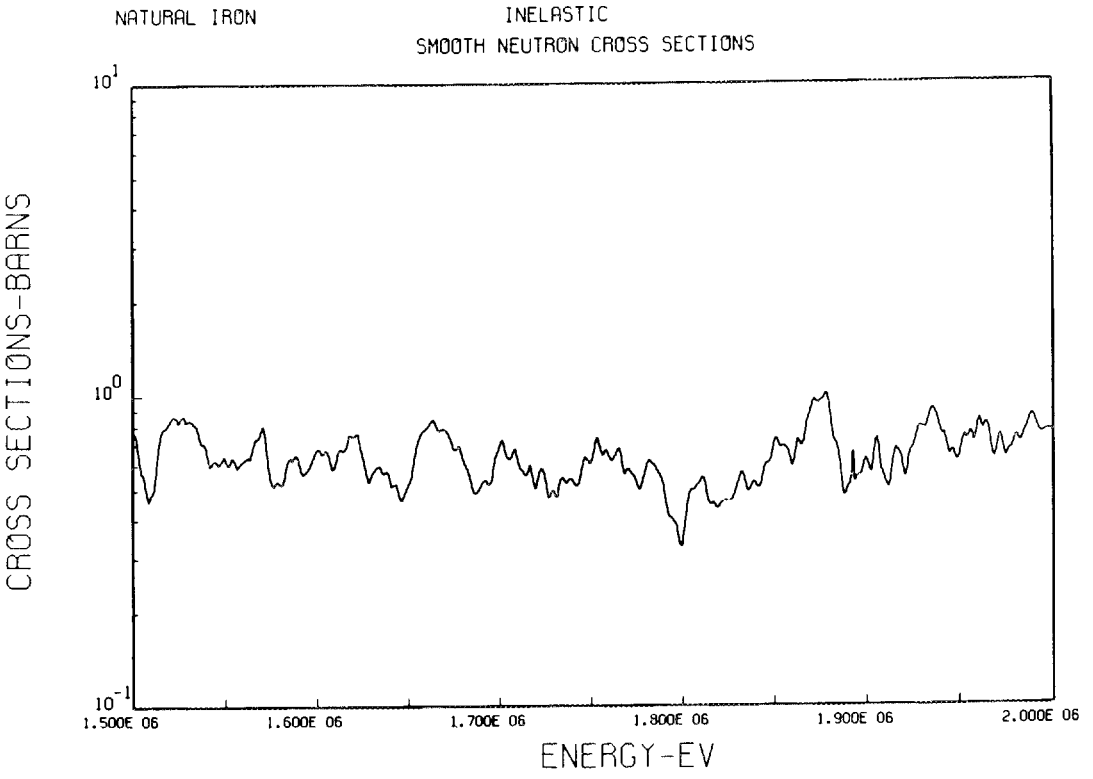

Fig. 41. The Evaluated Inelastic Scattering Cross Section from 1.5 to 2 MeV.

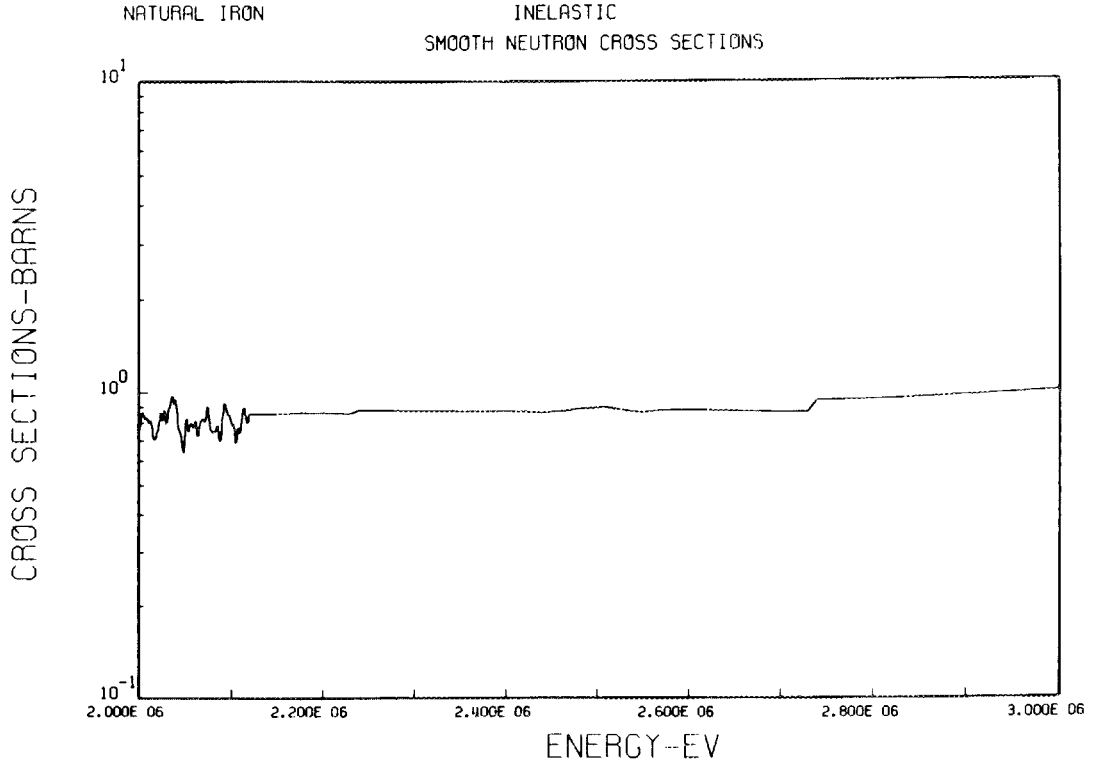

Fig. 42. The Evaluated Inelastic Scattering Cross Section From 2 to 3 MeV.

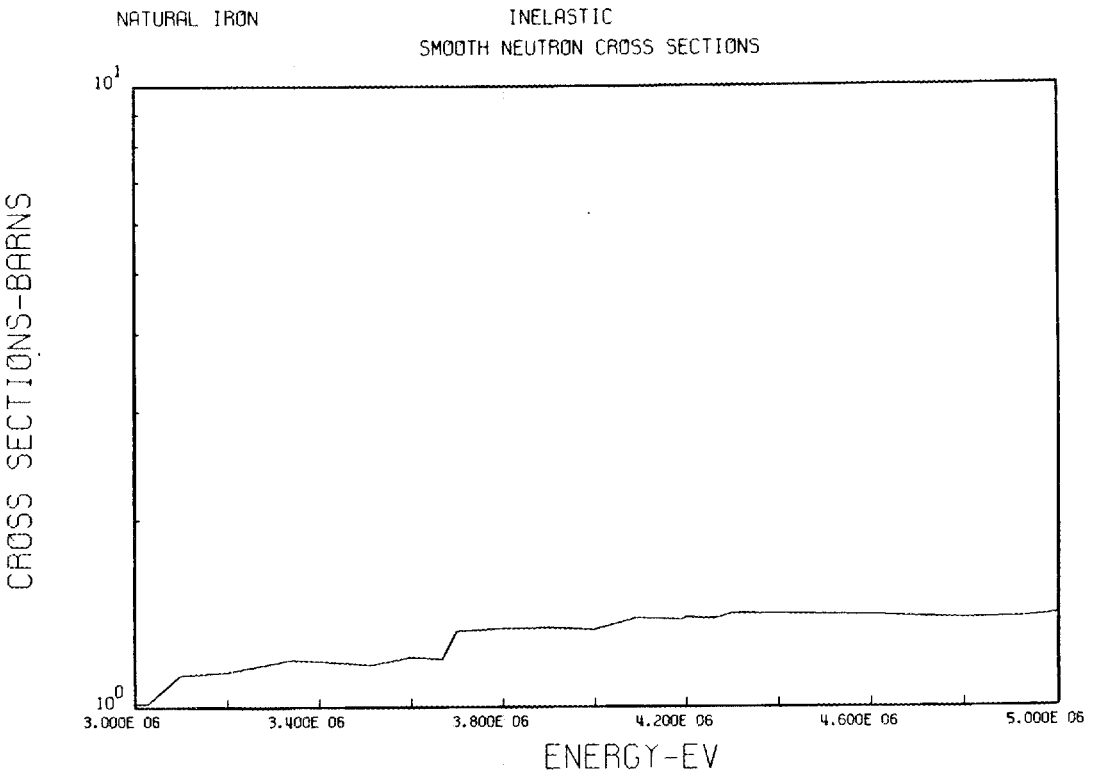

Fig. 43. The Evaluated Inelastic Scattering Cross Section From 3 to 5 MeV.

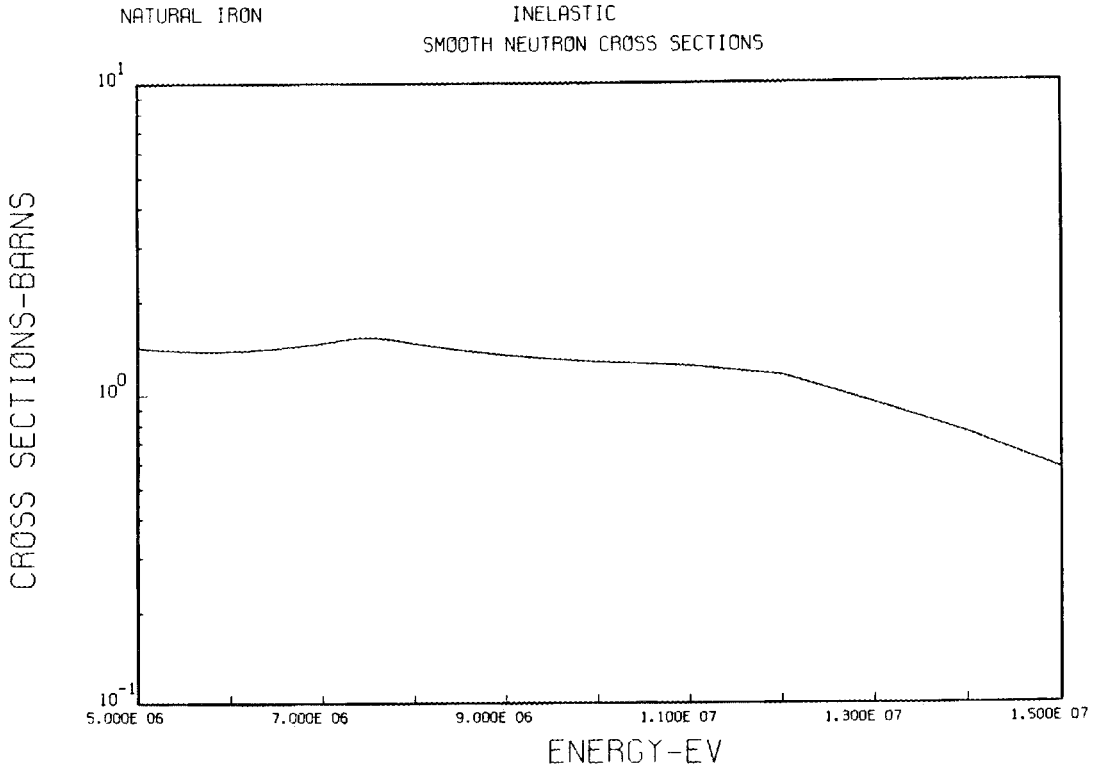

Fig. 44. The Evaluated Inelastic Scattering Cross Section From 5 to 15 MeV.

The Capture Cross Section

The capture cross section was taken from the U.K. evaluation (DFN-91).[31] These data were obtained by the U.K. in the energy range 1 keV to 60 keV by using resonance parameters based on the measurements of Hockenbury *et al.*[32] These data are, in general, lower than the data of DFN-64 and consequently lower than those of ENDF-1101[4] and ENDF-1108.[45] The U.K. adopted J. J. Schmidt's[46] evaluation below 1 keV and above 60 keV except that above 60 keV a constant value of 9 mb was assumed which joins smoothly to Schmidt's curve just above 100 keV. The data are shown in Figs. 45–48.

Cross Sections for the (n,α), (n,p), and (n,2n) Reactions

The (n,α) and (n,p) cross sections were taken from the U.K. evaluation (DFN-91) which were in turn derived from J. J. Schmidt's evaluation.[46] The cross sections for the (n,2n) reaction were taken from the evaluation by Azziz *et al.* (ENDF-1122).[45]

The secondary neutron energy distribution of the (n,2n) reaction was also taken from the evaluation of Azziz *et al.* The form is Maxwellian:

$$f(E \rightarrow E') = NE' e^{-E'/\theta(E)}$$

where $\theta = 0.433\sqrt{E}$ (in MeV), E is incident neutron energy, E′ is emergent neutron energy, and N is a normalization constant. The curves for the (n,α), (n,p), and (n,2n) cross sections are shown in Figs. 49–51.

The Nonelastic Cross Section

The nonelastic cross section obtained by adding the evaluated partial cross sections is shown in Figs. 52–62.

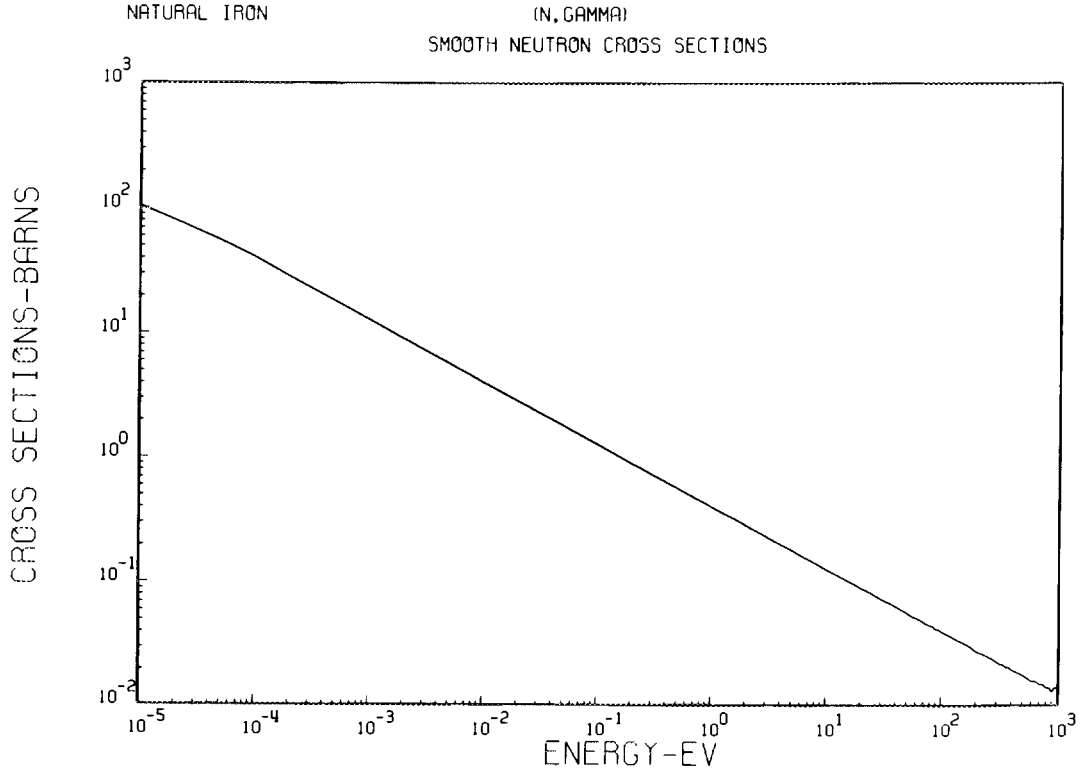

Fig. 45. The Evaluated Capture Cross Section For Neutron Energies 10^{-5} eV to 1 keV.

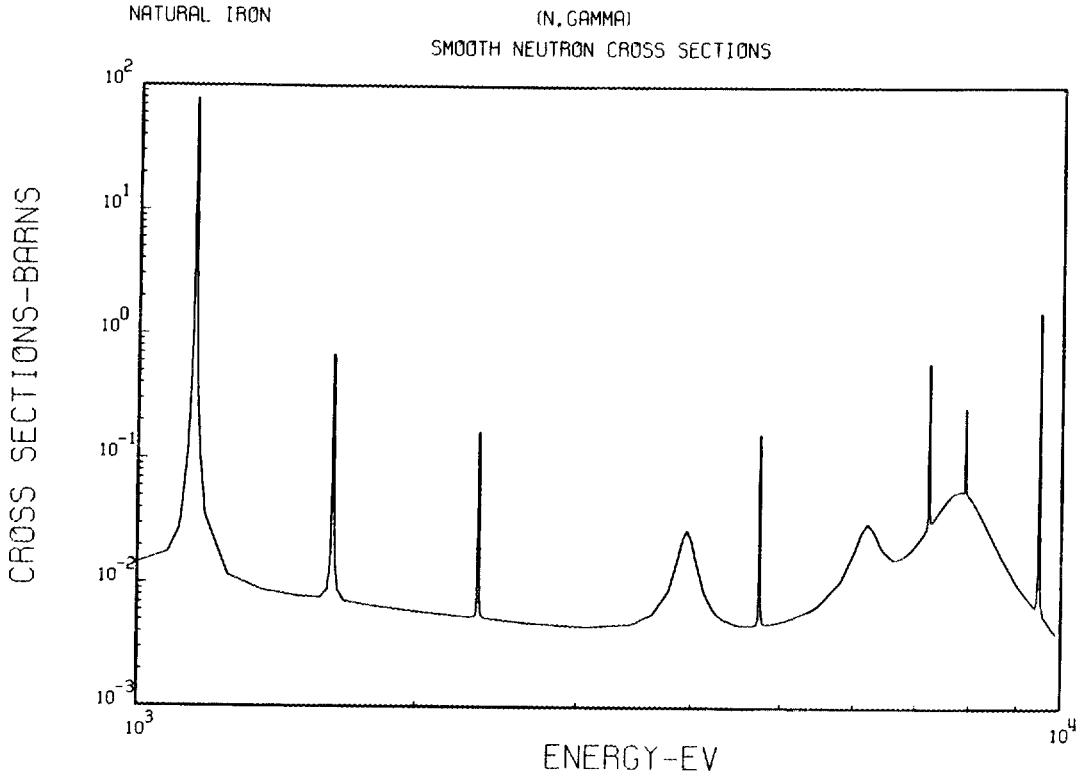

Fig. 46. The Evaluated Capture Cross Section For Neutron Energies 1 keV to 10 keV.

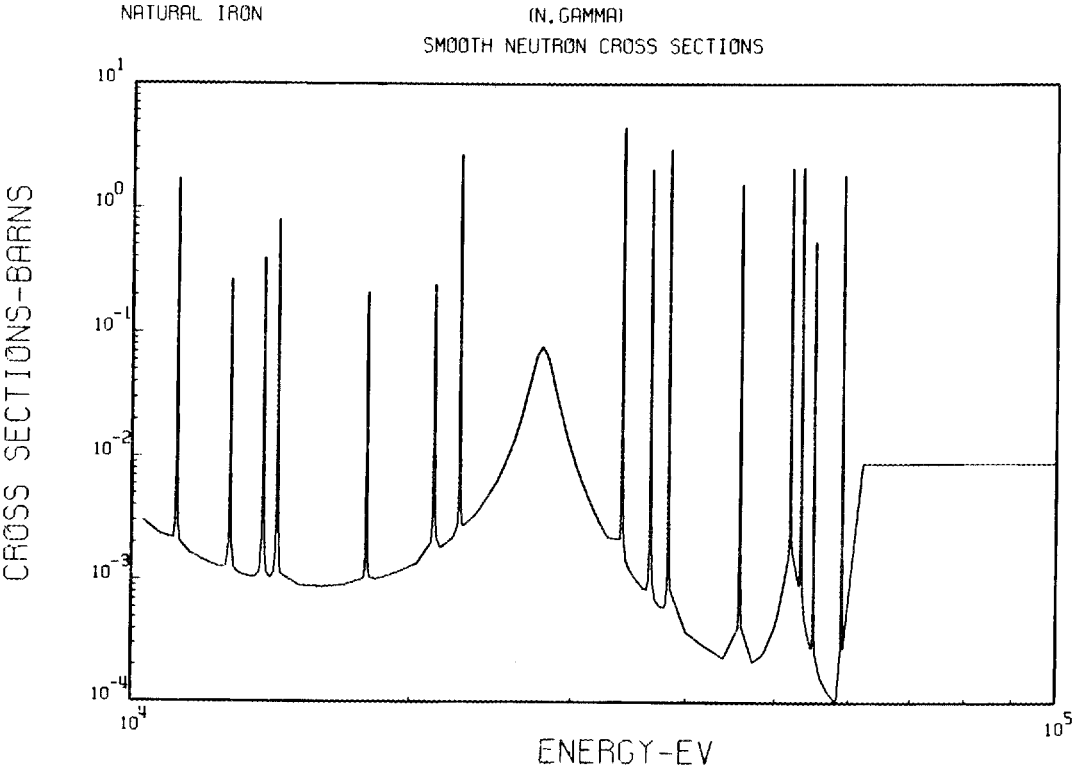

Fig. 47. The Evaluated Capture Cross Section For Neutron Energies 10 to 100 keV.

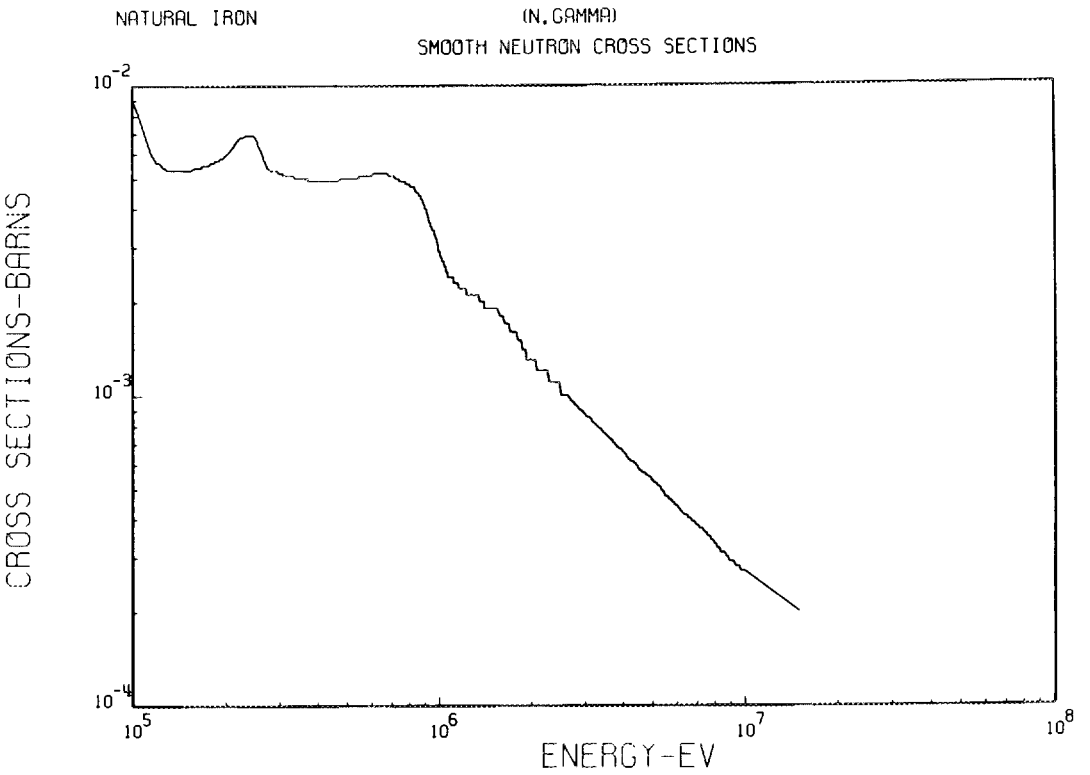

Fig. 48. The Evaluated Capture Cross Section For Neutron Energies 100 keV to 15 MeV.

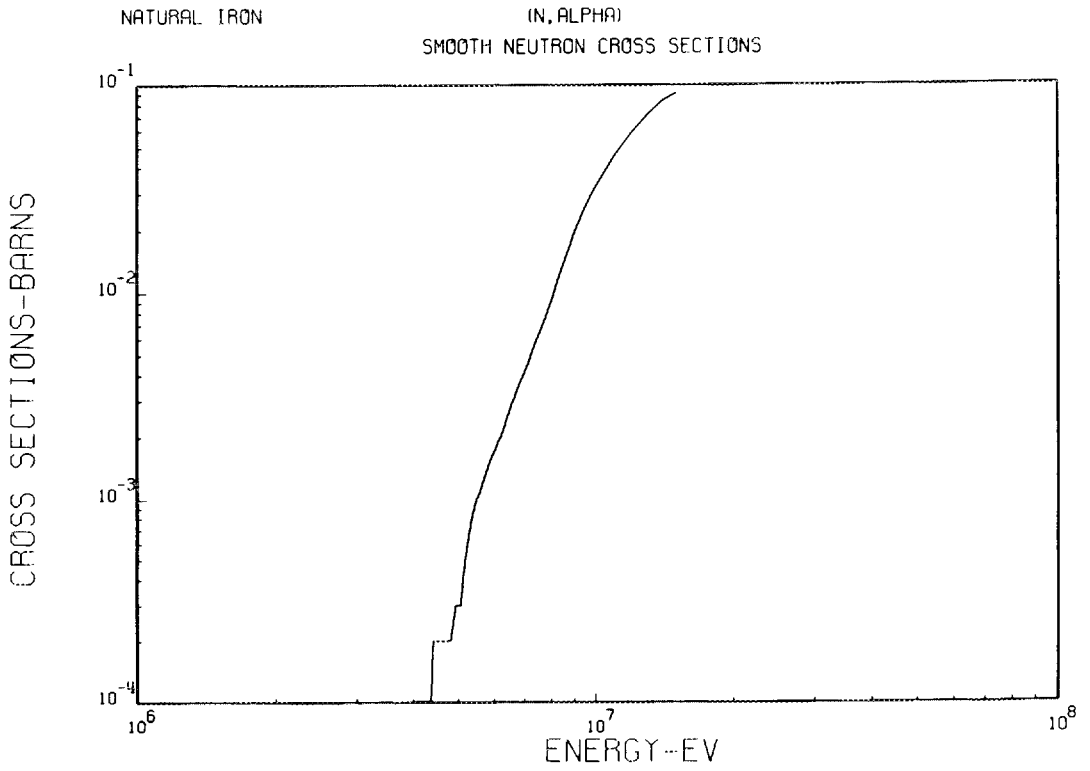

Fig. 49. The Evaluated (n,α) Cross Section.

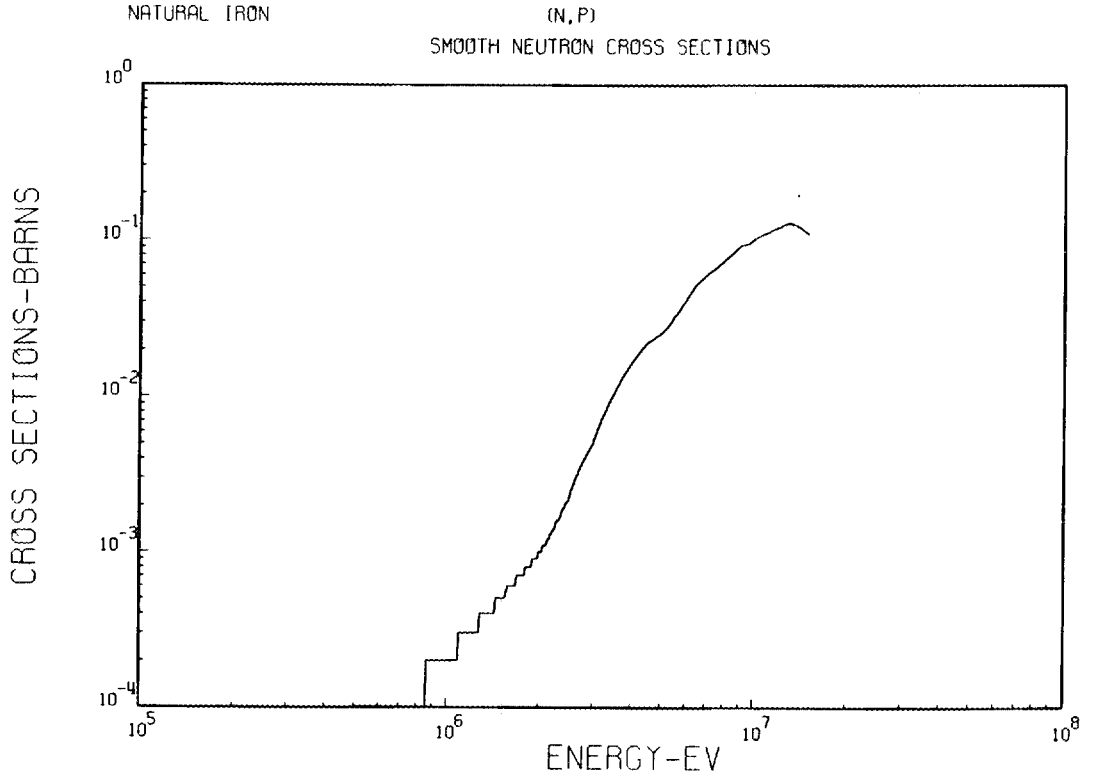

Fig. 50. The Evaluated (n,p) Cross Section.

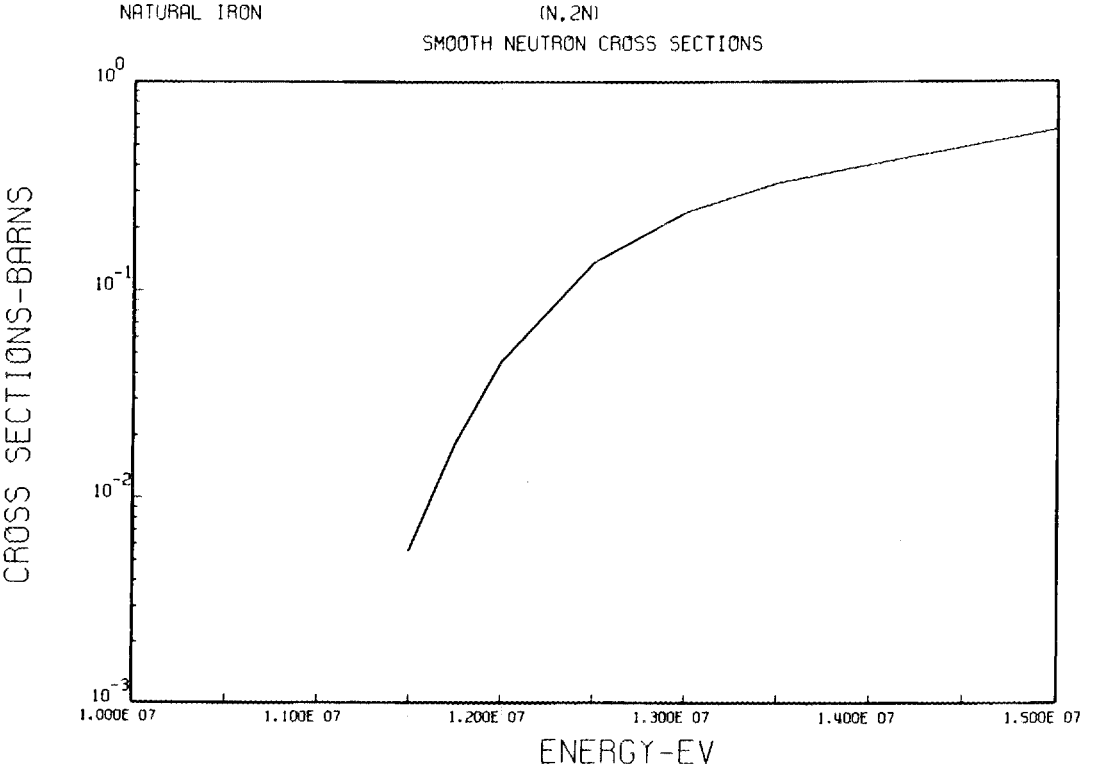

Fig. 51. The Evaluated (n,2n) Cross Section.

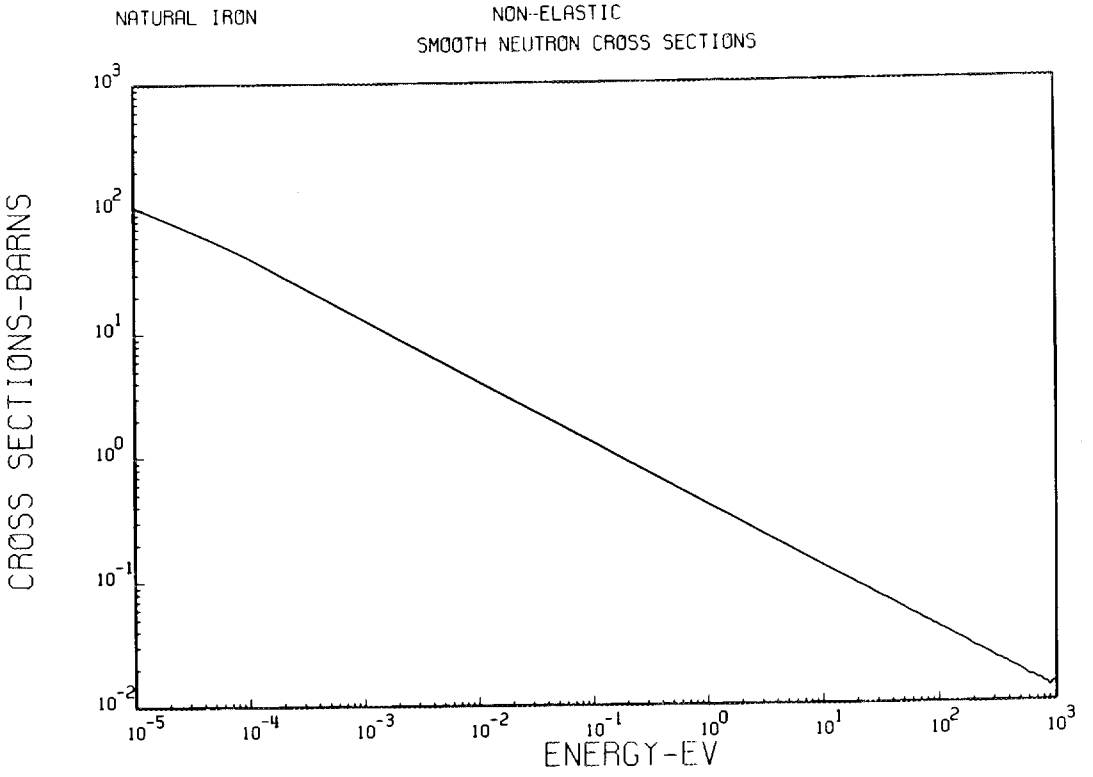

Fig. 52. The Evaluated Nonelastic Cross Section for Neutron Energies 10^{-5} eV to 1 keV.

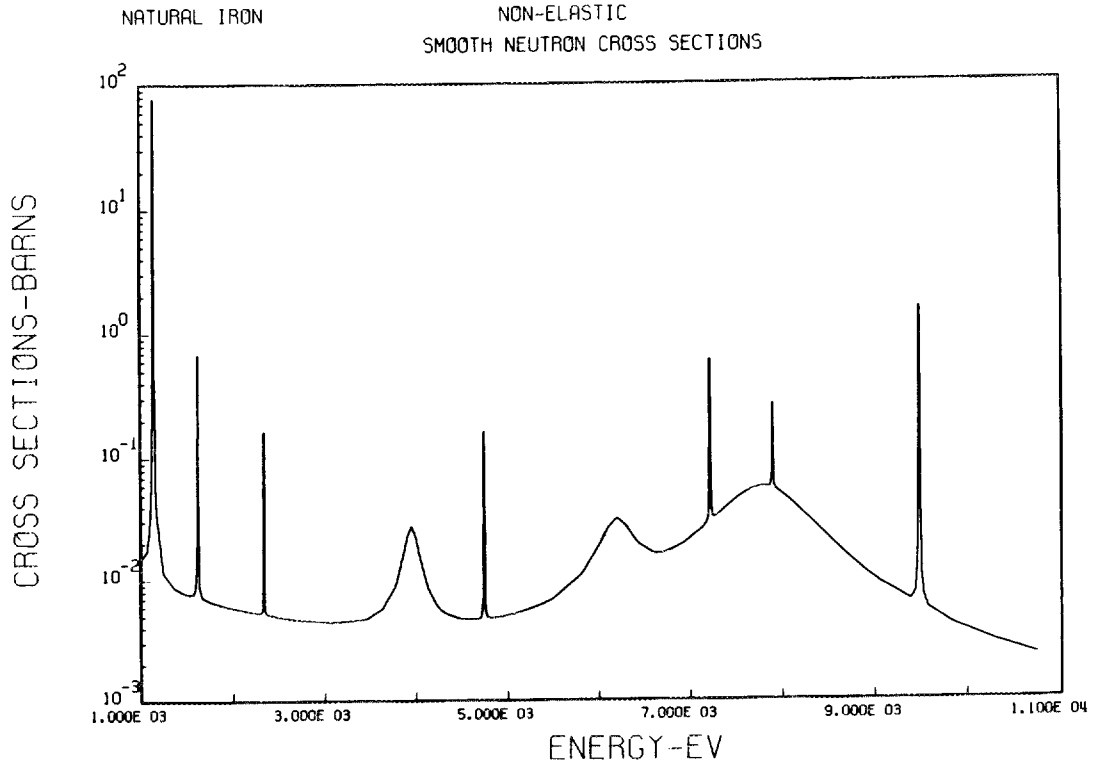

Fig. 53. The Evaluated Nonelastic Cross Section for Neutron Energies 1 to 11 keV.

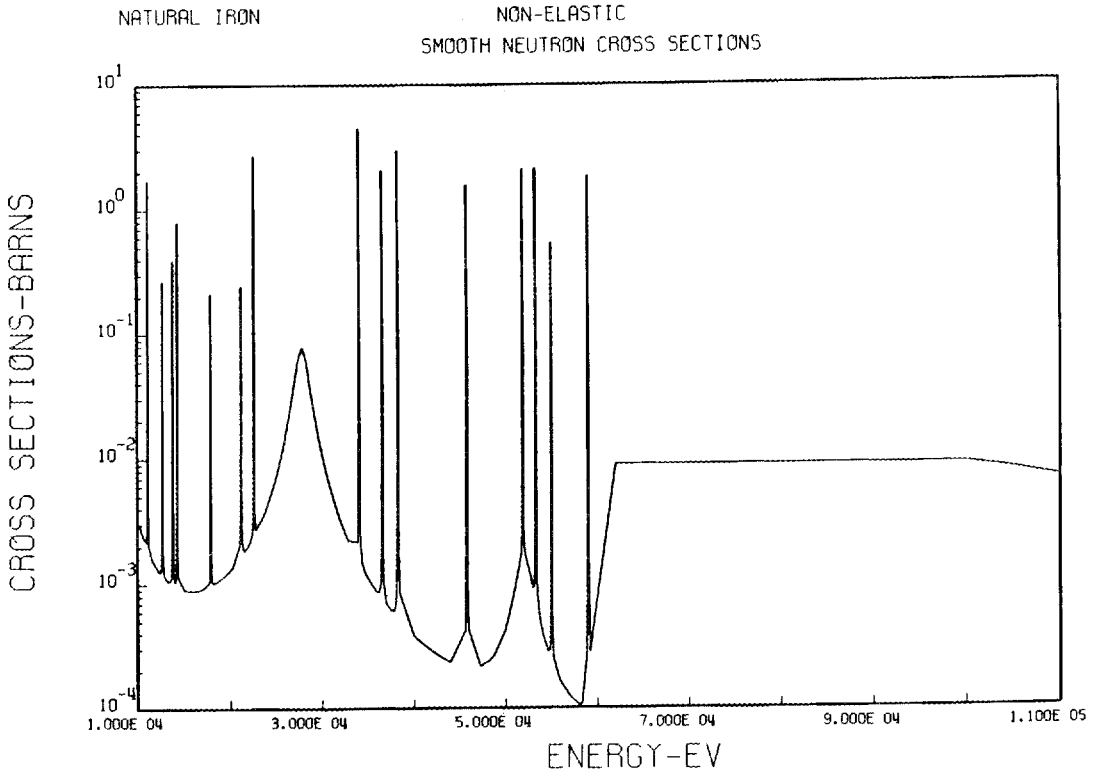

Fig. 54. The Evaluated Nonelastic Cross Section for Neutron Energies 10 to 110 keV.

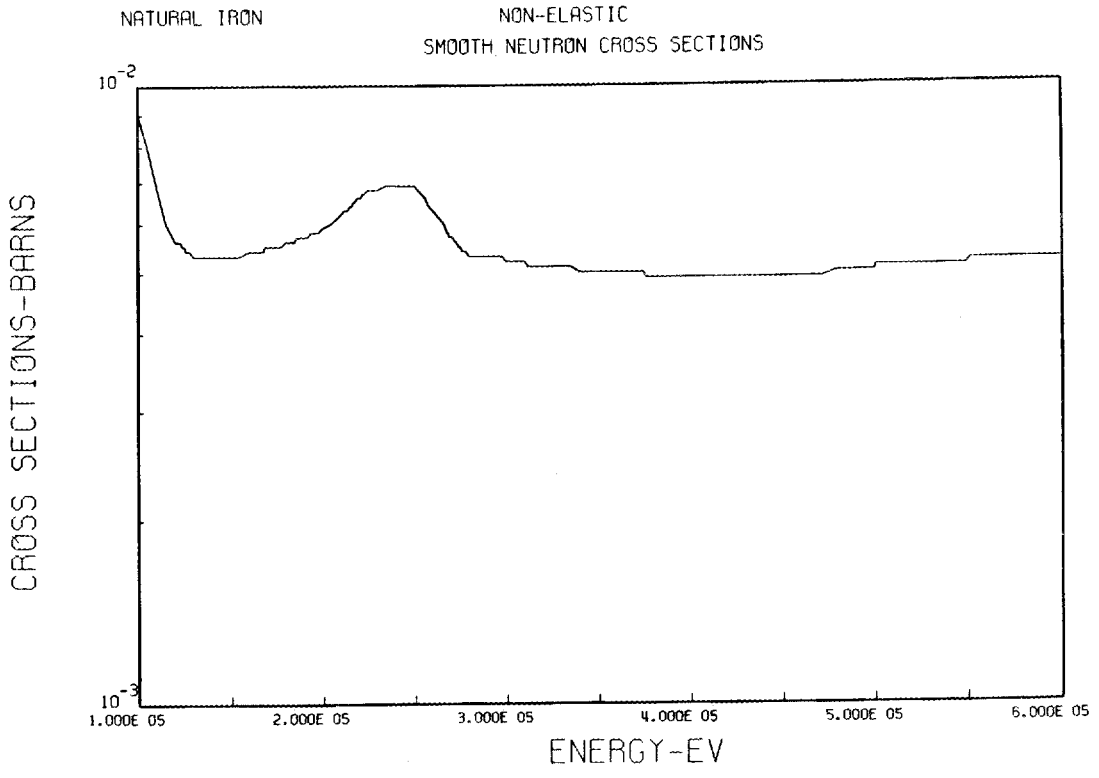

Fig. 55. The Evaluated Nonelastic Cross Section for Neutron Energies 100 to 600 keV.

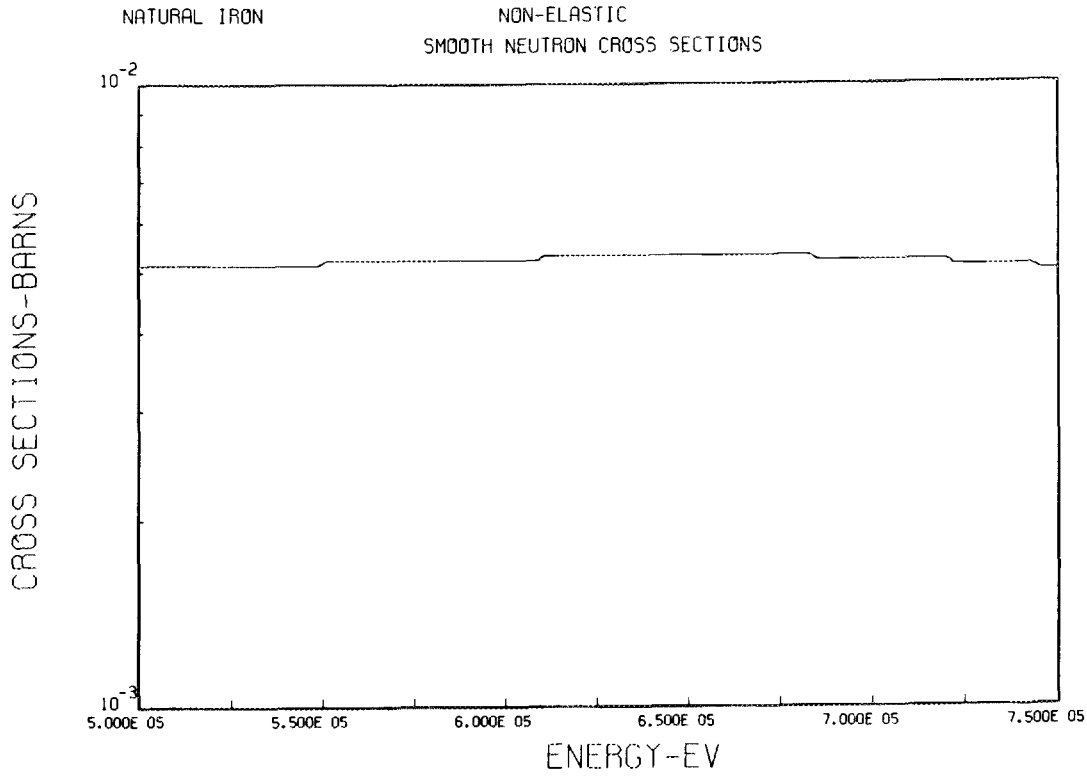

Fig. 56. The Evaluated Nonelastic Cross Section for Neutron Energies 500 to 750 keV.

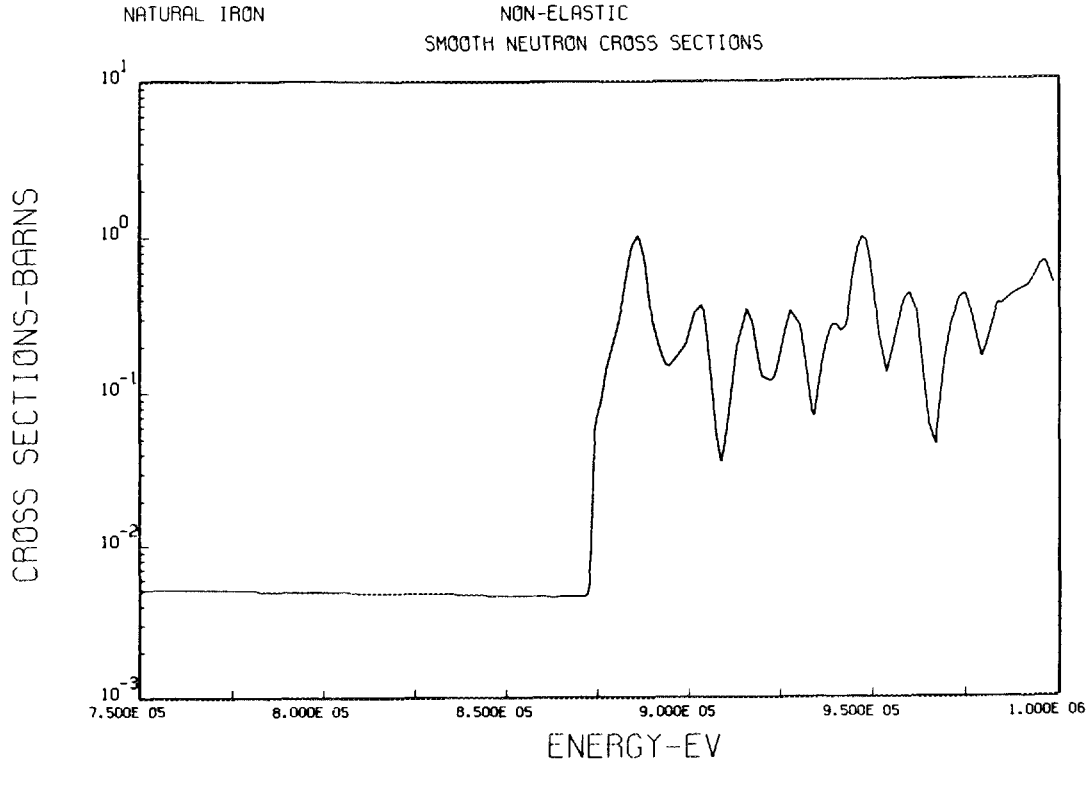

Fig. 57. The Evaluated Nonelastic Cross Section for Neutron Energies 750 keV to 1 MeV.

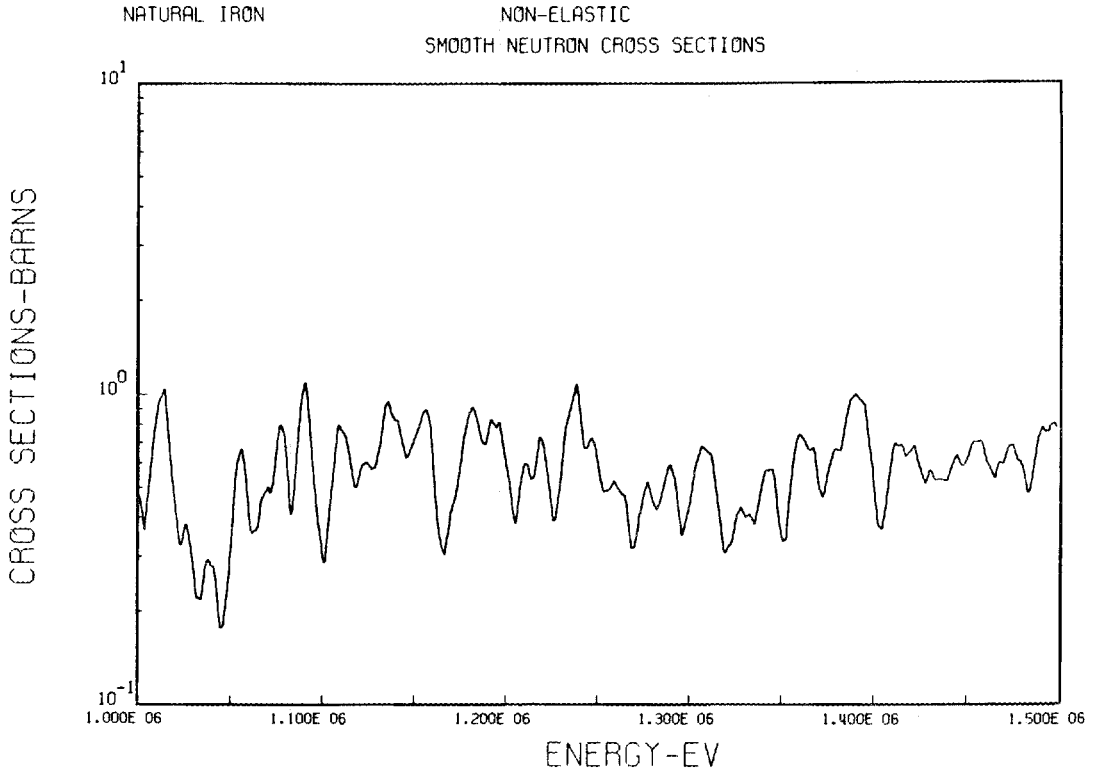

Fig. 58. The Evaluated Nonelastic Cross Section for Neutron Energies 1 to 1.5 MeV.

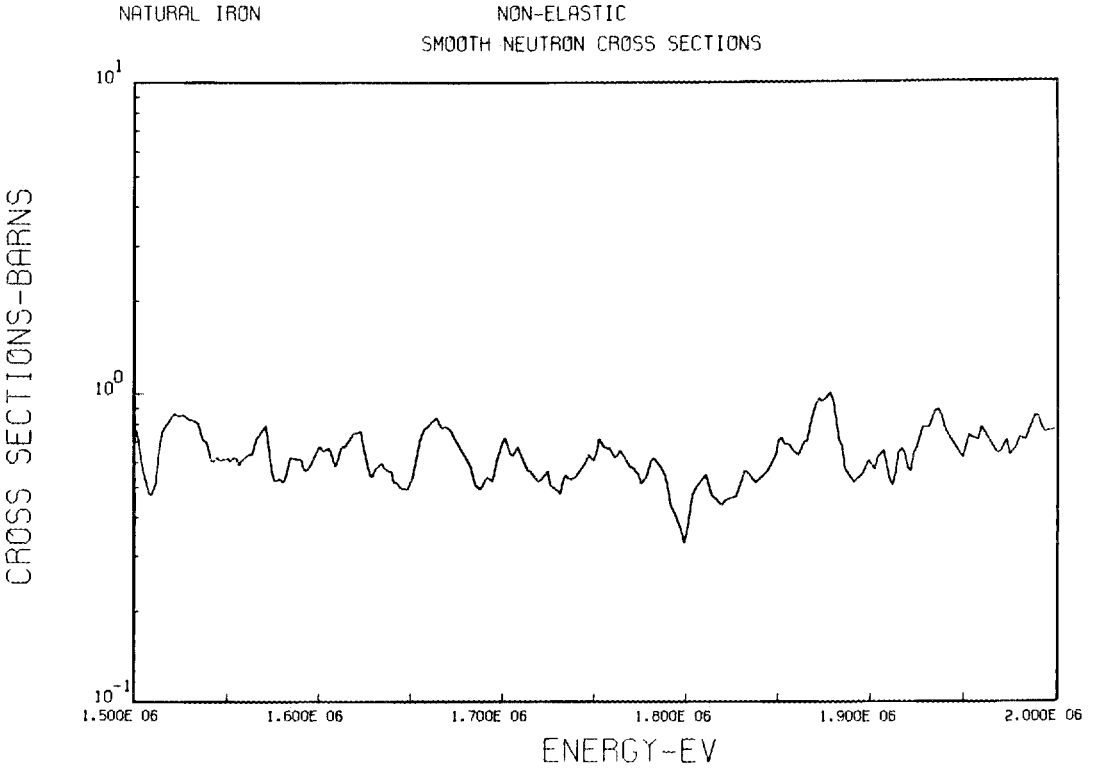

Fig. 59. The Evaluated Nonelastic Cross Section for Neutron Energies 1.5 to 2 MeV.

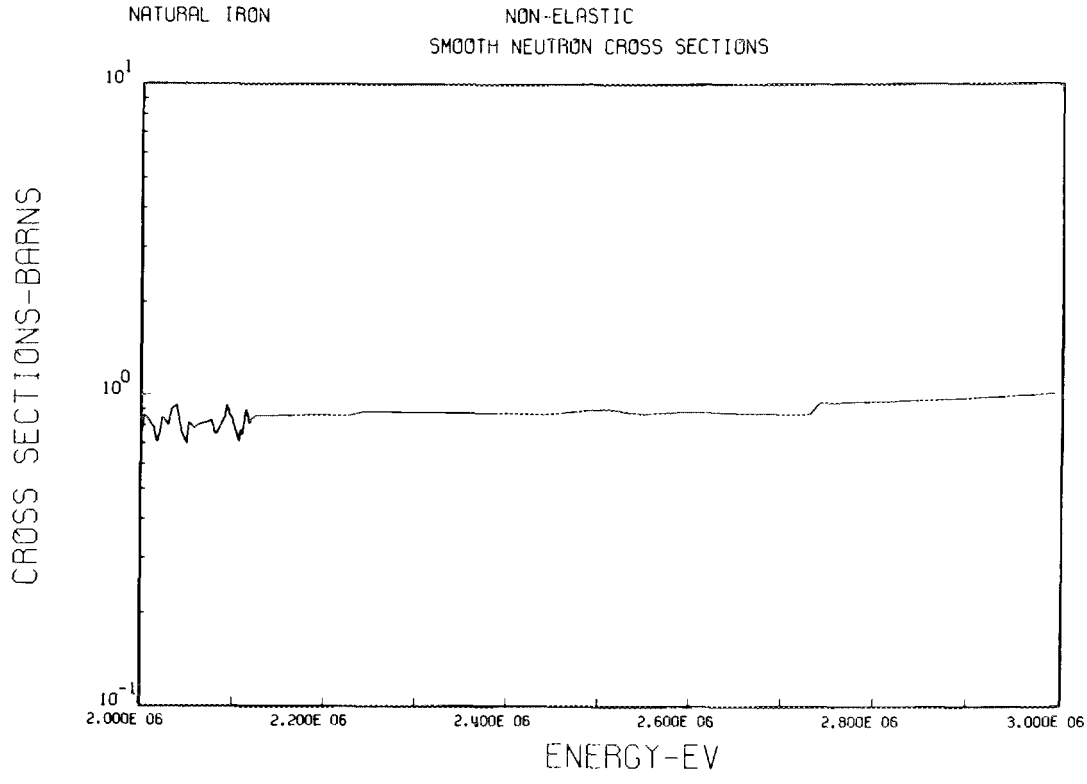

Fig. 60. The Evaluated Nonelastic Cross Section for Neutron Energies 2 to 3 MeV.

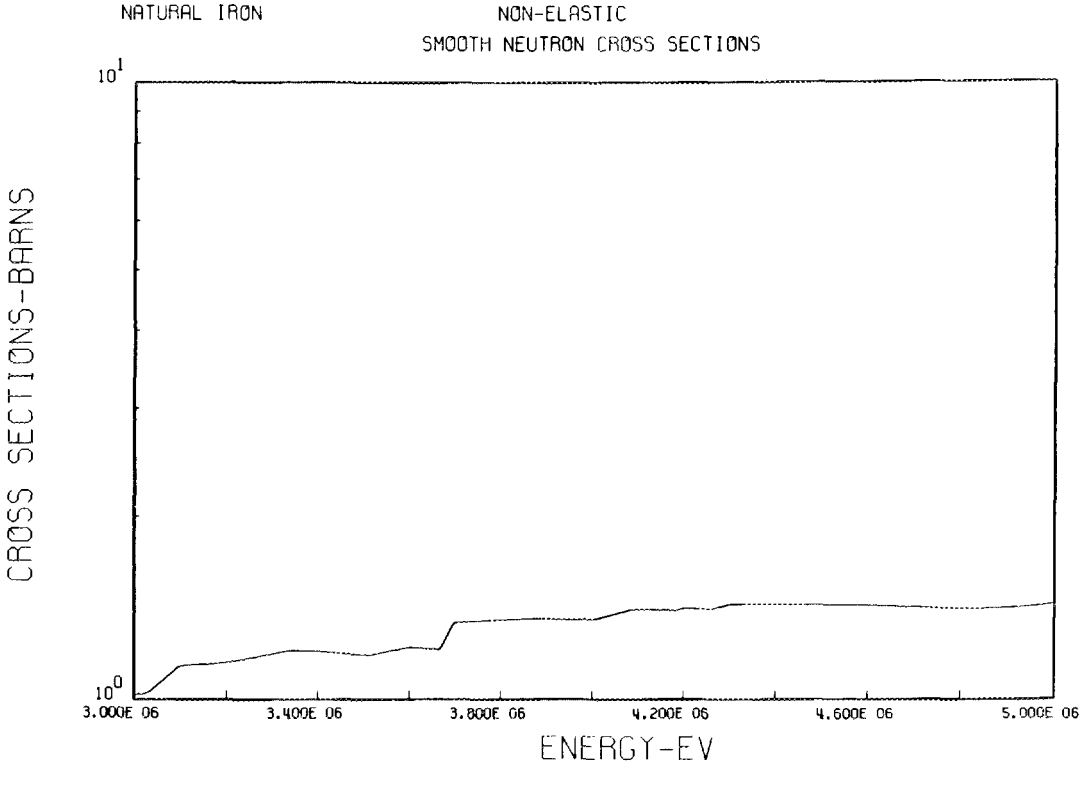

Fig. 61. The Evaluated Nonelastic Cross Section for Neutron Energies 3 to 5 MeV.

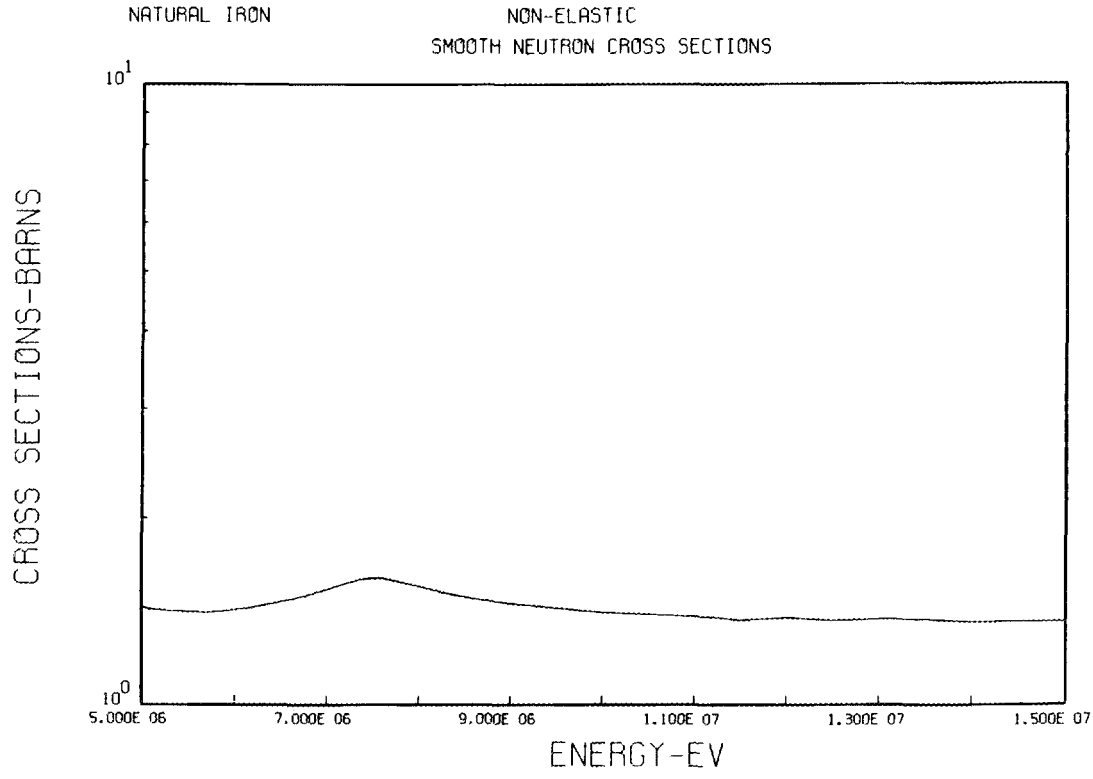

Fig. 62. The Evaluated Nonelastic Cross Section for Neutron Energies 5 to 15 MeV.

IV. GAMMA-RAY PRODUCTION CROSS SECTIONS

Only gamma rays resulting from neutron capture and neutron inelastic scattering have been considered. Gamma rays resulting from (n,α), (n,p), and (n,2n) reactions could be important for the higher energy range (10 MeV to 15 MeV) if the neutrons in this energy range are abundant enough in a given shield. However, in most shields this is not the case.

Neutron Capture Gamma-Ray Production

The multiplicities and gamma-ray energy distributions of gamma rays resulting from neutron capture were calculated by White[47] after intensities of primary lines had been fitted to experimental data. White used the code DUCAL[48] to calculate the de-excitation spectra from capture states in ^{56}Fe and ^{54}Fe extending from thermal-neutron energies to 1 MeV. Intensities of primary lines were matched with experimental data of Chrien *et al.*,[49] B. B. V. Raju *et al.*,[50] and N. C. Rasmussen *et al.*[51] The rest of the spectra were generated by the code; however, in this case most of the binding energy resides in the primary lines. For higher neutron energies the same parameters were used as for the lower energy case except that the capture state was changed. S-, p-, and d-waves were included. The states of ^{55}Fe were obtained from the Nuclear Data Group,[22] and the states of ^{57}Fe were obtained from the Nuclear Data Group and a calculation by Fu.[52] The branching ratios that were not known experimentally for the states were obtained from an *ad hoc* calculation which presumes knowledge of E2/M1 and M1/E1 ratios for all states. These were taken to be 0.2 and 0.25, respectively. White then used the code AVA[53] to average the de-excitation spectra over 12 neutron energy groups to obtain gamma-ray energy distributions and multiplicities for each group. The code AVA averages the gamma-ray spectra over the capture cross section. The capture cross section is calculated in two energy regions – namely, the resolved resonance region and the unresolved resonance region. In the resolved resonance region the resonance parameters used were then derived from Hockenbury's measurements[32] by the U.K.[31]

The resonance treatment was single-level Breit-Wigner with no Doppler broadening. The energy groups are broad enough so that Doppler broadening is not important. In the unresolved region AVA incorporates a statistical model but with no competition from inelastic scattering, etc. This will introduce no error in this case since the inelastic scattering for ^{54}Fe is absent below 1 MeV and the inelastic scattering in ^{56}Fe introduces only a normalization constant which should be almost unity below 1 MeV. The statistical model was Hauser-Feshbach with width fluctuation corrections, and the analog of the penetrability for gamma rays was 2π times an average radiative width times a level density given by Gilbert and Cameron.[25] The gamma-ray multiplicities are shown in Table XI, and the probability densities of emitting gamma rays with energies in 50-keV bins are shown in Figs. 63–74.

Table XI. Capture Gamma-Ray Multiplicities

Neutron Energy Range	Multiplicity (Photons/Event)
10^{-5}–250 eV	2.1630
250–500 eV	2.1556
500–3000 eV	2.3577
3.0–4.5 keV	2.1592
4.5–6.0 keV	2.1575
6–12 keV	2.7338
12–20 keV	2.0939
20–40 keV	2.7726
40–60 keV	2.7917
60–200 keV	2.6261
200–400 keV	2.6629
0.4–15 MeV	2.7384

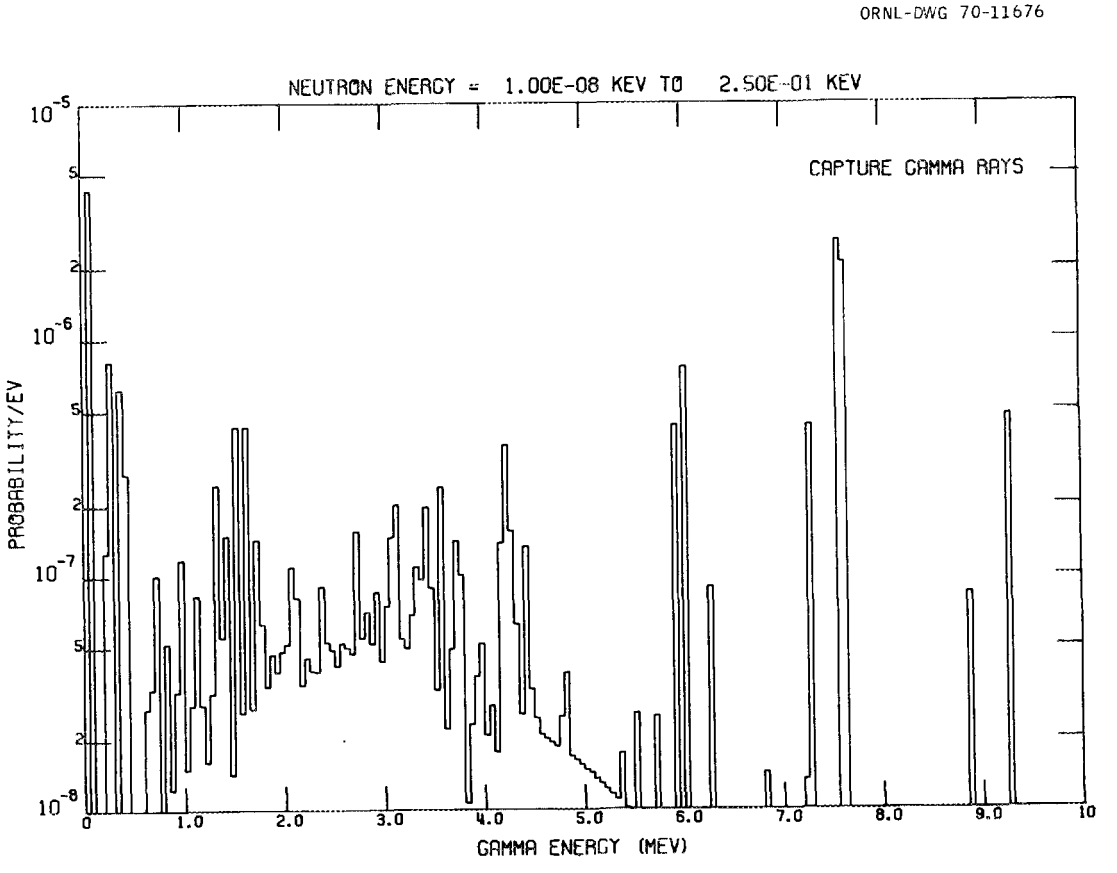

Fig. 63. Energy Distribution of Gamma Rays Resulting From the Radiative Capture of Neutrons in the Energy Range 10^{-5} to 250 eV.

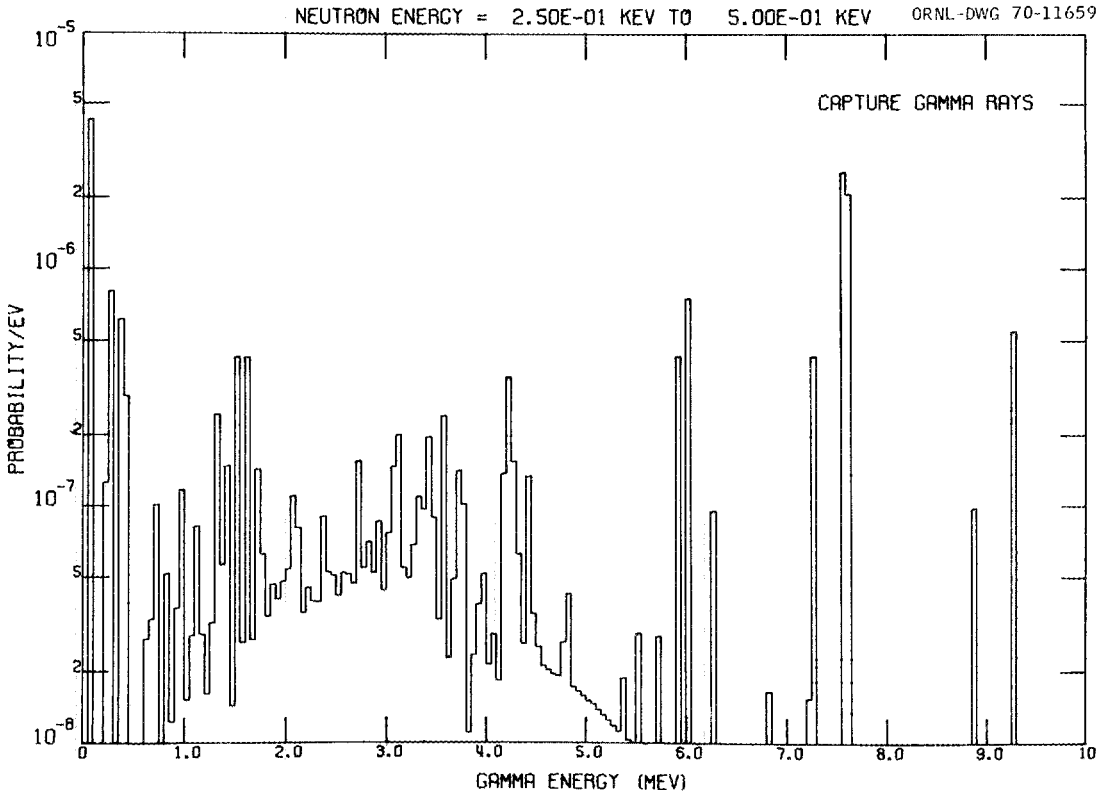

Fig. 64. Energy Distribution of Gamma Rays Resulting From the Radiative Capture of Neutrons in the Energy Range 250 to 500 eV.

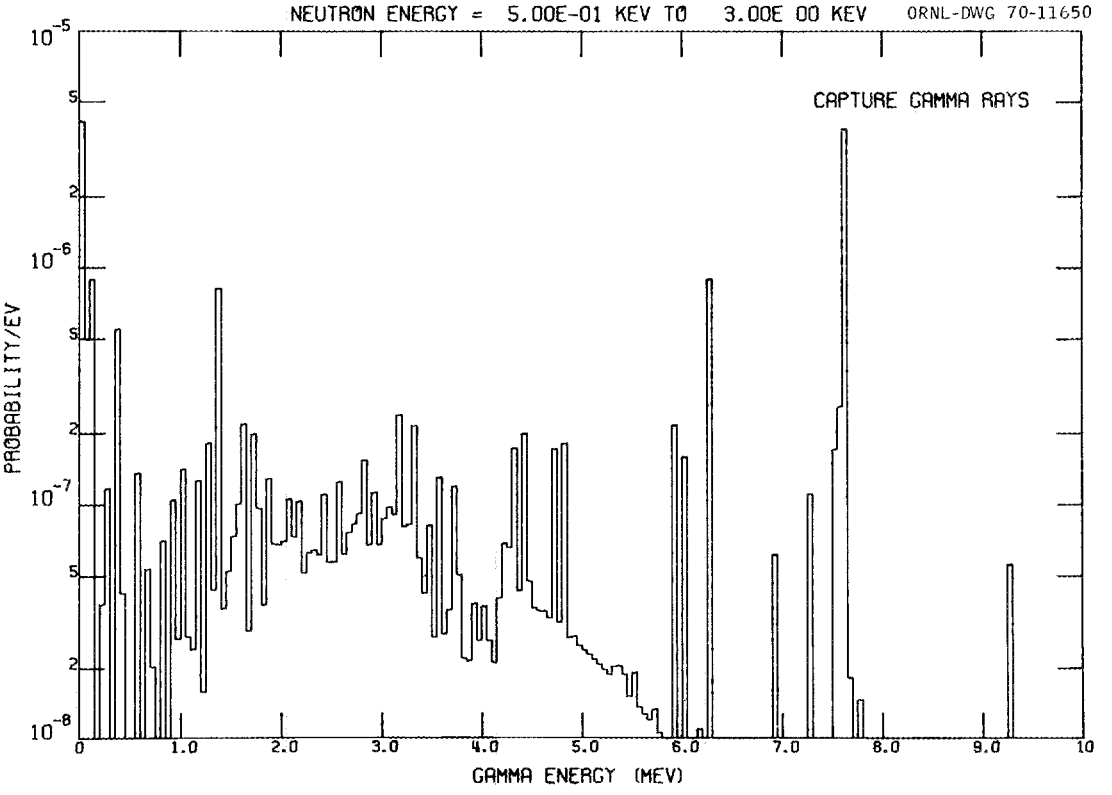

Fig. 65. Energy Distribution of Gamma Rays Resulting From the Radiative Capture of Neutrons in the Energy Range 0.5 to 3 keV.

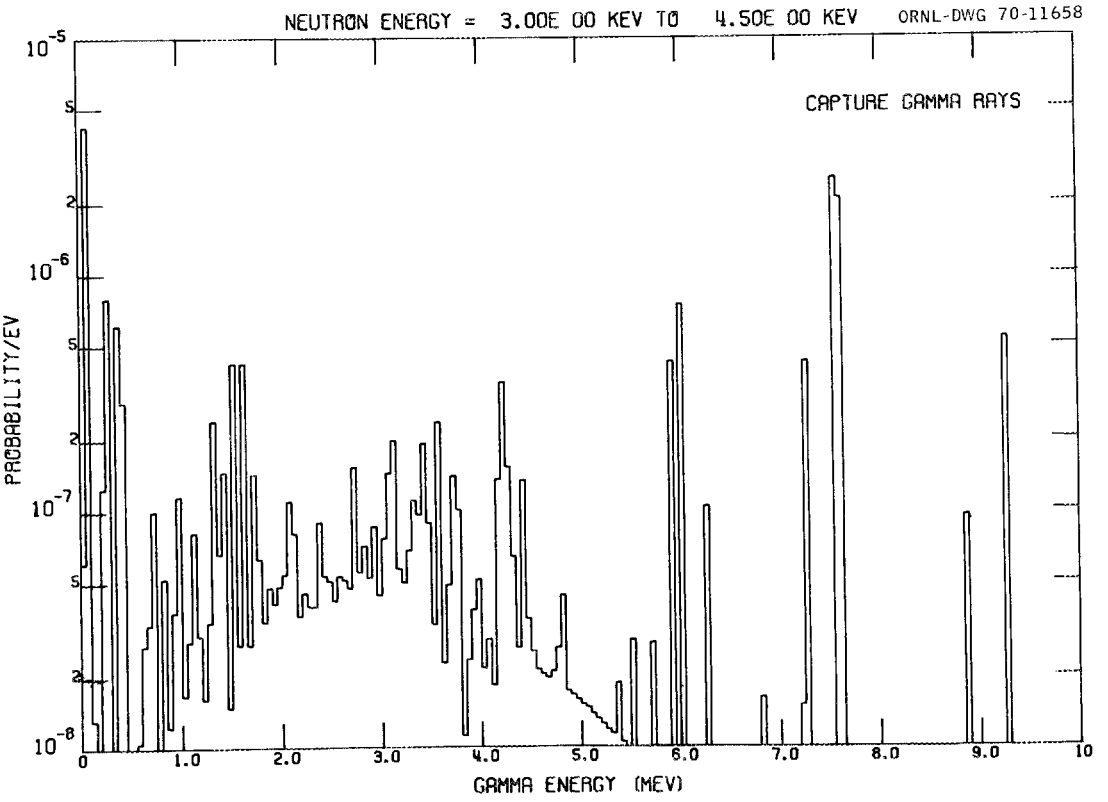

Fig. 66. Energy Distribution of Gamma Rays Resulting From the Radiative Capture of Neutrons in the Energy Range 3 to 4.5 keV.

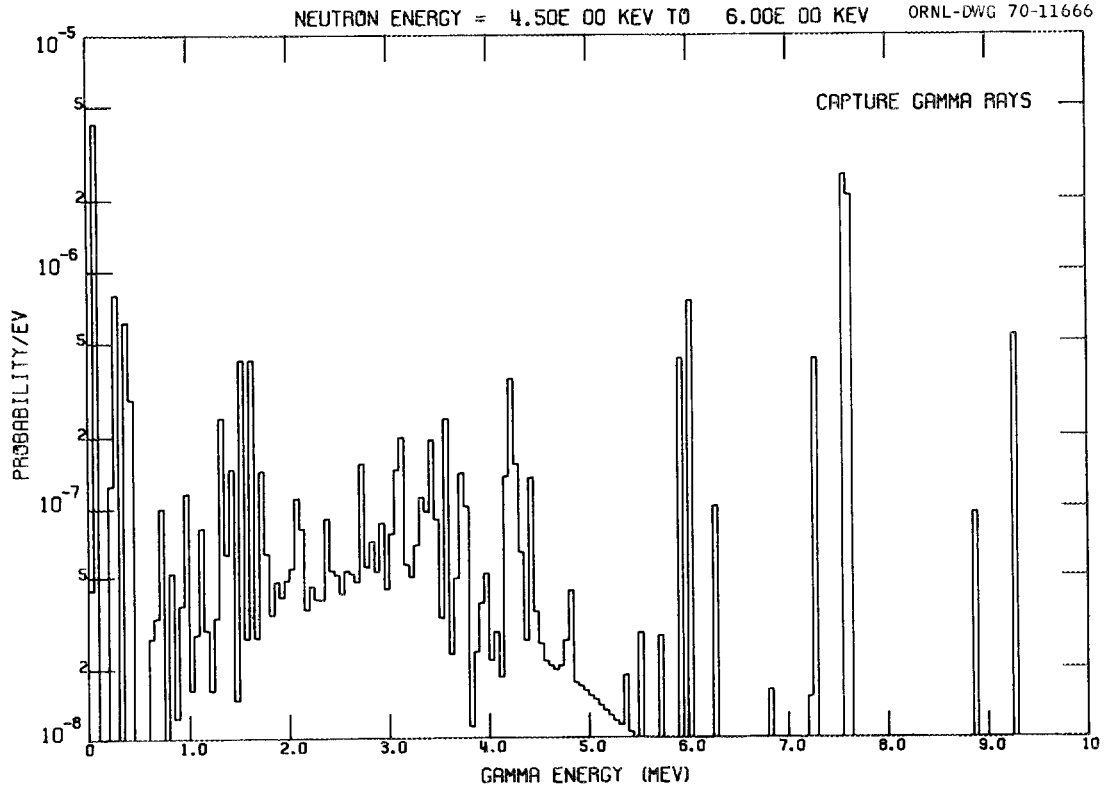

Fig. 67. Energy Distribution of Gamma Rays Resulting From the Radiative Capture of Neutrons in the Energy Range 4.5 to 6 keV.

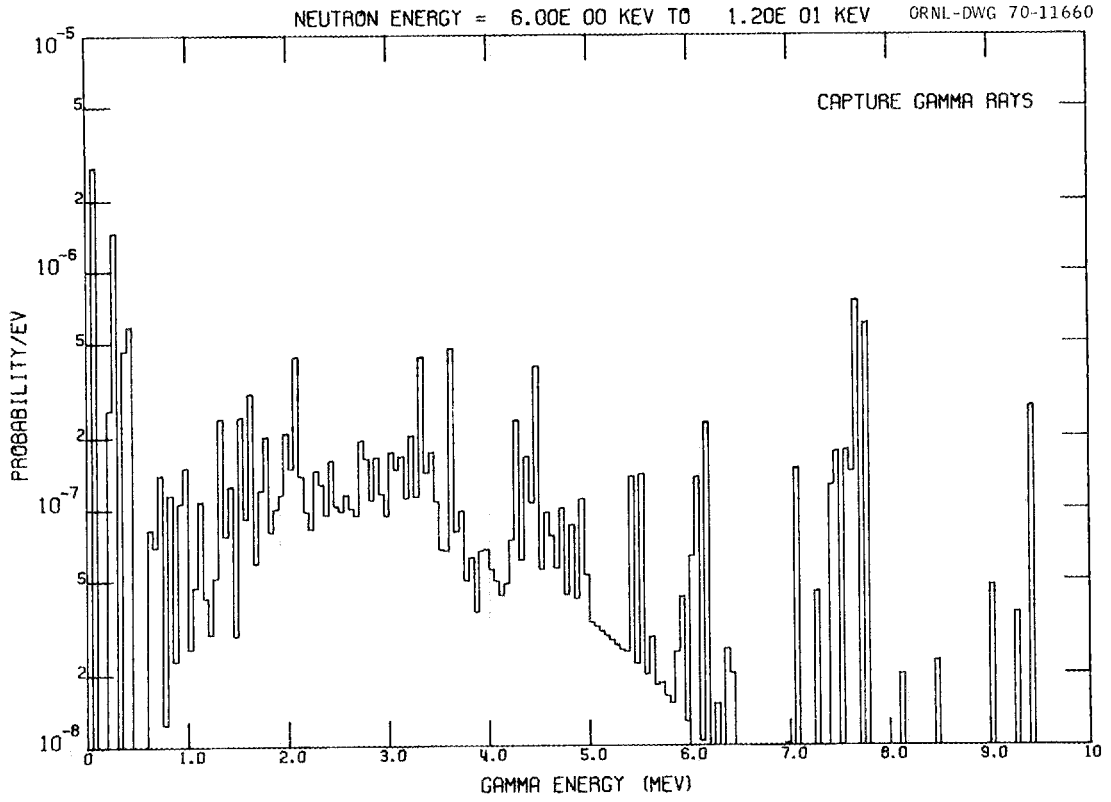

Fig. 68. Energy Distribution of Gamma Rays Resulting From the Radiative Capture of Neutrons in the Energy Range 6 to 12 keV.

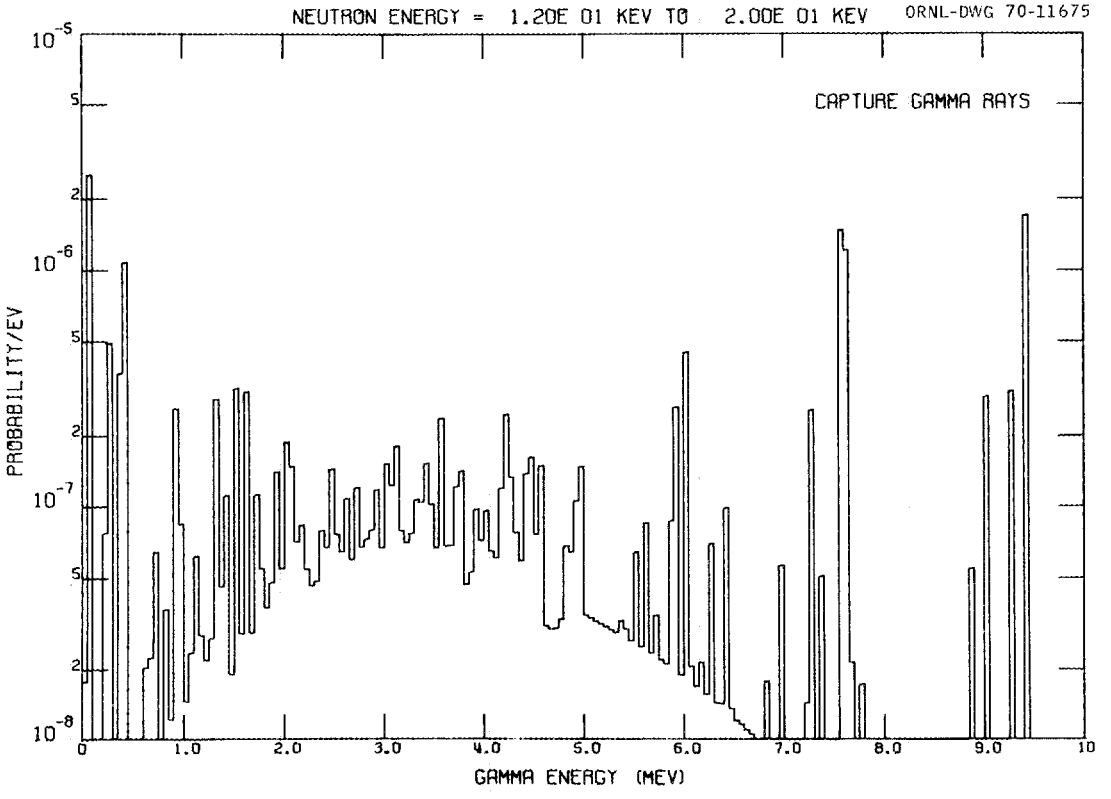

Fig. 69. Energy Distribution of Gamma Rays Resulting From the Radiative Capture of Neutrons in the Energy Range 12 to 20 keV.

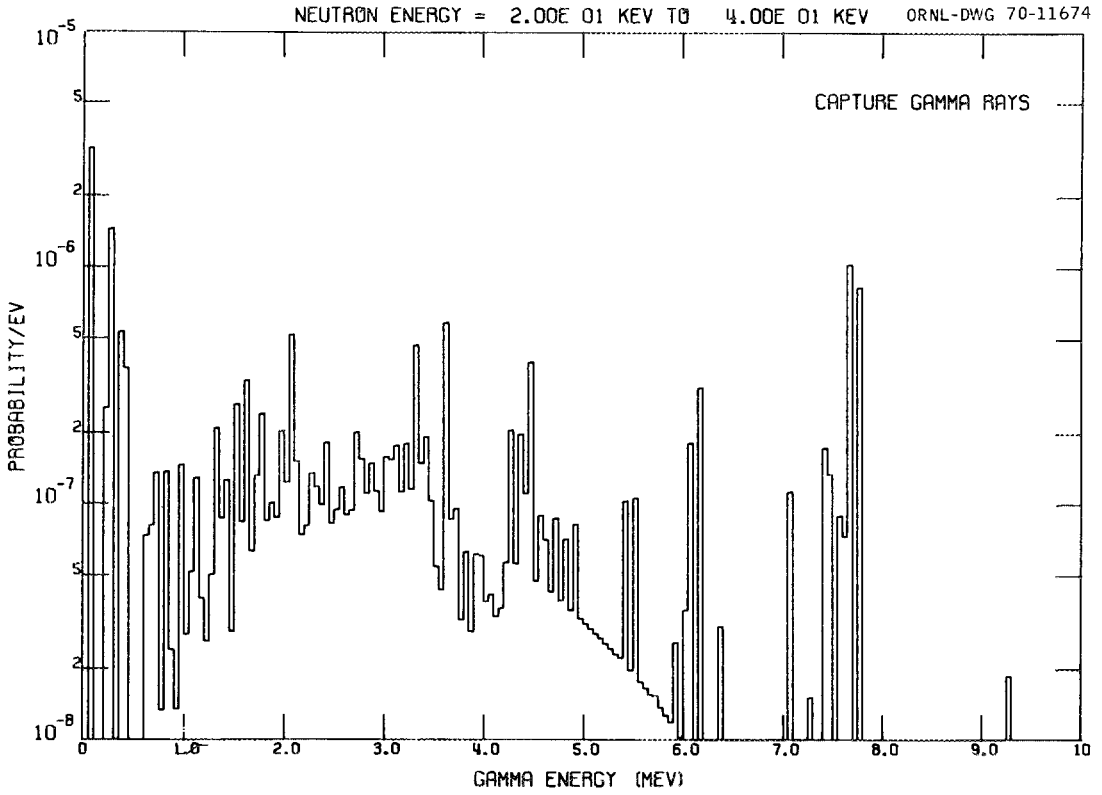

Fig. 70. Energy Distribution of Gamma Rays Resulting From the Radiative Capture of Neutrons in the Energy Range 20 to 40 keV.

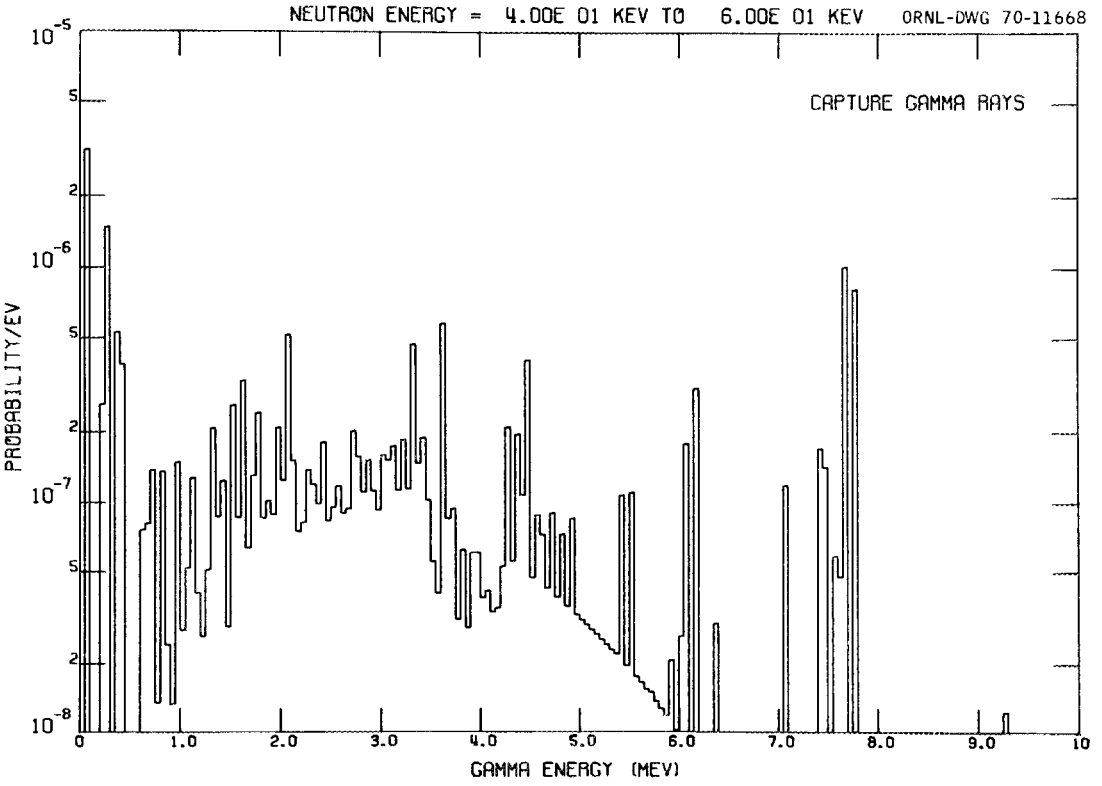

Fig. 71. Energy Distribution of Gamma Rays Resulting From the Radiative Capture of Neutrons in the Energy Range 40 to 60 keV.

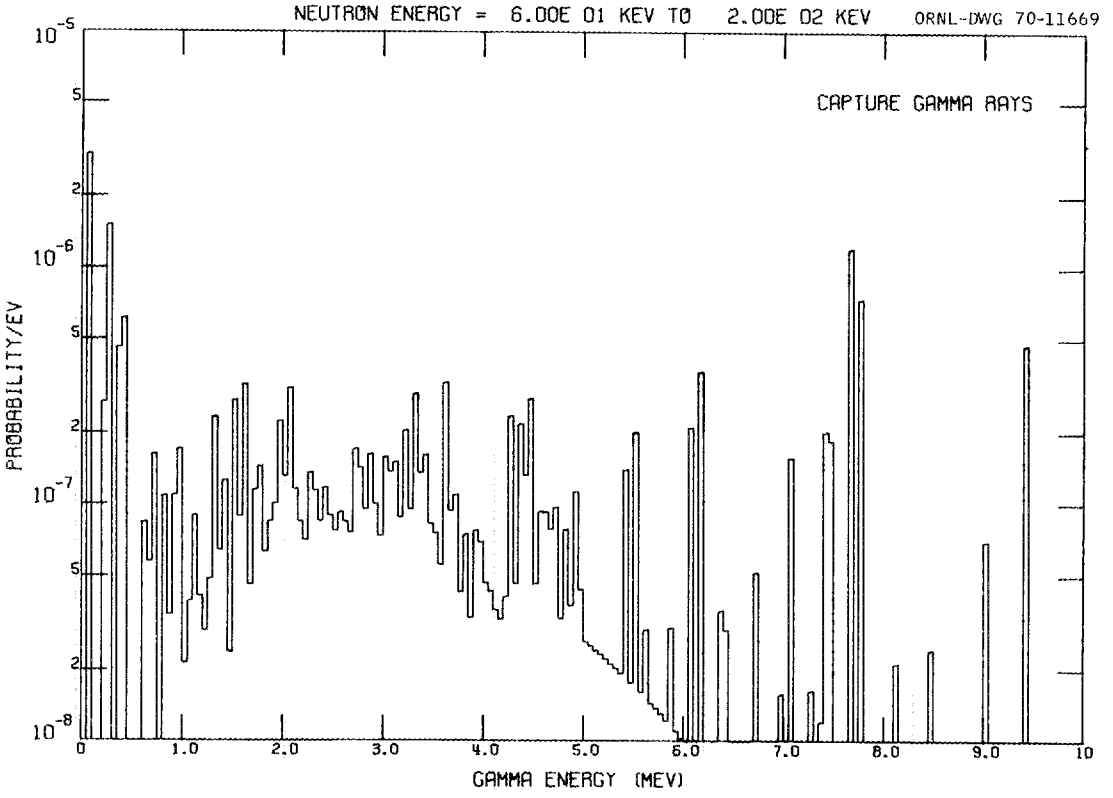

Fig. 72. Energy Distribution of Gamma Rays Resulting From the Radiative Capture of Neutrons in the Energy Range 60 to 200 keV.

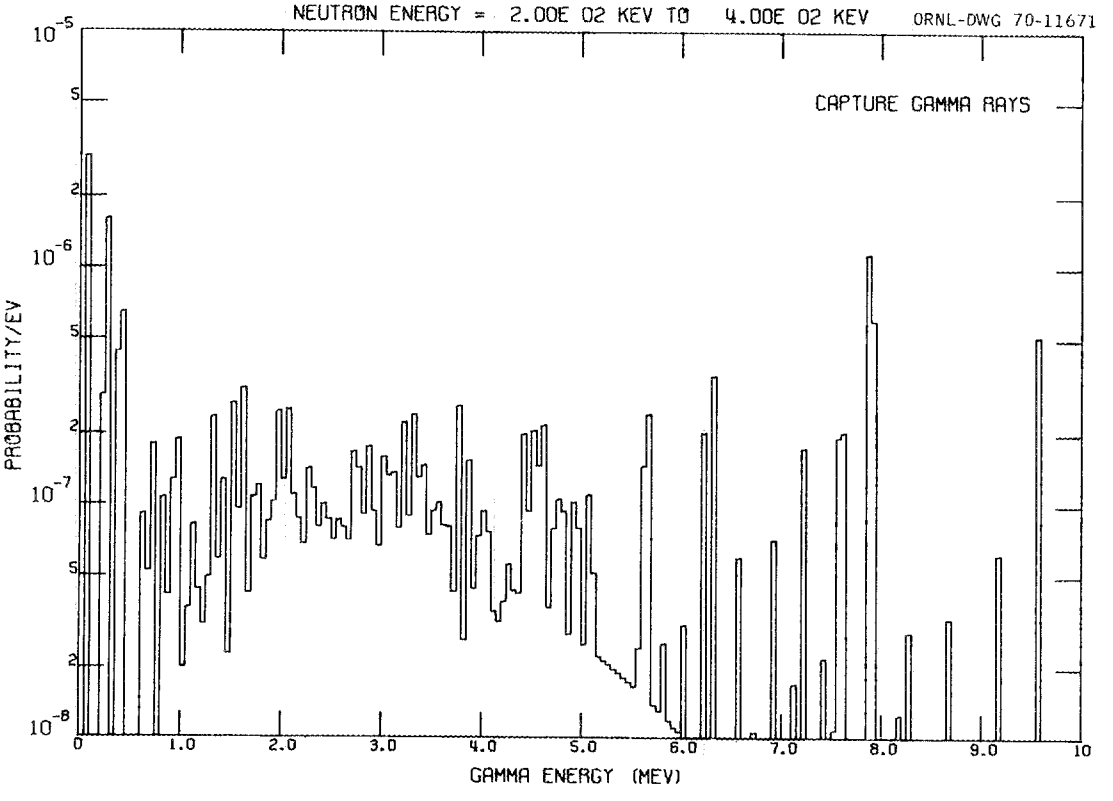

Fig. 73. Energy Distribution of Gamma Rays Resulting From the Radiative Capture of Neutrons in the Energy Range 200 to 400 keV.

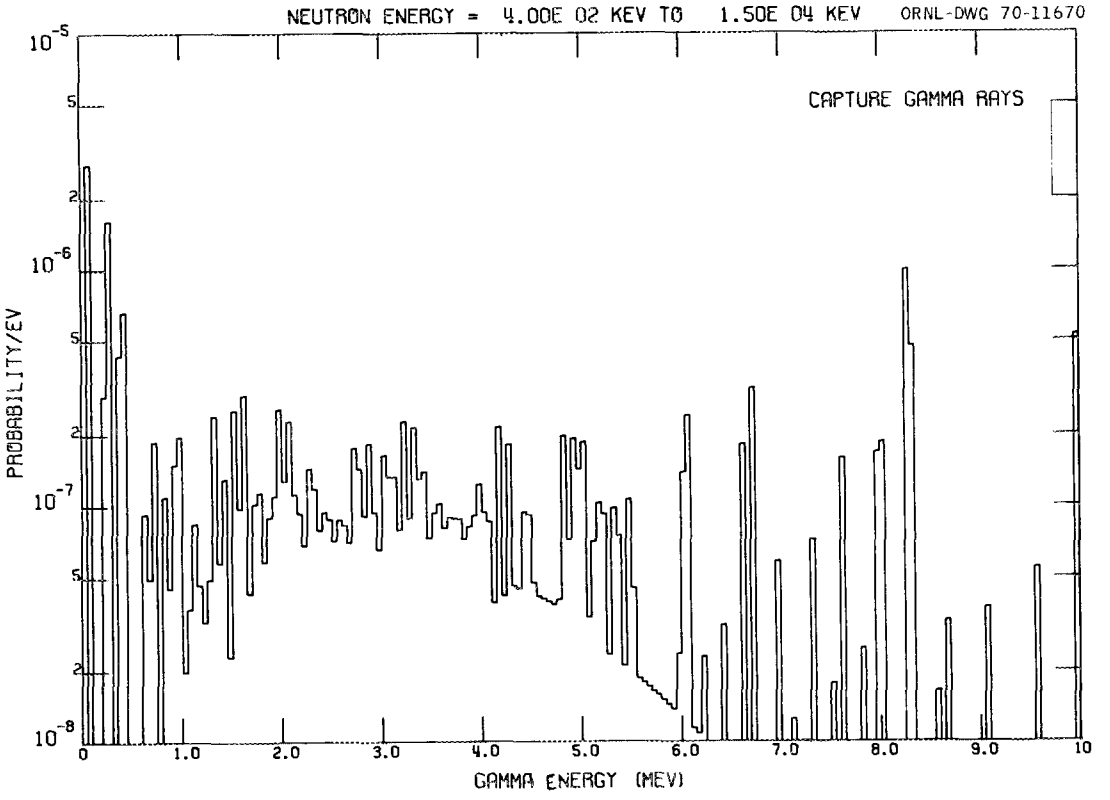

Fig. 74. Energy Distribution of Gamma Rays Resulting From the Radiative Capture of Neutrons in the Energy Range 0.4 to 15 MeV.

Neutron Inelastic Scattering Gamma-Ray Production

Since the calculations of the inelastic scattering cross sections described previously were successful, we decided to calculate the gamma-ray production arising from de-excitation of states excited by inelastic scattering of neutrons. We realized that the 41 nuclear states for ^{56}Fe used in the neutron calculations would not be sufficient and that the use of a continuum model would either entail undesirable approximations such as spin and parity independence of the spectra or involve a large data handling problem. Extensive shell-model calculations had been performed by McGrory,[54] so we naturally thought of using the states predicted by these calculations for energies above 4 MeV. When the cumulative number of levels was plotted versus excitation energy and compared with that predicted by the level density models which we had already used successfully, the number of states predicted by the shell model was found to be deficient. We then assumed that the shell-model calculations provided levels with correct spin-parity distribution and that the level density formula predicted correctly the total number of levels of all spins and parities. Therefore, in the statistical model calculations the excitation energy spectra were divided into three regions. The first region extended to 5.25 MeV and the levels were treated as discrete levels. The second energy region extended to 9 MeV and the levels were discrete but weighted by the number of levels the level density formula would have predicted. The third energy region extended beyond 9 MeV and was considered to be a continuum region. A total of 255 levels were used which had spins less than 6.

The computer program HELGA, which is a modification of HELENE,[19] was used to generate the gamma-ray production data. These calculations only included the discrete gamma-ray cascade, although a continuum model was programmed. The gamma rays had energies less than 9 MeV. These were collected into 50-keV energy bins rather than treating each gamma ray separately. The branching ratios were taken from Henrichsen *et al.*,[20] but those that were not known experimentally were calculated in the program by assuming the E2/M1 and M1/E1 ratios to be 0.2 and 0.25, respectively.

The calculations were compared with measurements made by Dickens[55] for three neutron energies. These results appeared to be in satisfactory agreement and are

shown in Tables XII–XIV. Other comparisons were made with a measurement by Maerker and Muckenthaler[56] and with calculations of Celnik and Spielberg.[57] The neutron energies were integrated over a reactor neutron spectrum for these cases. The agreement here was also satisfactory, although some 60 mbns should be added to the 1.0- to 1.5-MeV calculated value due to ^{54}Fe. The results are shown in Table XV. The 0.846-MeV gamma ray is anisotropic to a small extent as indicated by the experimental results. We did not incorporate the anisotropy because it is small and it is probably unimportant to the calculation of secondary gamma-ray dose as indicated by Straker.[58] The production cross sections are presented as multiplicities, relative to the total inelastic cross section in Table XVI, and probability densities of emitting gamma rays with energies in 50-keV bins as shown in Figs. 75–96 for the energy range 2.122 MeV to 15 MeV. This excludes the gamma ray from the first excited state of ^{54}Fe. The gamma rays from this state of ^{54}Fe and the first excited state of ^{56}Fe in the energy range 0.861 MeV to 2.122 MeV are given in the evaluation as relative to their excitation cross sections and, hence, have multiplicities of unity.

Table XII. Differential Cross Sections for Gamma-Ray Production Via Neutron Inelastic Scattering in Iron
E_n = 5.35 MeV

Differential Cross Sections (mbns/sr.)

E_γ (keV)	Calculation	Experiment	
		55°	90°
846	109.9	85.0	81.7
1038	5.4	5.7	5.7
1168 + 1175	1.5	2.1	2.2
1238	28.8	23.9	22.6
1811	9.9	9.3	10.6
2113	7.2	5.5	5.9
2523	5.2	5.3	4.5
3202	2.6	2.4	1.9
3445 + 3451	2.7	2.5	3.5
3548	3.4	2.0	2.2

Table XV. Gamma-Ray Production Cross Sections in Iron for a Reactor Spectrum (mbns)

Gamma-Ray Energy Interval (MeV)	This Calculation	Maerker's Experiment	Celnik's Calculation
0.5–1.0	905	600	1100
1.0–1.5	153	278	307
1.5–2.0	82	110	
2.0–2.5	83	101	198
2.5–3.0	77	74	
3.0–3.5	29	44	78
3.5–4.0	38	33	
4.0–4.5	12.7	8.7	14
4.5–5.0	8.9	5.6	
5.0–5.5	4.4	3.8	8.5
5.5–6.0	2.8	2.4	
6.0–6.5	1.7	2.1	2.0
6.5–7.0	0.6	<0.6	

Table XIII. Differential Cross Sections for Gamma-Ray Production Via Neutron Inelastic Scattering in Iron
E_n = 6.40

Differential Cross Sections (mbns/sr.)

E_γ (keV)	Calculation	Experiment	
		55°	90°
846	106.3	88.0	82.0
1038	5.6	6.5	6.1
1168 + 1175	1.1	2.5	2.1
1238	32.3	28.9	24.5
1811	8.0	9.9	8.9
2113	5.6	5.4	4.9
2523	4.2	3.5	3.4
3202	2.6	1.6	1.8
3445 + 3451	2.7	2.4	2.8
3548	2.8	2.2	2.5

Table XIV. Differential Cross Sections for Gamma-Ray Production Via Neutron Inelastic Scattering in Iron
E_n = 8.50

Differential Cross Sections (mbns/sr.)

E_γ (keV)	Calculation	Experiment	
		55°	90°
846	102.2	93.4	85.1
1038	7.0	7.9	6.4
1168 + 1175	0.8	2.2	1.9
1238	39.6	34.5	31.1
1811	6.6	9.2	8.5
2113	4.7	4.1	3.7
2523	3.6	2.4	2.2
3202	3.4	2.2	1.8
3445 + 3451	3.5	1.8	1.6
3548	2.1	2.0	1.4

Table XVI. Inelastic Scattering Gamma-Ray Multiplicities

Neutron Energy (MeV)	Multiplicity (Photons/Event)	Neutron Energy (MeV)	Multiplicity (Photons/Event)
2.122	1.000	5.200	1.983
2.240	1.031	5.440	2.011
2.500	1.080	5.740	2.054
2.740	1.200	6.000	2.087
3.000	1.310	6.440	2.159
3.340	1.539	7.240	2.300
3.700	1.678	7.670	2.407
4.000	1.764	8.000	2.480
4.500	1.886	8.560	2.605
4.750	1.929	9.090	2.711
5.000	1.963	15.000	3.904

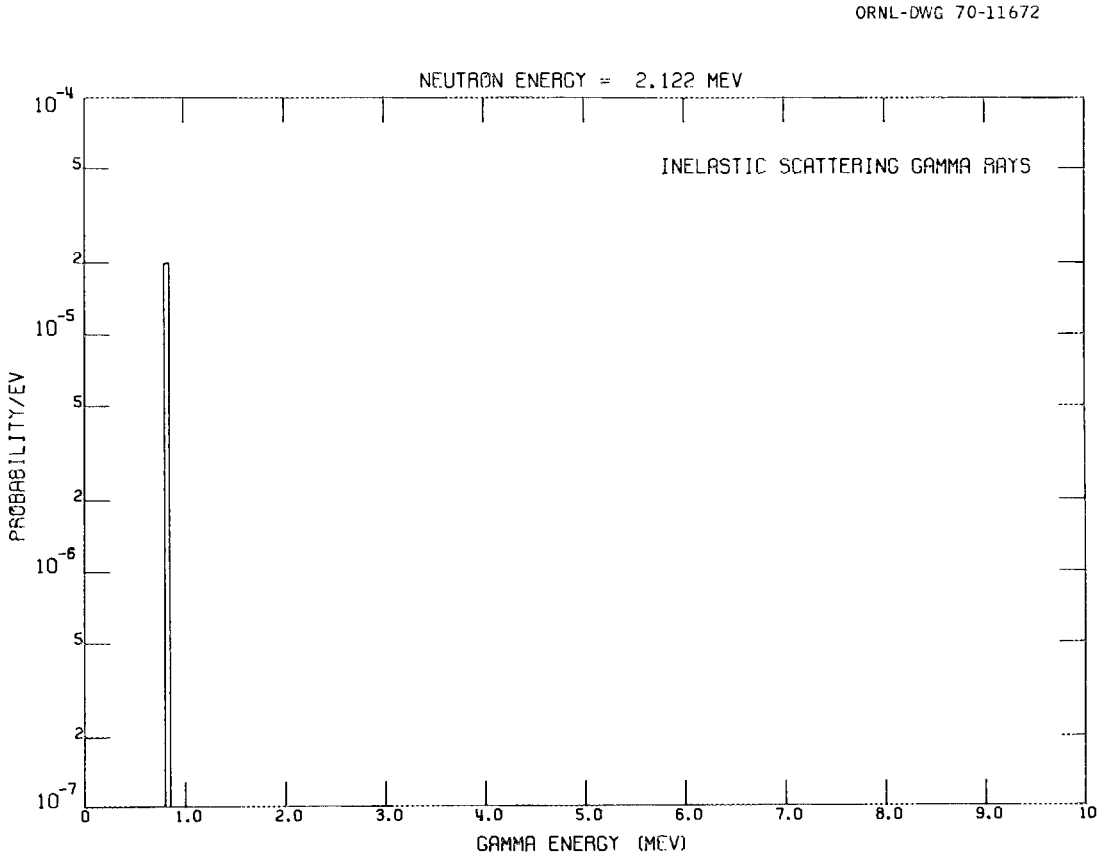

Fig. 75. Energy Distribution of Gamma Rays Resulting From Inelastic Scattering of 2.122-MeV Neutrons.

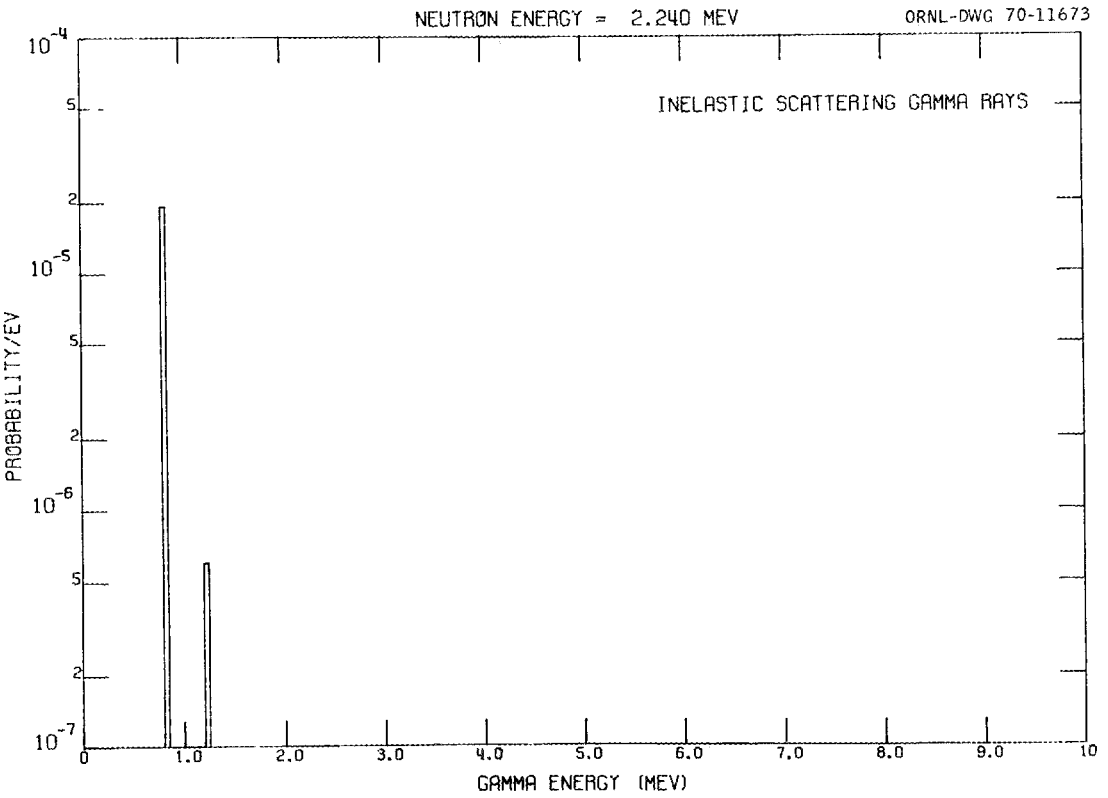

Fig. 76. Energy Distribution of Gamma Rays Resulting From Inelastic Scattering of 2.24-MeV Neutrons.

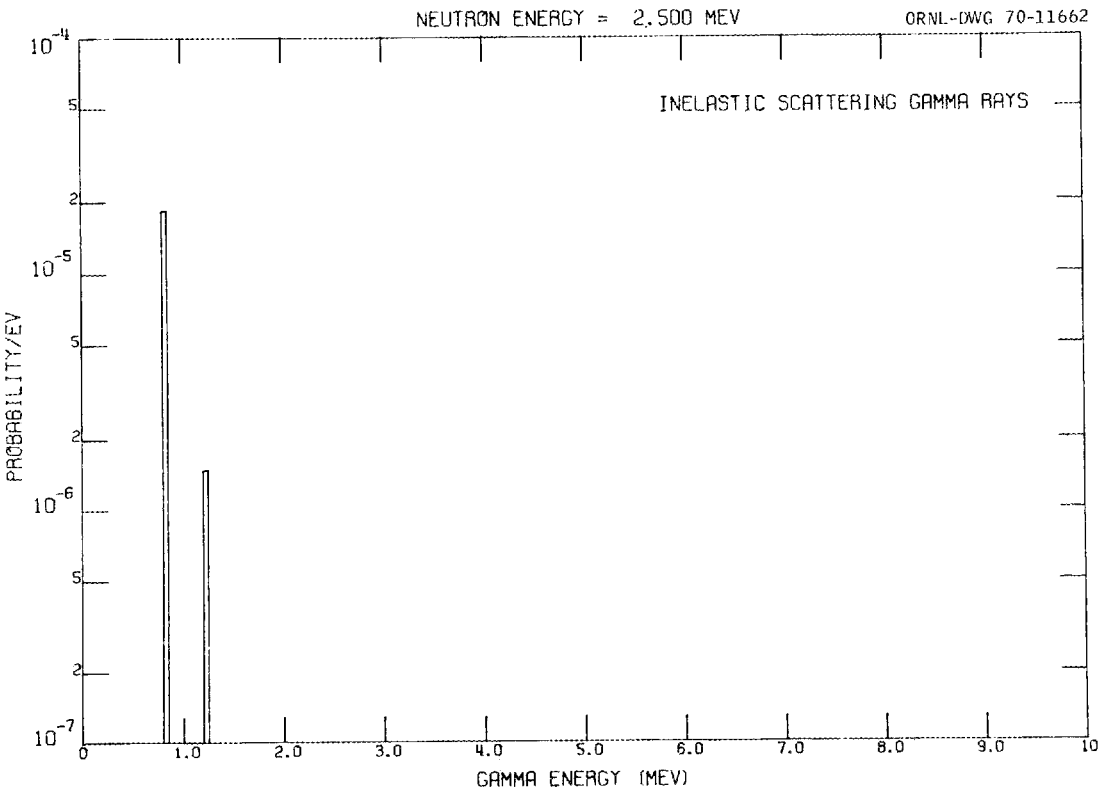

Fig. 77. Energy Distribution of Gamma Rays Resulting From Inelastic Scattering of 2.5-MeV Neutrons.

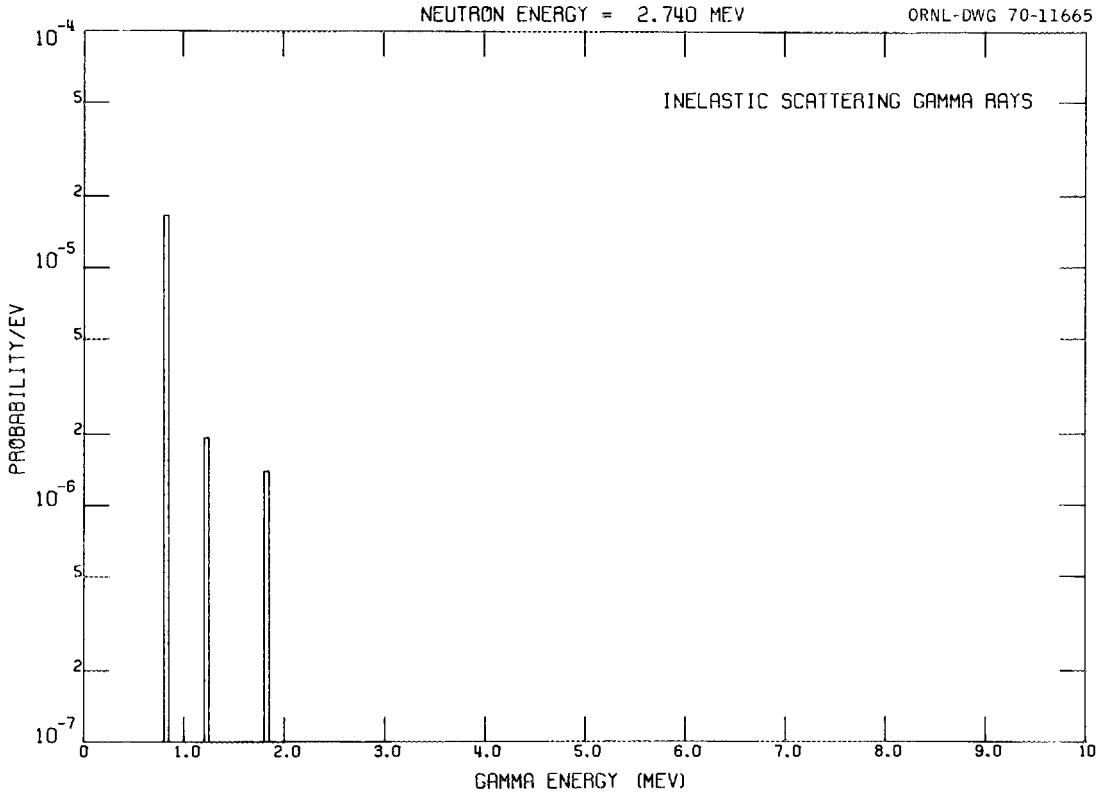

Fig. 78. Energy Distribution of Gamma Rays Resulting From Inelastic Scattering of 2.74-MeV Neutrons.

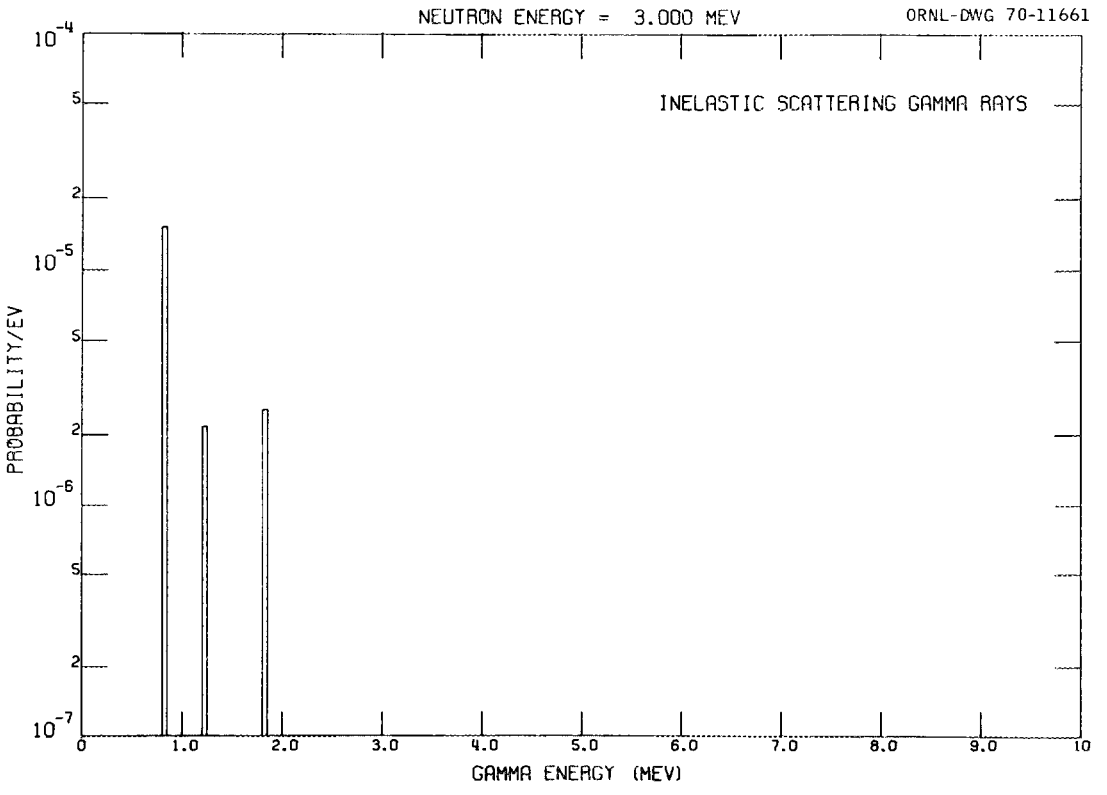

Fig. 79. Energy Distribution of Gamma Rays Resulting From Inelastic Scattering of 3.0-MeV Neutrons.

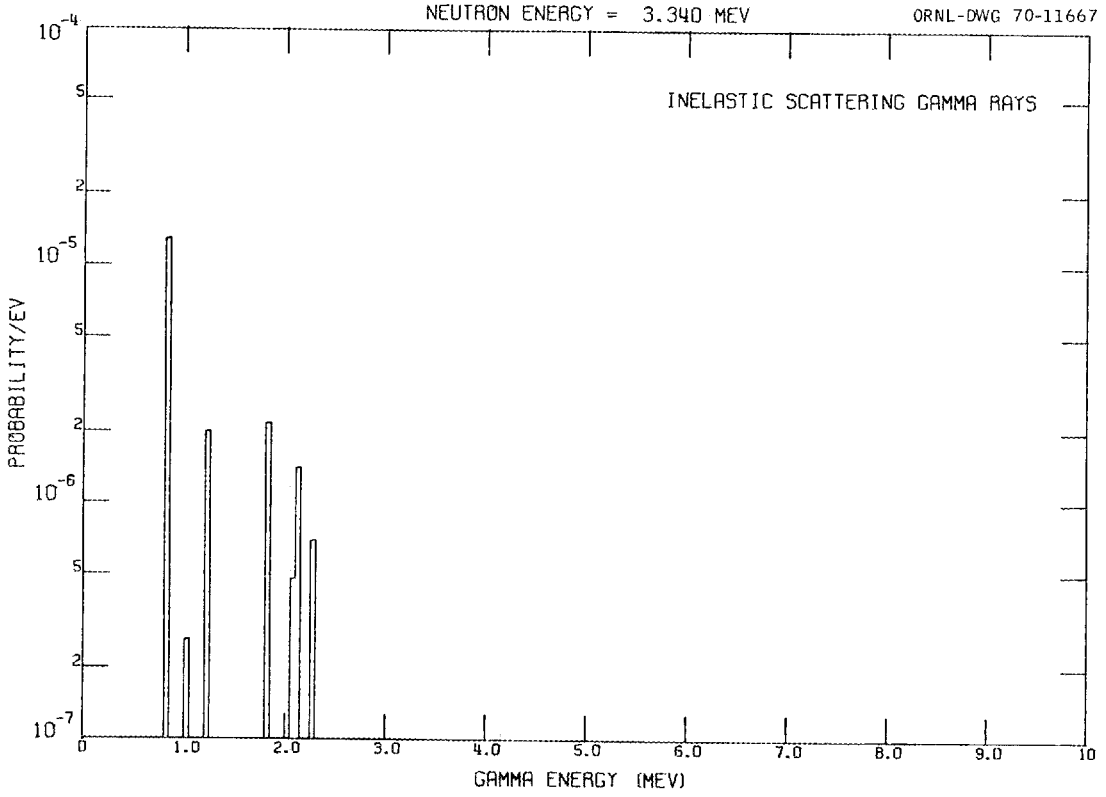

Fig. 80. Energy Distribution of Gamma Rays Resulting From Inelastic Scattering of 3.34-MeV Neutrons.

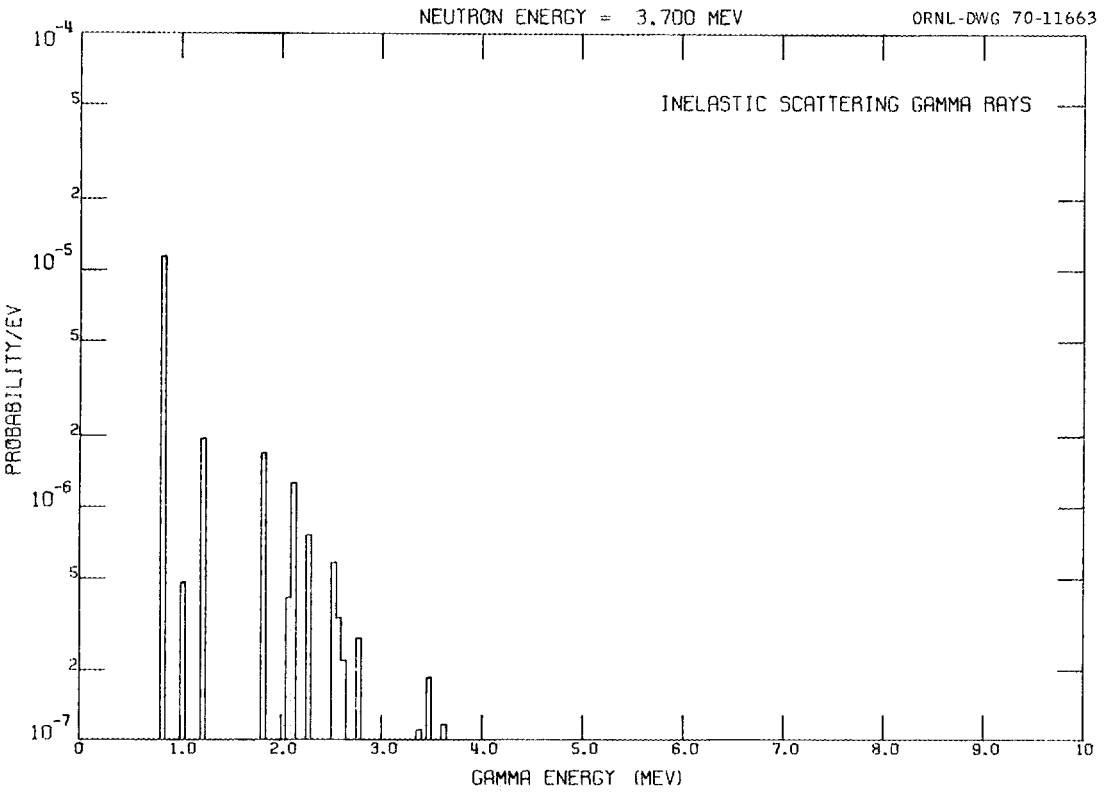

Fig. 81. Energy Distribution of Gamma Rays Resulting From Inelastic Scattering of 3.7-MeV Neutrons

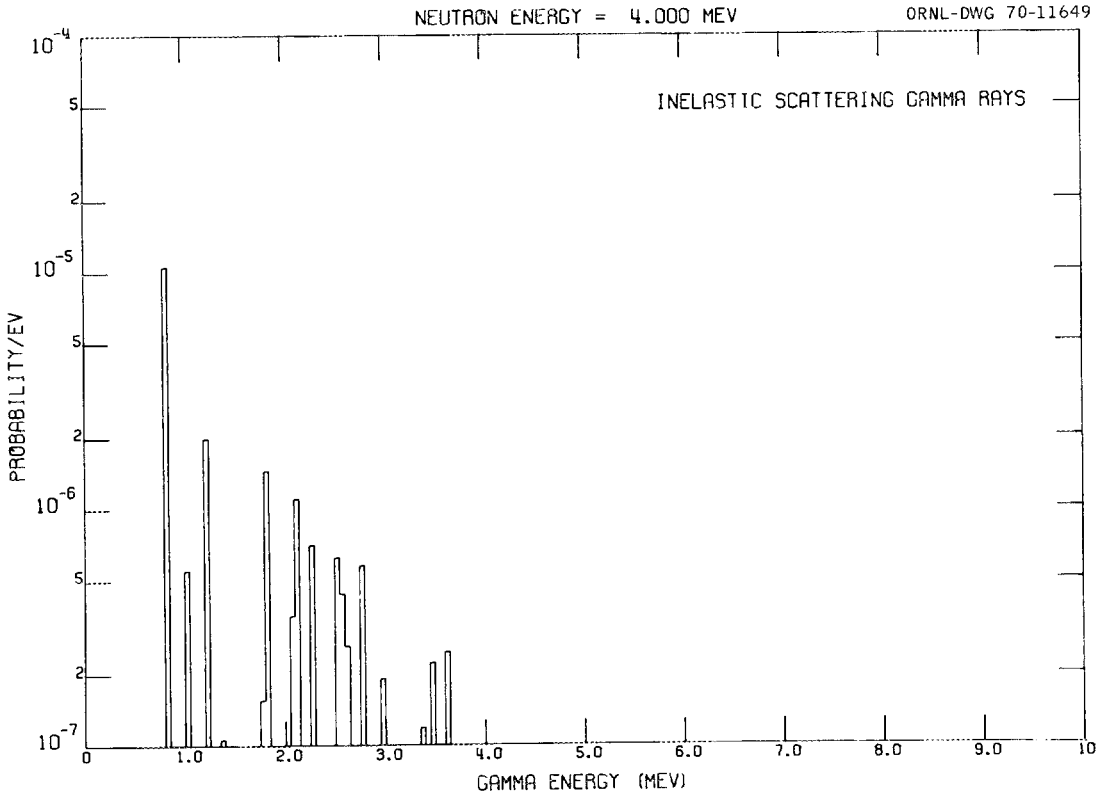

Fig. 82. Energy Distribution of Gamma Rays Resulting From Inelastic Scattering of 4.0-MeV Neutrons.

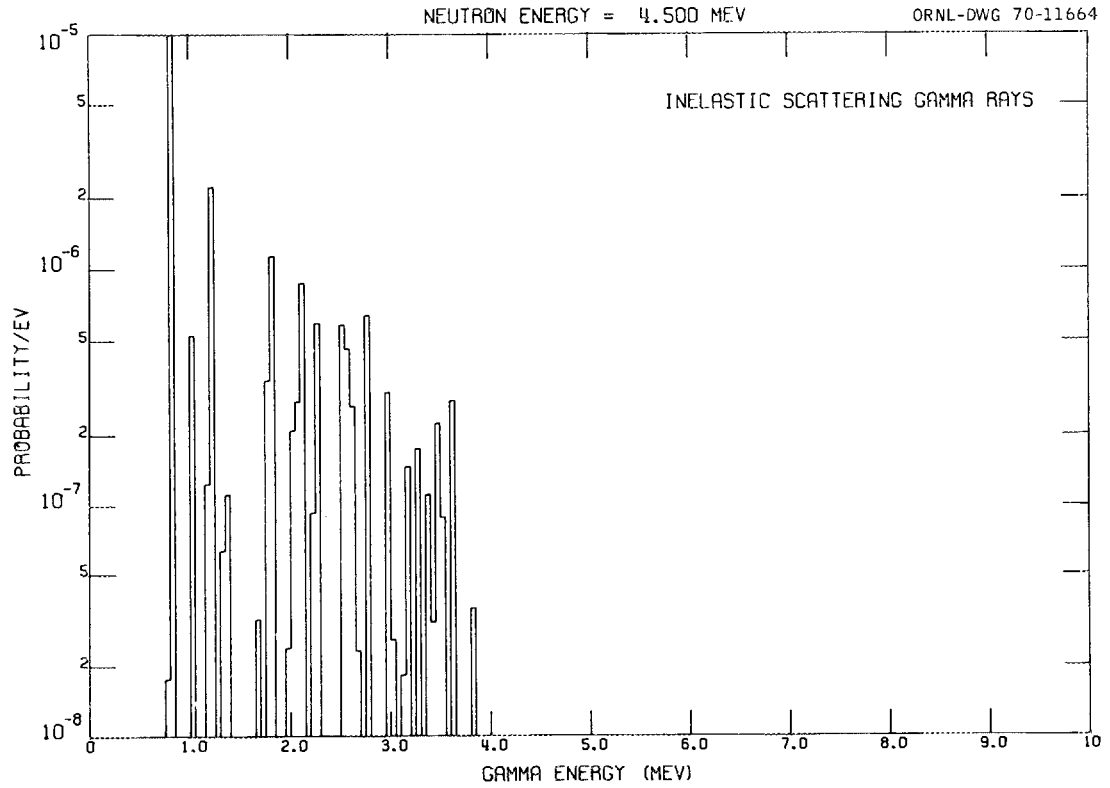

Fig. 83. Energy Distribution of Gamma Rays Resulting From Inelastic Scattering of 4.5-MeV Neutrons.

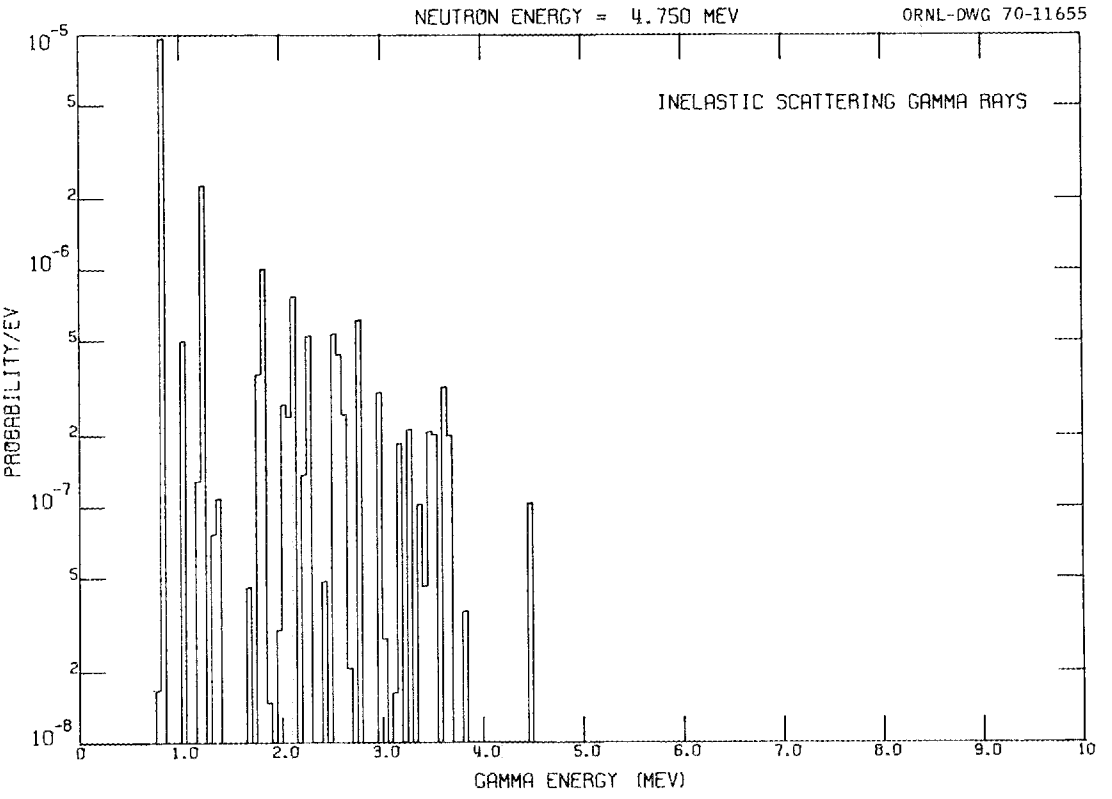

Fig. 84. Energy Distribution of Gamma Rays Resulting From Inelastic Scattering of 4.75-MeV Neutrons.

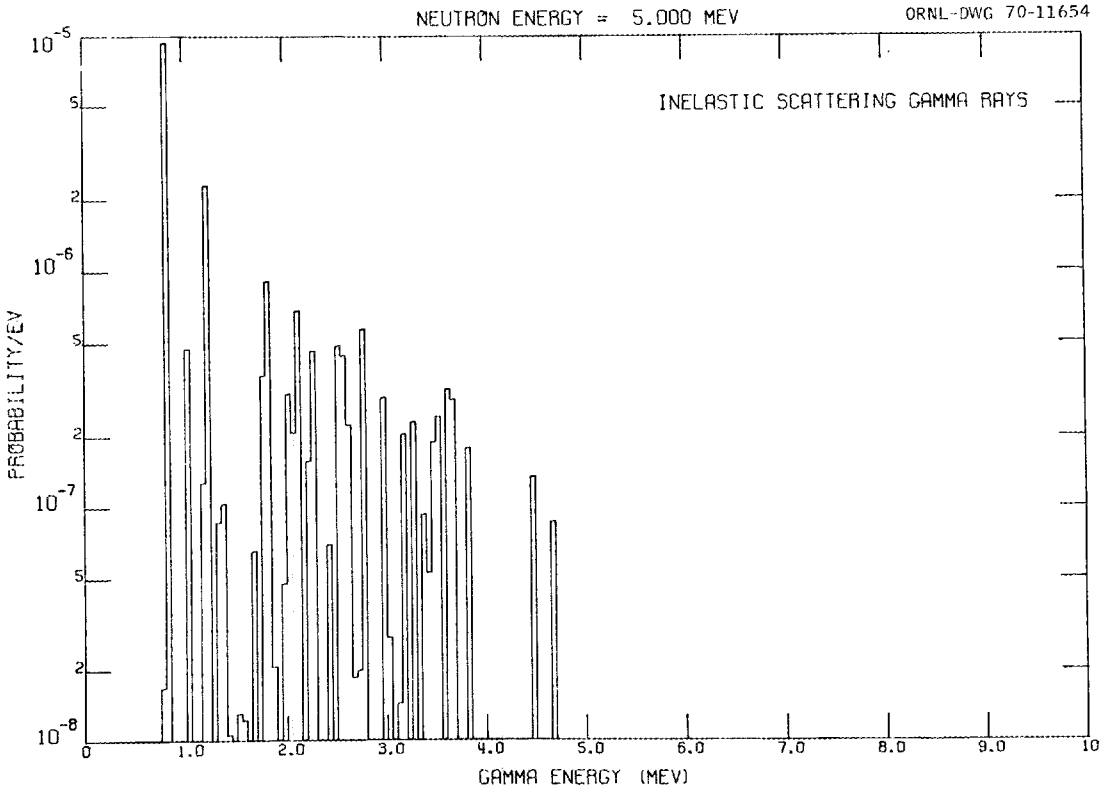

Fig. 85. Energy Distribution of Gamma Rays Resulting From Inelastic Scattering of 5.0-MeV Neutrons.

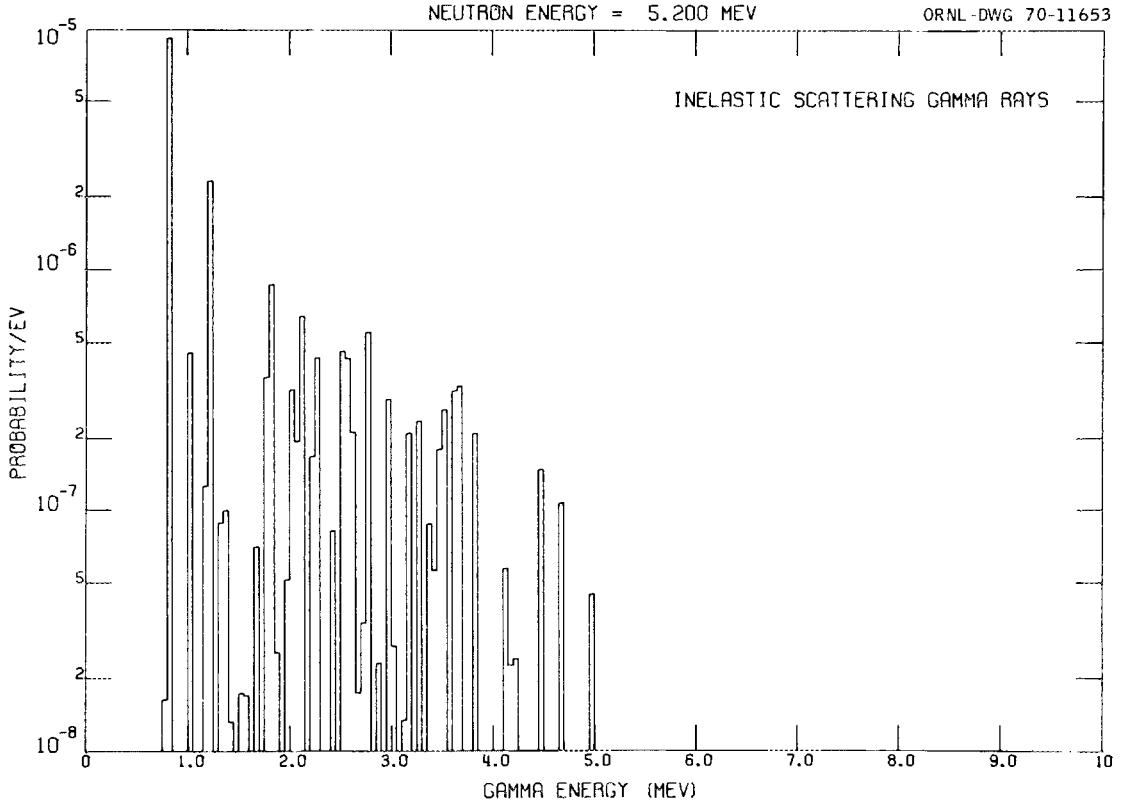

Fig. 86. Energy Distribution of Gamma Rays Resulting From Inelastic Scattering of 5.2-MeV Neutrons.

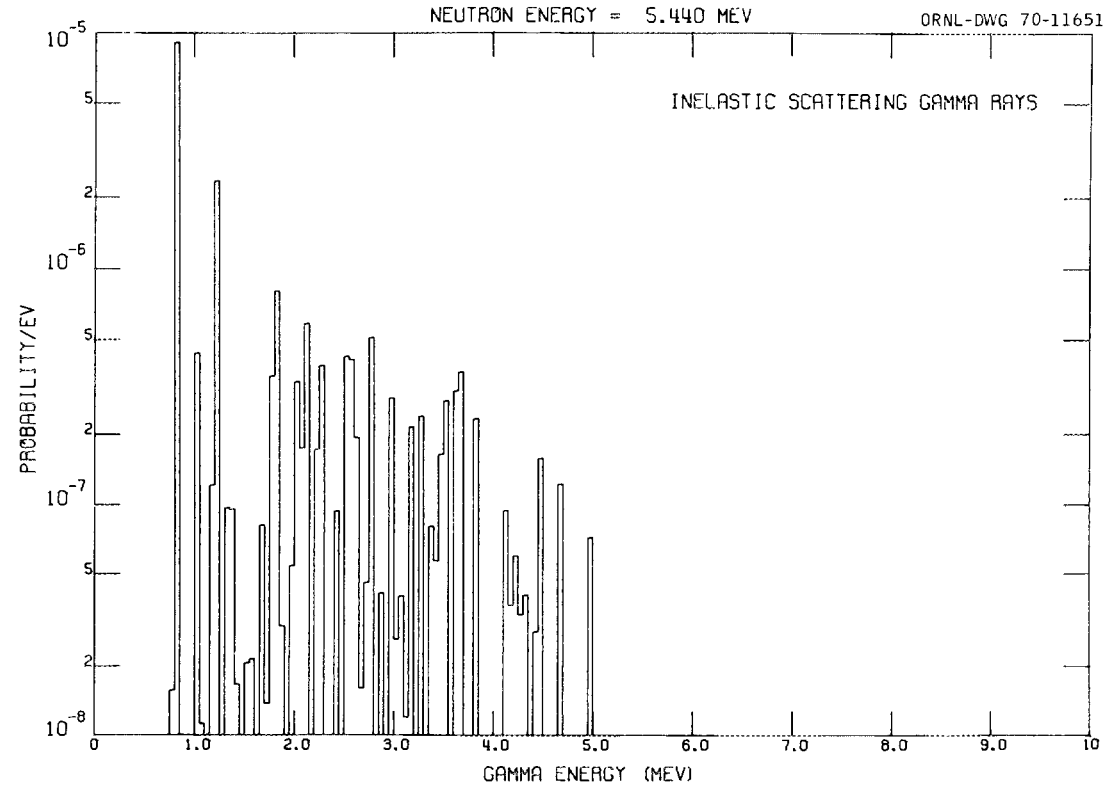

Fig. 87. Energy Distribution of Gamma Rays Resulting From Inelastic Scattering of 5.44-MeV Neutrons.

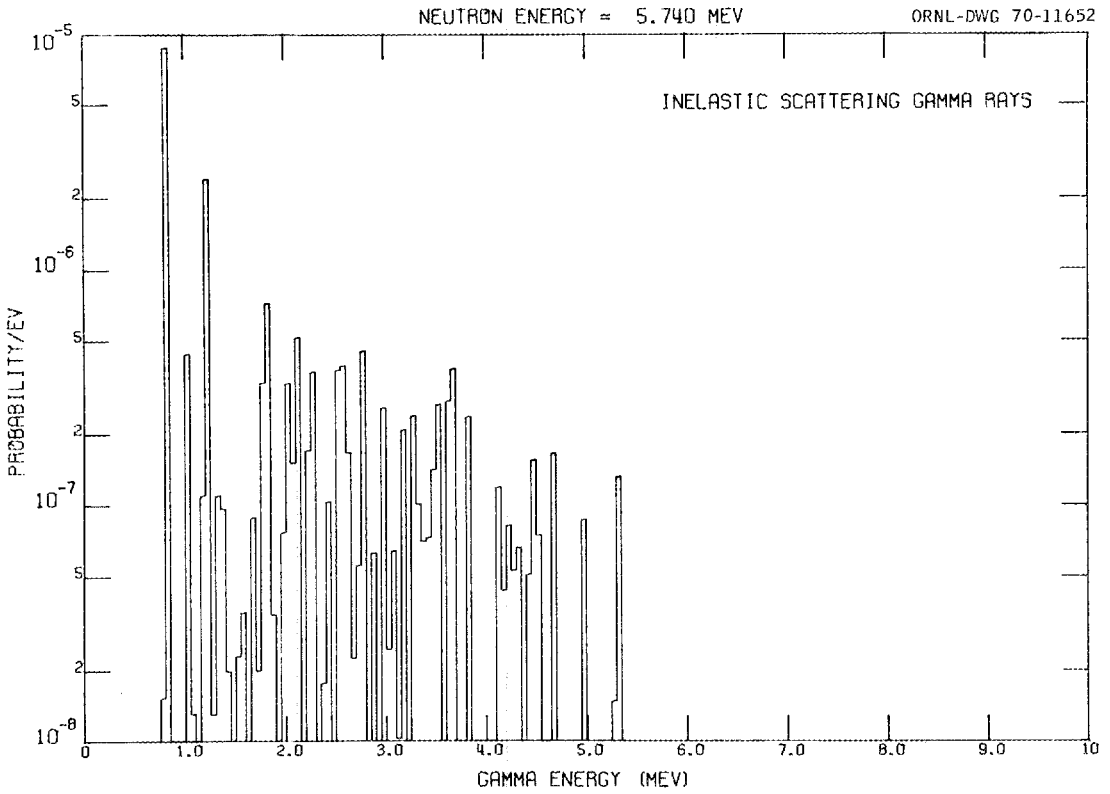

Fig. 88. Energy Distribution of Gamma Rays Resulting From Inelastic Scattering of 5.74-MeV Neutrons.

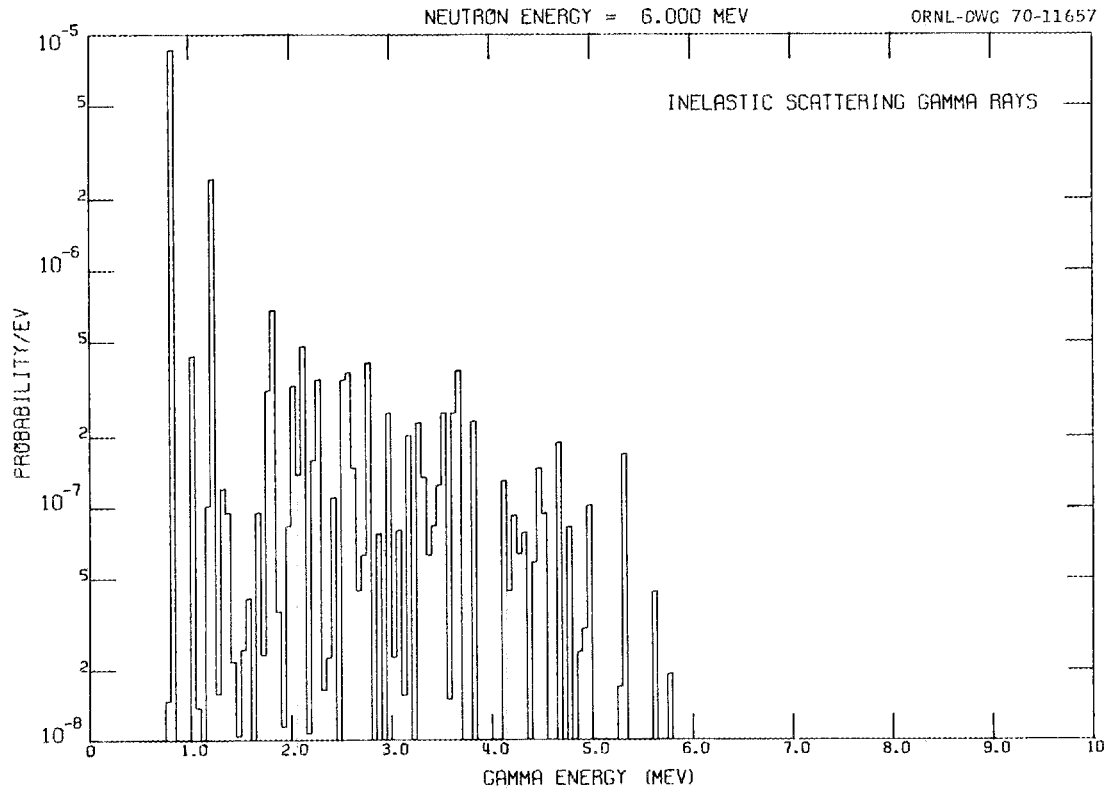

Fig. 89. Energy Distribution of Gamma Rays Resulting From Inelastic Scattering of 6-MeV Neutrons.

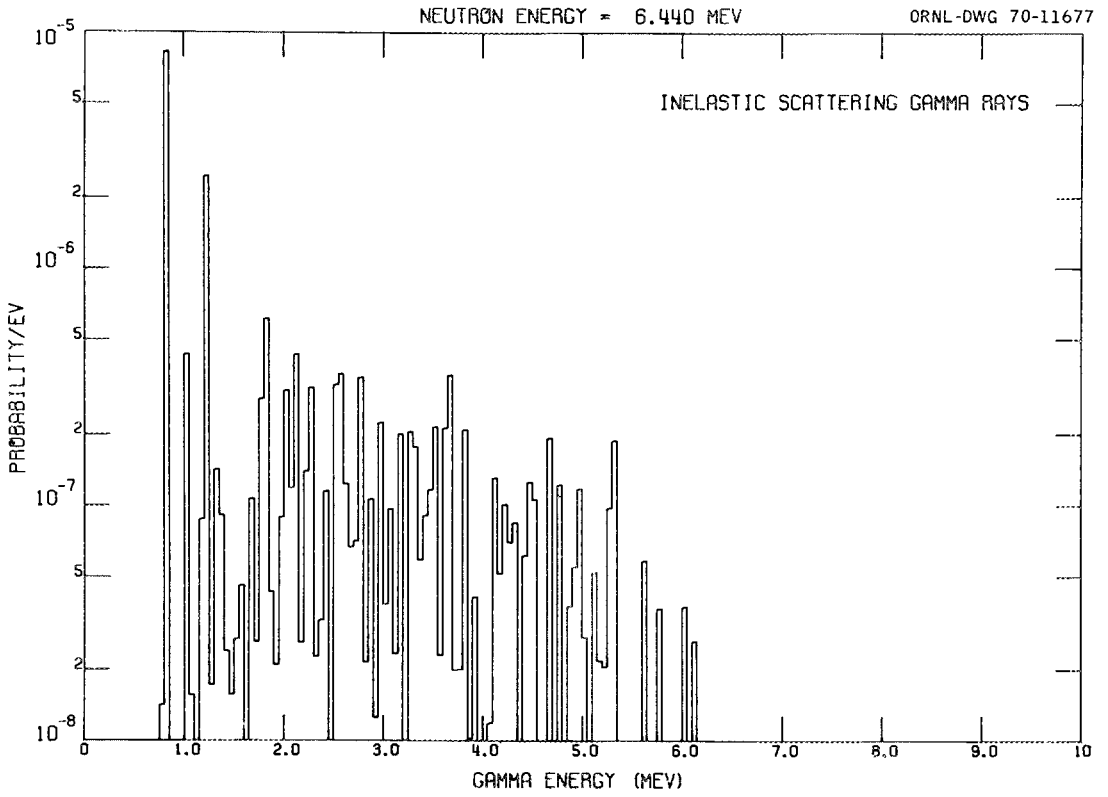

Fig. 90. Energy Distribution of Gamma Rays Resulting From Inelastic Scattering of 6.44-MeV Neutrons.

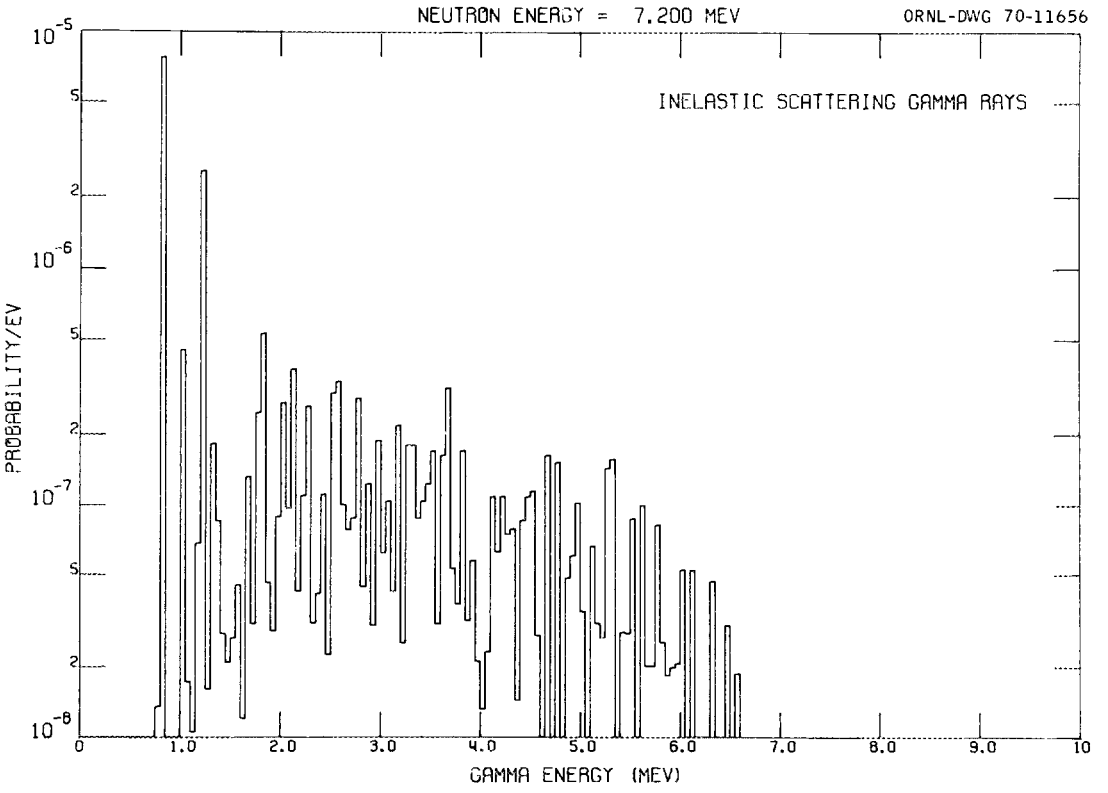

Fig. 91. Energy Distribution of Gamma Rays Resulting From Inelastic Scattering of 7.2-MeV Neutrons.

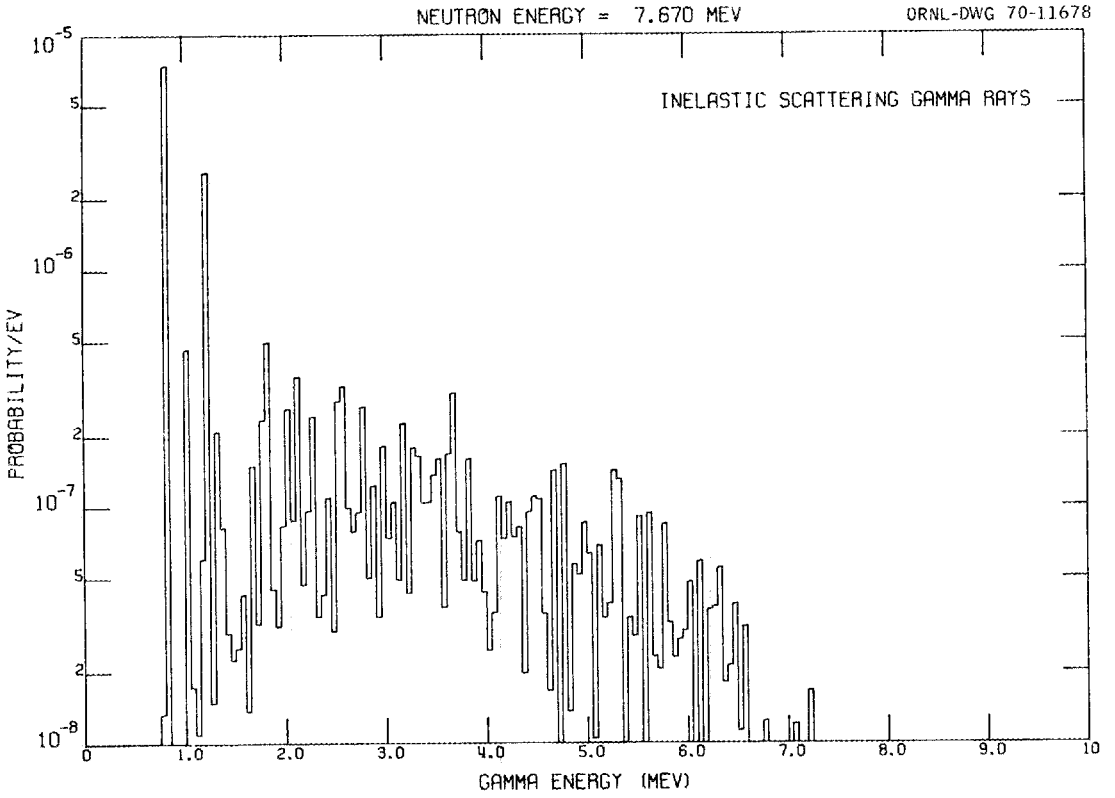

Fig. 92. Energy Distribution of Gamma Rays Resulting From Inelastic Scattering of 7.67-MeV Neutrons.

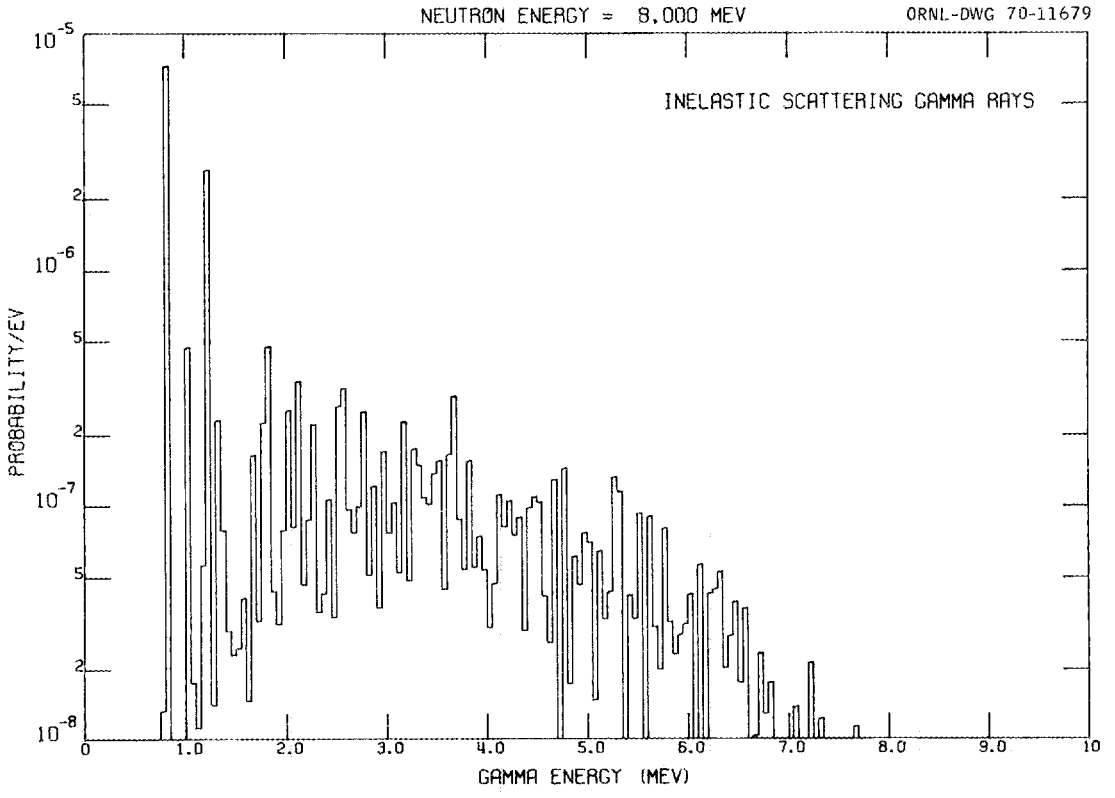

Fig. 93. Energy Distribution of Gamma Rays Resulting From Inelastic Scattering of 8-MeV Neutrons.

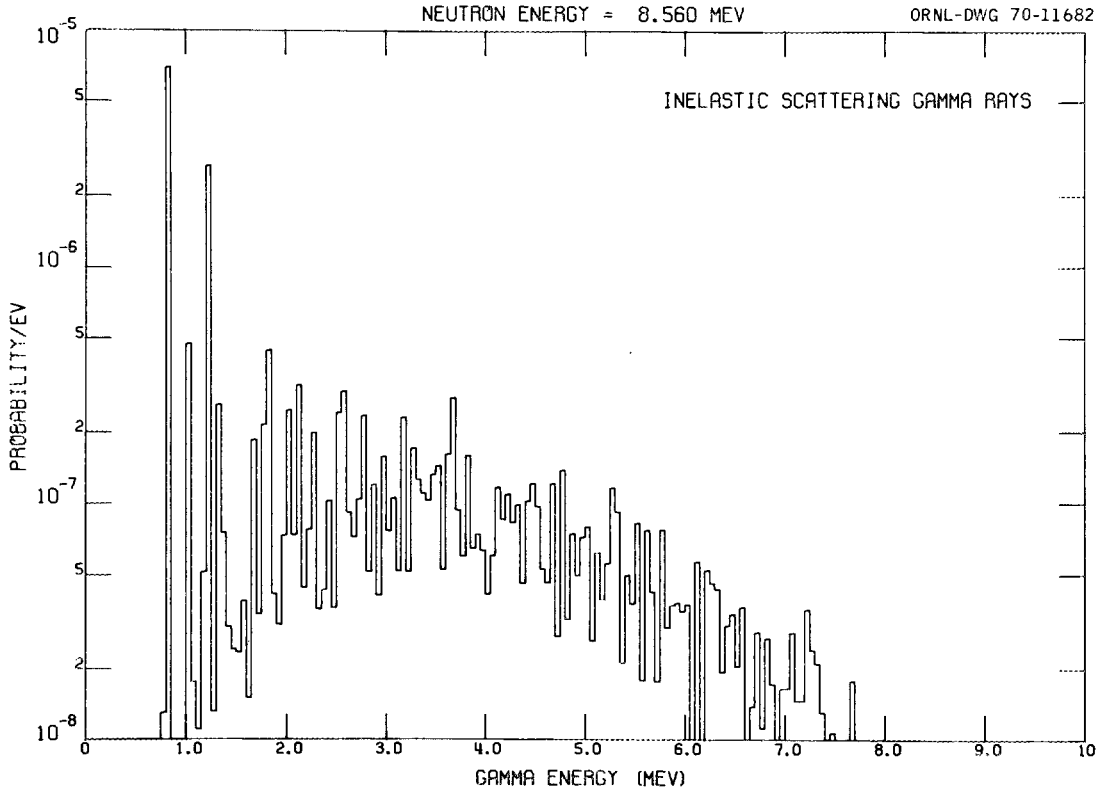

Fig. 94. Energy Distribution of Gamma Rays Resulting From Inelastic Scattering of 8.56-MeV Neutrons.

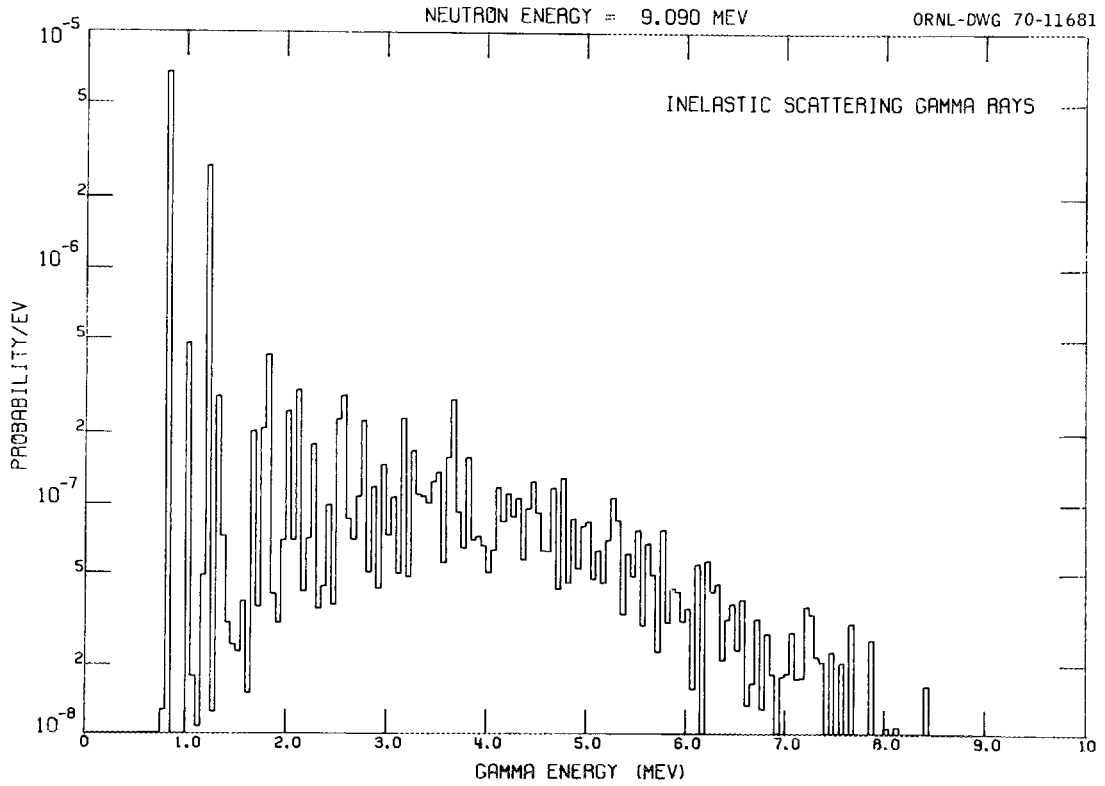

Fig. 95. Energy Distribution of Gamma Rays Resulting From Inelastic Scattering of 9.09-MeV Neutrons.

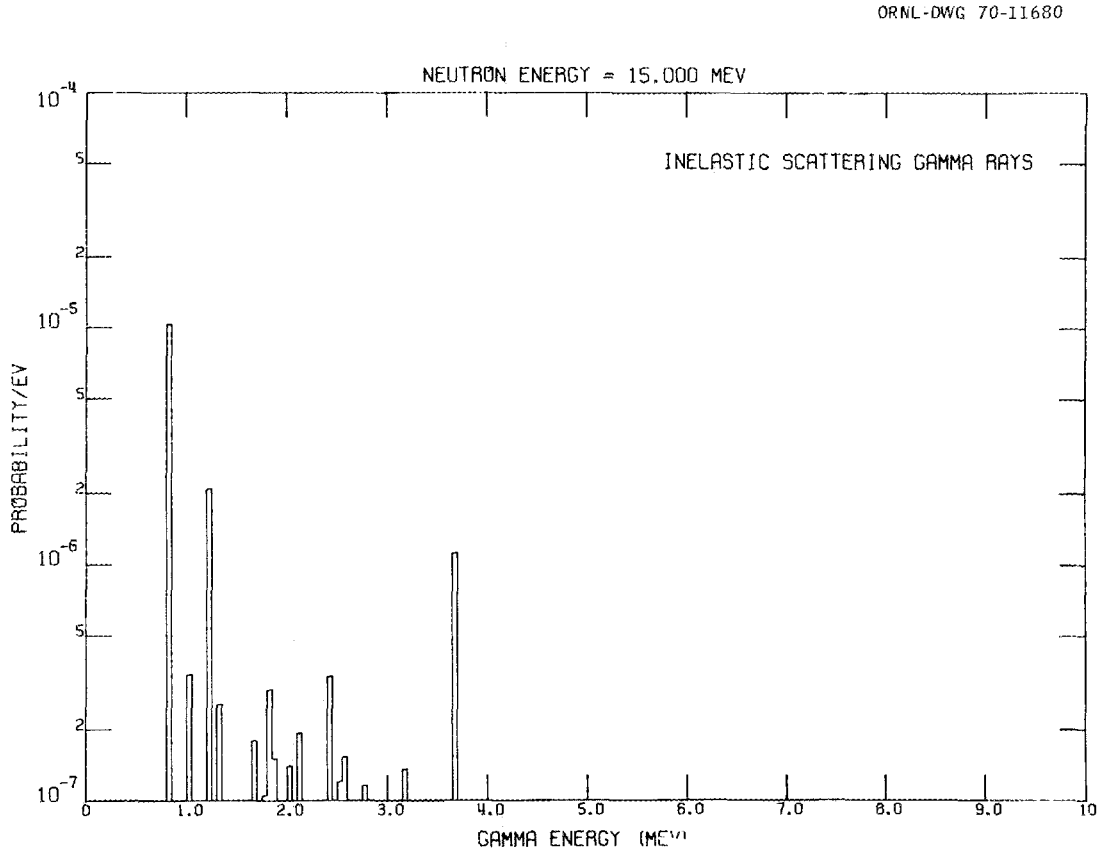

Fig. 96. Energy Distribution of Gamma Rays Resulting From Inelastic Scattering of 15-MeV Neutrons.

V. PHOTON INTERACTION CROSS SECTIONS

Cross sections for photons interacting with iron were obtained from an evaluation by McMaster *et al.*[59] in the energy range 1 keV to 1 MeV and from a compilation by Plechaty and Terrall[60] for the energy range 1 MeV to 100 MeV. The interactions considered were total, coherent scattering, incoherent scattering, pair production plus triplet production, and photoelectric. Only the integrated cross sections were incorporated into the evaluation. These are shown in Figs. 97–101.

VI. CONCLUSIONS

Previous natural iron ENDF/B evaluations have been improved by this re-evaluation in the following areas:

1. The elastic angular distributions have been brought into better agreement with experiment from 0.3 to 15 MeV.
2. The integrated cross sections for inelastic scattering to discrete levels in ^{56}Fe have been extended beyond 5 MeV and smoothed (as appropriate to experimental energy resolutions) by statistical model calculations which agree with experimental data.
3. Experimental data showing resonant structure in the integrated cross section for inelastic scattering to the 0.846-MeV level in ^{56}Fe have been included from threshold to 2.1 MeV.
4. Recently observed structure in the neutron inelastic continuum has been incorporated.
5. Gamma-ray-production cross sections and photon interaction cross sections were included where they had been nonexistent in previous evaluations.

Outside the above areas, previous evaluations and sets of cross sections were combined to agree best, in our opinion, with the latest data.

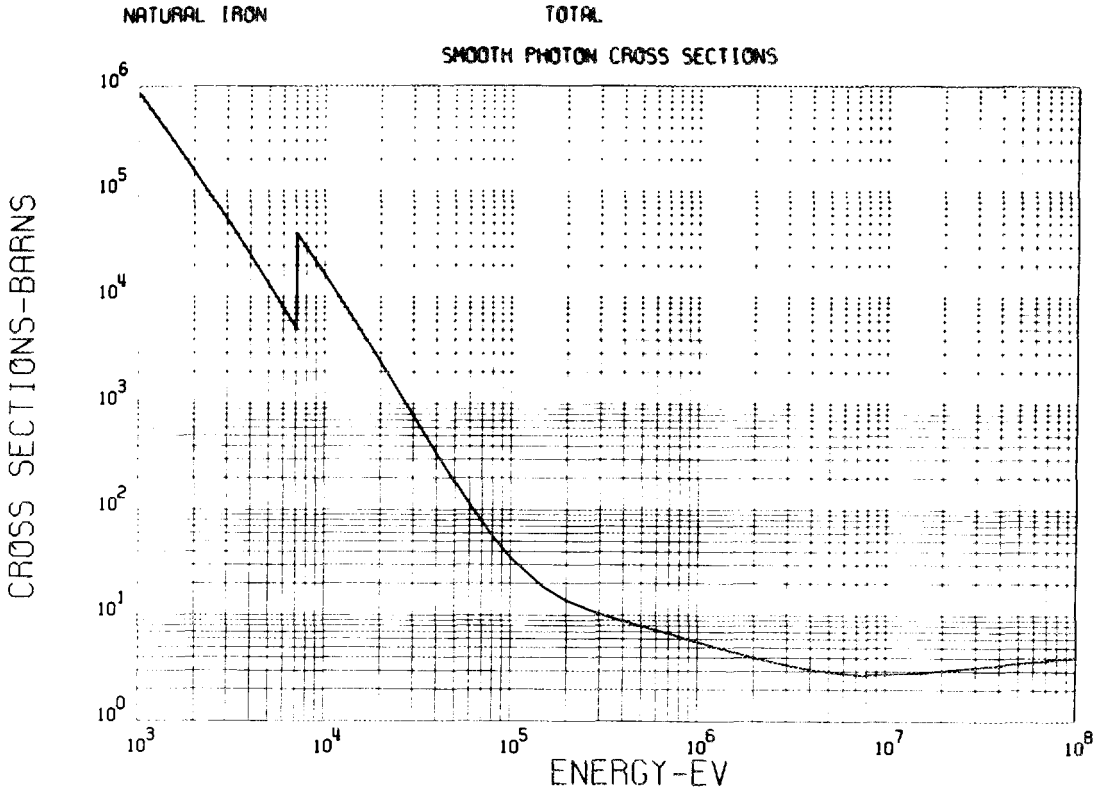

Fig. 97. The Evaluated Photon Total Cross Section.

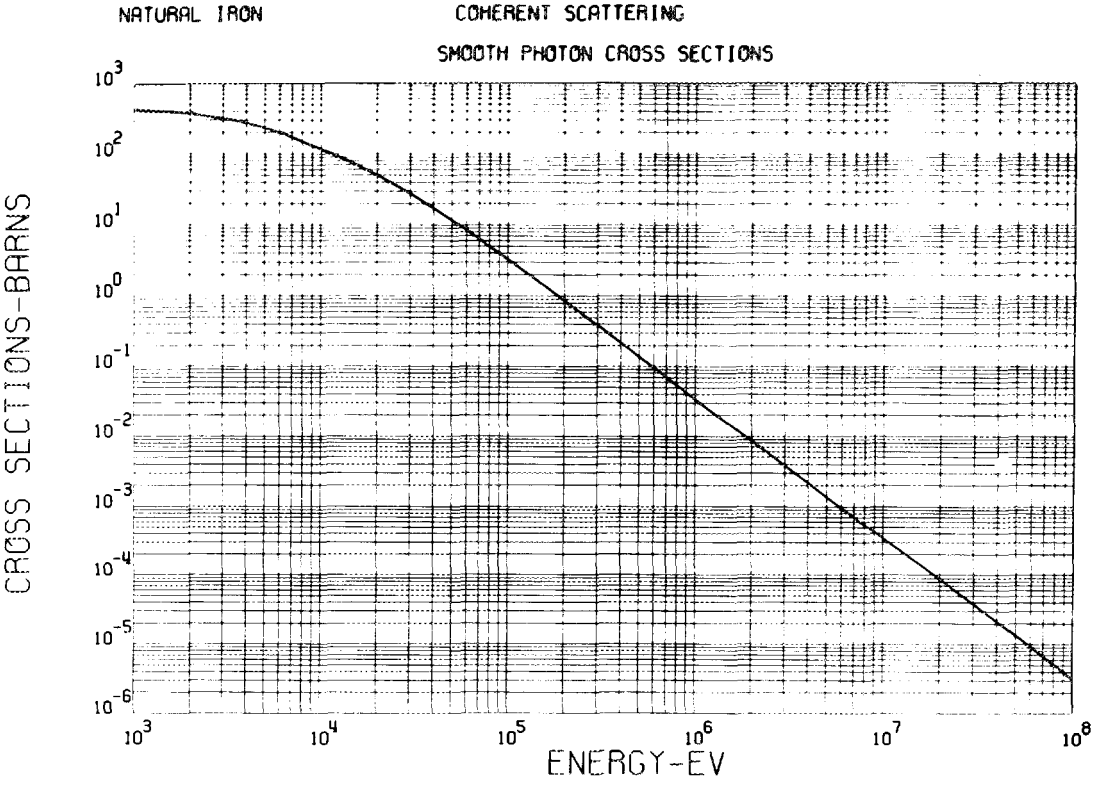

Fig. 98. The Evaluated Photon Coherent Scattering Cross Section.

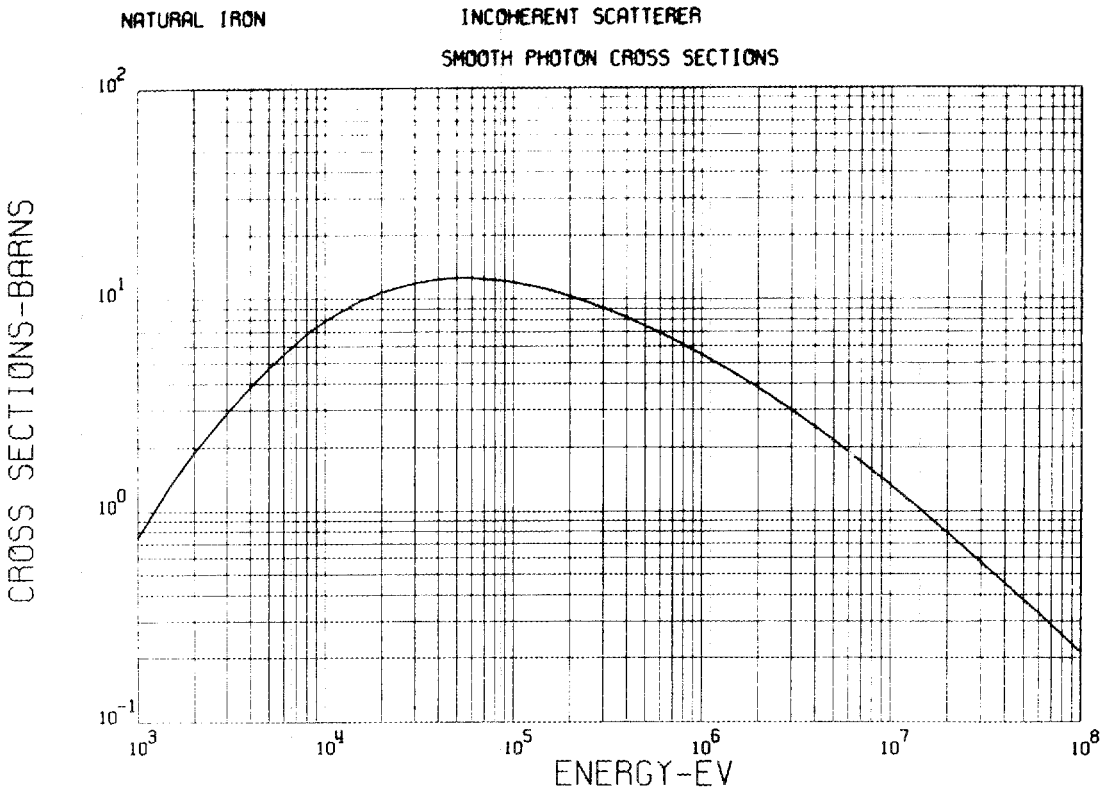

Fig. 99. The Evaluated Photon Incoherent Scattering Cross Section.

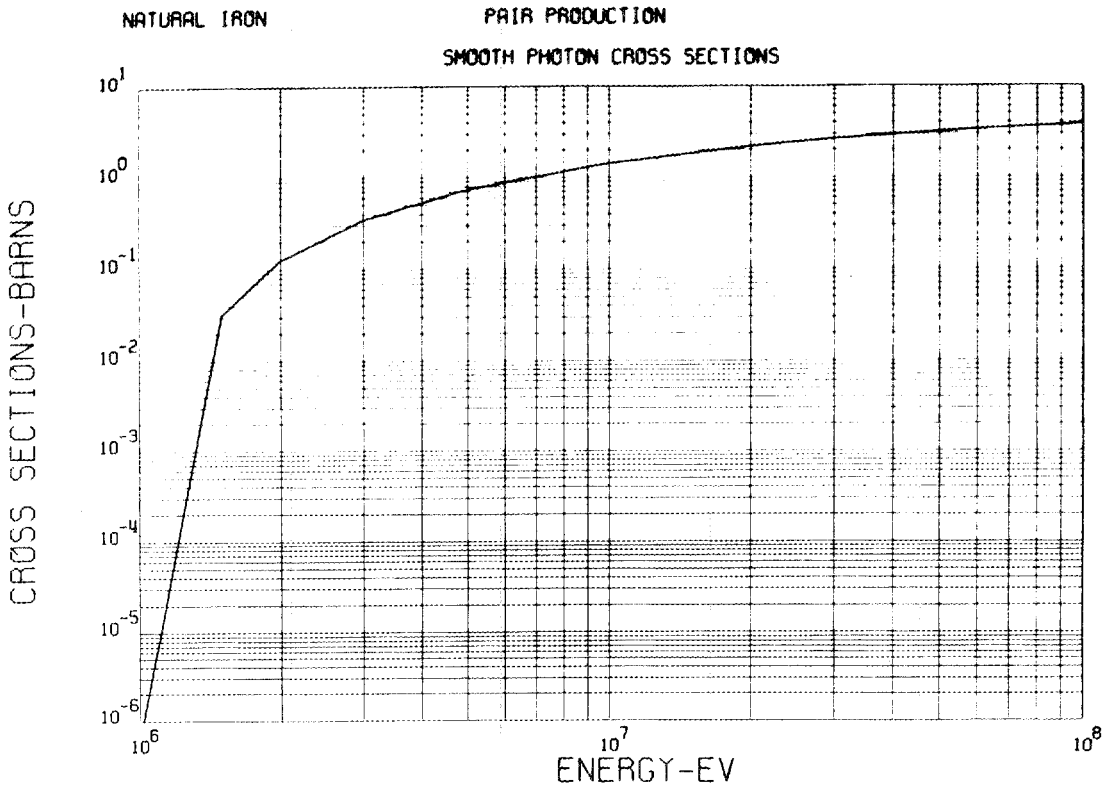

Fig. 100. The Evaluated Photon Pair + Triplet Production Cross Section.

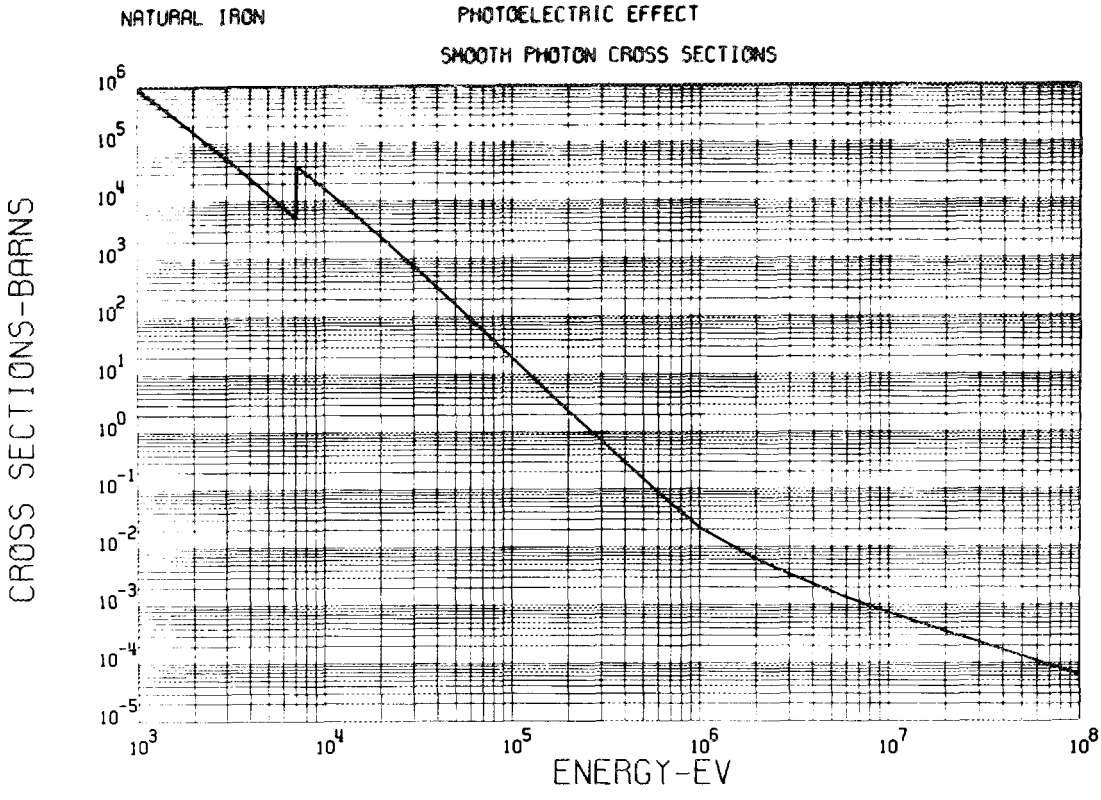

Fig. 101. The Evaluated Photon Photoelectron Cross Section.

Where experimental data are lacking or sparse, our evaluation is necessarily weakened. More data on the following would strengthen future evaluations:

1. Elastic scattering angular distributions below ~4 MeV. Considering the fluctuations in the total cross section, the elastic scattering cross section and angular distributions must also fluctuate as indicated by Cox's data from 0.6 to 1.2 MeV.
2. The cross sections for inelastic scattering to discrete levels in ^{56}Fe and ^{54}Fe. No doubt the cross sections for scattering to the higher levels fluctuate in a manner similar to the fluctuations in the cross section for scattering to the 0.846-MeV level in ^{56}Fe.
3. Neutron inelastic continuum data. A constant nuclear temperature has been assumed here to describe the evaporation portion of the neutron inelastic continuum. It may well vary above 8.5 MeV.
4. Capture and inelastic gamma-ray yields. Models had to be used here to compute the gamma-ray energy distributions. The models entailed assumptions whose validity must be tested.

We made no effort to correlate the fluctuations in the cross section for inelastic scattering to the 0.846-MeV level in ^{56}Fe with fluctuations in the total cross section. Between 0.87 and 2 MeV some suspiciously sharp and low dips appear in the elastic scattering cross section which results from subtracting the nonelastic (essentially the 0.846-MeV level inelastic cross section in this energy region) from the total cross section.

It is difficult to say what difference the use of this evaluation will make on reactor and shield calculations over the use of previous evaluations. Reactor calculations probably will not be affected. In shield calculations the elastic angular distributions should make little difference since the predominant forward peaks are comparable in this and previous evaluations. The improved inelastic description may produce a noticeable effect on neutron spectra in special problems. Gamma-ray-production cross sections were not considered in previous evaluations.

The detail put into this evaluation may be burdensome for some applications. Whether this is offset by better agreement between calculation and experiment must be determined by tests.

We would appreciate being informed of any discrepancies among experiments and calculations using this evaluation, since we plan to revise the evaluation as new information becomes available.

VII. ACKNOWLEDGMENTS

We are grateful to F. G. Perey for his suggestion on the treatment of the structure portion of the continuum and for many useful discussions. We gratefully acknowledge the help of R. Q. Wright of the ORNL Mathematics Division in the manipulation and plotting of the cross sections. We are also indebted to J. E. White of the ORNL Mathematics Division for his calculations of the capture gamma-ray production cross sections and to Margaret B. Emmett of the Mathematics Division for plotting the gamma-ray production energy distributions.

REFERENCES

1. W. E. Kinney and F. G. Perey, "Neutron Elastic- and Inelastic-Scattering Cross Sections for ^{56}Fe in the Energy Range 4.19 to 8.56 MeV," ORNL-4515 (June 1970).
2. B. Holmqvist, *Arkiv Fysik* **38**, 403 (1968).
3. R. L. Macklin *et al.*, Oak Ridge National Laboratory, private communication.
4. D. C. Irving and E. A. Straker, "Evaluation of the Cross Sections of Iron: ENDF/B Mat-1101," ORNL-TM-2891 (ENDF-138) (1970).
5. D. T. Goldman and J. R. Roessen, *Chart of the Nuclides*, Ninth Ed., Revised to July 1966, Prepared by Knolls Atomic Power Laboratory.
6. Creve Maples, George W. Goth, and Joseph Cerny, "Nuclear Reaction Q Values," *Nuclear Data* **A2**, Nos. 5 and 6 (1966).
7. F. G. Perey and B. Buck, *Nucl. Phys.* **32**, 353 (1962).
8. W. Hauser and H. Feshbach, *Phys. Rev.* **87**, 366 (1952).
9. C. E. Porter and R. G. Thomas, *Phys. Rev.* **104**, 483 (1956).
10. L. Dresner, "The Effect of Fluctuations in the Widths on Neutron Reaction Cross Sections," ORNL-CF-57-6-2 (1957).
11. G. R. Satchler, *Nucl. Phys.* **55**, 1 (1964).
12. F. G. Perey, Oak Ridge National Laboratory, private communication.
13. R. W. Hill, *Phys. Rev.* **109**, 2105 (1958).
14. R. M. Wilenzick *et al.*, *Nucl. Phys.* **62**, 511 (1965).
15. Norman A. Bostrom *et al.*, WADC-TR-59-31 (1959).
16. J. C. Hopkins and M. G. Silbert, *Nucl. Sci. Eng.* **19**, 431 (1964).
17. J. H. Coon *et al.*, *Phys. Rev.* **111**, 250 (1958).
18. W. B. Gilboy and J. H. Towle, *Nucl. Phys.* **64**, 130 (1965).
19. S. K. Penny, "HELENE – A Computer Program to Calculate Nuclear Cross Sections Employing the Hauser-Feshbach Model, Porter-Thomas Width Fluctuations, and Continuum States," ORNL-TM-2590 (1969).
20. A. Aspinall *et al.*, *Nucl. Phys.* **46**, 33 (1963); A. Sperduto and W. W. Buechner, *Phys. Rev.* **134**, B142 (1964); A. D. Katsanos *et al.*, *Phys. Rev.* **141**, 1053 (1966); G. Brown *et al.*, *Nucl. Phys.* **77**, 365 (1966); B. L. Cohen and R. Middleton, *Phys. Rev.* **146**, 748 (1966); J. R. MacDonald and M. A. Grace, *Nucl. Phys.* **A92**, 593 (1967); P. F. Henrichsen *et al.*, *Nucl. Phys.* **A101**, 81 (1967); K. Vaughan *et al.*, *Nucl. Phys.* **A130**, 62 (1969).
21. M. N. Rao *et al.*, *Nucl. Phys.* **A121**, 1 (1968).
22. Nuclear Data Group, Nuclear Data Sheets B3, Nos. 3–4, Academic Press (1970).
23. R. H. Bassel, private communication.

24. C. M. Perey *et al.*, "Distorted-Wave Born Analysis of 11-MeV Proton Scattering," *Neut. Phys. Div. Ann. Progr. Rept. for Period Ending May 31, 1967,* ORNL-4134 (1967).
25. A. Gilbert and A. G. W. Cameron, *Can. J. Phys.* **43,** 1446 (1965).
26. R. H. Bassel, R. M. Drisko, and G. R. Satchler, "The Distorted Wave Theory of Direct Nuclear Reactions. I: 'Zero-Range' Formalism Without Spin-Orbit Coupling, and the Code SALLY," ORNL-3240 (1962).
27. M. D. Goldberg *et al.*, "Neutron Cross Sections, Vol. IIA; Z = 21 to 40," BNL-325, 2nd ed., Suppl. 2 (1966).
28. S. Cierjacks *et al.*, "High Resolution Total Neutron Cross Sections Between 0.5 and 30 MeV," KFK-1000 (June 1968).
29. A. D. Carlson and R. J. Cerbone, "High Resolution Measurements of the Total Neutron Cross Sections of Nitrogen and Iron," GA-9149 (March 1969).
30. E. Barnard *et al.*, *Nucl. Phys.* **A118,** 321 (1968).
31. J. S. Story, U.K.A.E.A. Winfrith, private communication (1970).
32. R. W. Hockenbury *et al.*, *Phys. Rev.* **178,** 1746 (1969).
33. S. A. Cox, *Bull. Am. Phys. Soc.* **8,** 478 (1963).
34. J. T. Wells, A. B. Tucker, and W. E. Meyerhof, *Phys. Rev.* **131,** 1644 (1963).
35. I. O. Korzh and M. T. Skylar, *UKR. FIZ.Zh* **8,** 1389 (1963).
36. M. V. Pasechnik *et al.*, *At. En.* (*USSR*) **16,** 207 (1964).
37. K. Tsukada *et al.*, *EAN(J)* **3,** 18 (1966).
38. C. O. Muehlhause *et al.*, *Phys. Rev.* **103,** 720 (1956).
39. H. H. Landon *et al.*, *Phys. Rev.* **112,** 1192 (1958).
40. Lawrence Cranberg and Jules S. Levin, *Phys. Rev.* **103,** 343 (1956).
41. J. R. Beyster, M. Walt, and E. W. Salmi, *Phys. Rev.* **104,** 1319 (1956).
42. R. L. Becker, W. G. Guindon, and G. J. Smith, *Nucl. Phys.* **89,** 154 (1966).
43. M. K. Machwe, D. W. Kent, Jr., and S. C. Snowdon, *Phys. Rev.* **114,** 1563 (1959).
44. W. D. Whitehead and S. C. Snowdon, *Phys. Rev.* **92,** 114 (1953).
45. Nestor Azziz *et al.*, "Iron, Nickel, and Chromium Neutron Cross Sections From 0 to 15 MeV," WCAP 7281 (ENDF-129) (August 1969).
46. J. J. Schmidt, "Neutron Cross Sections for Fast Reactor Materials, Part I: Evaluation," KKFK-120 (EANDC-E 35 U).
47. J. E. White, Oak Ridge National Laboratory, private communication (1970).
48. K. J. Yost, *Nucl. Sci. Eng.* **32,** 62 (1968).
49. R. E. Chrien *et al.*, "Gamma Rays Following Resonant Neutron Capture in ^{56}Fe," BNL-14104 (1970).
50. B. B. V. Raju *et al.*, "The Measurement of Thermal Neutron Capture Gamma Rays in Iron, Cobalt, and Scandium," AAEC/TM 512 (July 1969).
51. Norman C. Rasmussen *et al.*, "Thermal Neutron Capture Gamma-Ray Spectra of the Elements," AECRL-69-0071 (MTNE-85) (January 1969).
52. C. Y. Fu, Oak Ridge National Laboratory, private communication.
53. S. K. Penny, "AVA" (to be published).
54. J. B. McGrory, *Phys. Rev.* **160,** 915 (1967).
55. J. K. Dickens, Oak Ridge National Laboratory, private communication (1970).
56. R. E. Maerker and F. J. Muckenthaler, "Gamma-Ray Spectra Arising From Fast-Neutron Interactions in Elements Found in Soils, Concretes, and Structural Material," ORNL-4475 (1970).
57. J. Celnik and D. Spielberg, "Gamma Spectral Data for Shielding and Heating Calculations," UNC-5140 (1966).
58. E. A. Straker, Technical Note, *Nucl. Sci. Eng.* **41,** 147 (1970).
59. W. H. McMaster *et al.*, "Compilation of X-Ray Cross Sections," UCRL-50174, Sec. II, Rev. 1 (1969).
60. Ernest F. Plechaty and John R. Terrall, "An Integrated System for Production of Neutrons and Photonic Calculational Constants: Vol. VI, Photon Cross Section 1 keV to 100 MeV," UCRL-50400 (1968).

ORNL-4617
(ENDF-139)
UC-34 – Physics

INTERNAL DISTRIBUTION

1–3. Central Research Library
4. ORNL – Y-12 Technical Library Document Reference Section
5–54. Laboratory Records Department
55. Laboratory Records, ORNL R.C.
56–57. L. S. Abbott
58. R. G. Alsmiller, Jr.
59. A. A. Brooks
60. C. E. Burgart
61. H. C. Claiborne
62–66. C. E. Clifford
67. F. L. Culler, Jr.
68. J. K. Dickens
69. M. B. Emmett
70. R. M. Freestone, Jr.
71. C. Y. Fu
72. J. A. Harvey
73. L. B. Holland
74. J. D. Jenkins
75. W. H. Jordan
76–77. W. E. Kinney
78. K. Kumar
79. J. Lucius
80. H. G. MacPherson
81. R. E. Maerker
82–83. F. C. Maienschein
84. G. L. Morgan
85. F. J. Muckenthaler
86. F. R. Mynatt
87. R. B. Parker
88. R. W. Peelle
89–138. S. K. Penny
139. F. G. Perey
140. R. W. Roussin
141. M. J. Skinner
142. A. H. Snell
143. E. A. Straker
144. A. M. Weinberg
145. L. Weston
146. J. E. White
147. R. Q. Wright
148. E. R. Cohen (consultant)
149. H. Feshbach (consultant)
150. H. Goldstein (consultant)
151. C. R. Mehl (consultant)
152. H. T. Motz (consultant)

EXTERNAL DISTRIBUTION

153–339. Given DASA Shielding and Initial Radiation Distribution (updated August 1970)
340. W. H. Hannum, Division of Reactor Development and Technology, U.S. Atomic Energy Commission, Washington, D.C. 20546
341. P. B. Hemmig, Division of Reactor Development and Technology, U.S. Atomic Energy Commission, Washington, D.C. 20546
342. K. O. Laughon, AEC Site Representative, ORNL
343–467. National Neutron Cross Section Center
468. R. J. Howerton, Lawrence Radiation Laboratory, P.O. Box 808, Livermore, California 94551
469. J. Ferguson, Lawrence Radiation Laboratory, P.O. Box 808, Livermore, California 94551
470. D. C. Irving, Savannah River Laboratory, Aiken, South Carolina 29802
471. L. Stewart, Los Alamos Scientific Laboratory, P.O. Box 1663, Los Alamos, New Mexico 87544
472. John Story, UKAEA, Aldermaston, Berkshire, England
473. P. G. Young, Los Alamos Scientific Laboratory, P.O. Box 1663, Los Alamos, New Mexico 87544
474. J. A. Swartout, Union Carbide Corporation, New York, N.Y. 10017
475. Laboratory and University Division, AEC, ORO
476. Patent Office, AEC, ORO
477–710. Given distribution as shown in TID-4500 under Physics category (25 copies – NTIS)